공학박사학위논문

Modeling, State Estimation and Control of Lithium-ion Battery for Hybrid Energy System

하이브리드 에너지 시스템용 리튬 이온 전지에 대한 모델링, 상태 추정 및 제어

2012년 8월

서울대학교 대학원

화학생물공학부

조 성 우

Abstract

Modeling, State Estimation and Control of Lithium-ion Battery for Hybrid Energy System

Sungwoo Cho

School of Chemical & Biological Engineering

The Graduate School

Seoul National University

In recent years, energy storage systems have been highlighted in portable electronics and eco-friendly vehicle applications. In particular, lithium-ion batteries are used as principal or auxiliary power supply devices for the eco-friendly vehicle applications as hybrid energy systems due to high performance of voltage and power. The batteries in the eco-friendly vehicles either store excess power from the vehicle or supply insufficient power to vehicle motive power generator. Therefore, the performance of the lithium-ion battery is a key variable for the performance

evaluation of eco-friendly cars. The key variables of the lithium-ion battery are state-of-charge and state-of-health. Rigorous dynamic model is required to estimate the key variables as state. Therefore, the lithium-ion battery model for hybrid energy system is presented in this thesis. The estimation methodologies for state-of-charge and state-of-health are suggested based on the developed model. Finally, the developed model and estimation methodologies are applied to the optimal control logic of fuel cell hybrid electric vehicle as the hybrid energy system.

This thesis describes a state-of-charge estimation methodology for lithium-ion batteries in eco-friendly vehicles. The proposed methodology is intended for state-of-charge estimation under various operating conditions including changes in temperature, driving mode and power duty. The suggested methodology consists of a recursive estimator and employs an equivalent circuit as the electrochemical cell model. Model parameters are estimated by parameter map on experimental cell data with various temperatures and current conditions. The parameter map is developed by a least sum square error estimation method based on nonlinear programming. An adaptive estimator is employed and is based on the combination of current integration and battery model based estimation. The proposed state-of-charge estimation methodology is validated with experimental lithium-ion battery pack data under various driving schedules with low and ambient temperatures and sensor fault cases. The presented results show that the proposed model and methodology are appropriate for estimating state-of-charge under various conditions; power duty, temperature and sensor fault situations.

State-of-health estimation algorithms for the actual performance of a lithium-ion

battery as state-of-health are presented for on-line monitoring. The capacity is selected as the representative variable, which indicates the performance of the battery. Three algorithms are suggested to estimate the degree of capacity fading: principal algorithm, supplementary algorithm, and hybridized algorithm. The principal algorithm is based on a simplified equivalent circuit model and soft sensor technique. The soft sensor technique is based on a system identification methodology with variance inhibition based approach. The second algorithm is developed to compensate for the problem of computational load. Finally, both of the algorithms are combined in a hybridized algorithm to complement each other. The suitability of algorithms is demonstrated with on-line monitoring of fresh and aged cells using cyclic experiments. The results from diverse experiments for hybrid electric vehicle and plug-in hybrid electric vehicle applications demonstrate the appropriateness of the accuracy, reliability against the inaccurate previous estimated values and computational load. Consequently, the developed hybridized algorithm was appropriate for on-line estimation of the actual battery performance as quantitative values of capacity and power in real time.

The optimal control logic for lithium-ion battery / proton exchange membrane fuel cell hybrid energy system is developed using fuzzy logic controller. The developed lithium-ion battery model is applied to design of the control logic. The proton exchange membrane fuel cell system model with hydrogen recirculation and cathode humidifier is developed. The optimal controller is suggested by fuzzy logic control algorithm. Demanded power of the fuel cell hybrid electric vehicle is used with the fuzzy logic controller to calculate the output power from the fuel cell system. In addition, estimated state-of-charge and state-of-health are used as input

variables of the fuzzy logic controller. The fuzzy controller is validated with various operations for the eco-friendly vehicles as the hybrid energy system. The suggested control logic is appropriate for application in commercialization and practical usage of the eco-friendly vehicles.

This work could contribute to state estimation and control of the lithium-ion battery for the hybrid energy system. The developed models, state estimation methodologies and control logic could be implemented to on-line application for practical usage of the eco-friendly vehicle.

Keywords : Lithium-ion Battery, Hybrid Energy System, Equivalent Circuit Model, State of Charge, Capacity fading, Fuzzy control

***Student Number* : 2005-21277**

Contents

List of Figures

List of Tables

CHAPTER 1 : Introduction

1.1. Research motivation

In recent years, energy storage systems such as lithium-ion batteries have been highlighted in portable electronics and electric vehicle applications as hybrid energy system.[1] In particular, lithium-ion batteries have higher power, high energy density, and higher open circuit voltage than other types of batteries.[2] Thus, lithium-ion batteries are used as principal or auxiliary power supply devices for various types of electric vehicles: battery electric vehicles (BEVs), hybrid electric vehicles (HEVs) and plug-in hybrid electric vehicles (PHEVs).[3-6] In particular, sales of the electric vehicles have increased dramatically in the last decade and the lithium-ion battery has come under spotlight shown in Fig. 1-1.[7]

Especially, fuel cell hybrid electric vehicles (FCHEVs) are spotlighted as an ultimate application of the renewable eco-friendly vehicles.[8-9] The FCHEVs uses a fuel cell which uses the hydrogen gas or the reformed hydrogen gas as a fuel. The fuel cell produces the vehicle's on-board motive power instead of an internal combustion engine. Therefore, the FCHEVs fume out a fewer polluted exhaust gas than the conventional vehicles using the internal combustion engine.[10-13]

The difference between BEVs, HEVs, PHEVs and FCHEVs is based on type of the principal power supply device.[14-15] The principal power supply device for the HEVs is an internal combustion engine and battery serves as the auxiliary power supply device. The principal power source of the FCHEVs is changed to the fuel cell instead of the internal combustion engine. The battery in the FCHEVs plays a

same role as that in the HEVs. On the other hand, battery serves as the principal power supply device for PHEVs. The rechargeable battery in PHEVs could be fully charged by connection with a plug to external power source. The secondary batteries on PHEVs have large capacity and high performance power to be a principal power supply device. Furthermore, the batteries on the eco-friendly vehicle could be grown larger enough to serve a power supply role by themselves. In this case, the batteries could serve propulsive roles alone without any internal combustion engine or power supply unit like fuel cell. The vehicles with these types of batteries are called as BEVs.[16-18] The major characteristics of several eco-friendly vehicles are summarized in Table 1-1.[19-20]

For these types of the vehicles battery holds an important role as the motive force. The fuel cell or ICE generates power to battery system when the vehicle is just started. The power is supplied to both of powertrain and rechargeable battery system after starting mode, so called cruising mode. However, both of the ICE and the rechargeable battery generate more power at accelerating state as passing mode. Moreover, the wasted energy from the regenerative braking is converted to electrical energy and passed to the rechargeable battery system at braking mode.[18, 21-22] Likewise, the batteries in the vehicles either store excess power from the vehicle or supply power when it is insufficient to the vehicle according to the circumstances. Therefore, the performance of lithium-ion batteries is a key factor for the performance evaluation of eco-friendly cars. Thus many studies regarding the secondary battery have been carried out for a past decade.[23-24]

The state-of-charge (SOC) is equivalent to a fuel level for the battery pack in a battery electric vehicle and is the key to controlling the battery system and

estimating the maximum available power and state-of-health of the battery.[25-26] Therefore, the SOC estimation is an important aspect of hybrid electric vehicles and plug-in hybrid electric vehicle applications.

The regular daily use of eco-friendly vehicles worsens the performance of batteries over time in the vehicles through iterations of charge and discharge cycles. At first, the initial performance is equal to the performance of fresh batteries. However, the performance deteriorates over time. The performance of batteries is represented by the capacity and power. The capacity and power deteriorate over time, referred to as capacity and power fading.[27-29] The phenomenon of fading has a decisive effect on the efficiency of eco-friendly vehicles. The available maximum power from the battery decreases due to power fading. The charging capacity is reduced due to capacity fading. As a result, the role of the battery becomes secondary and the degree of hybridization of the engine and batteries decreases to the level of a conventional internal combustion vehicle. Therefore, the performance measurement of the state of the battery is a momentous issue in eco-friendly vehicle development.[30-31] State-of-health (SOH), which shows the state of a battery compared to its ideal condition, is typically the main parameter used to reflect the performance state. The on-line estimation of actual battery performance is especially highlighted in real world applications of eco-friendly vehicles.[32-33]

Power distribution problem for dual power sources is important issue for efficient operation of the eco-friendly vehicles as the hybrid energy system. Development of the power distribution control system plays an important role to operate the vehicle more efficiently and to maintain the durability of the system. The control system is developed to achieve maximum system's efficiency to minimize the fuel

consumption. Moreover, the SOC of the secondary battery has to be maintained in moderated range while operating the hybrid vehicle. When the battery is operated at very low or high SOC conditions, the capacity and power of the battery rapidly deteriorate. As a result, the life of the secondary battery is shortened than expected life length. Therefore, maintaining SOC of the battery is necessary to prevent frequent replacement of the secondary battery. The study of the optimal control of the hybrid energy system is an important issue for a last decade.[34-37]

Table 1-1. Characteristics of eco-friendly vehicles; BEV, HEV, PHEV and FCHEV

Type	BEV	PHEV	HEV	FCHEV
Propulsive unit	Electric motor	ICE / Electric motor	ICE / Electric motor	Electric motor
Power supply unit	Battery / Ultracapacitor	ICE generating unit / Battery / Integrated starter generator / Ultracapacitor	ICE generating unit / Battery / Integrated starter generator / Ultracapacitor	Fuel cell / Battery / Ultracapacitor
Energy source	Electric grid charging facilities as plug	Electric grid charging facilities as plug / Gasoline stations	Gasoline stations	Hydrogen infrastructures
Advantages	Zero emission / Independence on crude oils / High energy efficiency	Very low emission / Long driving range / Higher fuel economy	Low emission / Very long driving range / Higher fuel economy / Commercially available	Almost zero emission / High energy efficiency / Independence on crude oils / Satisfied driving range
Disadvantages	High cost / Short driving range	In development / Dependence on crude oils / Complexity	Dependence on crude oils / Complexity	High cost / In development

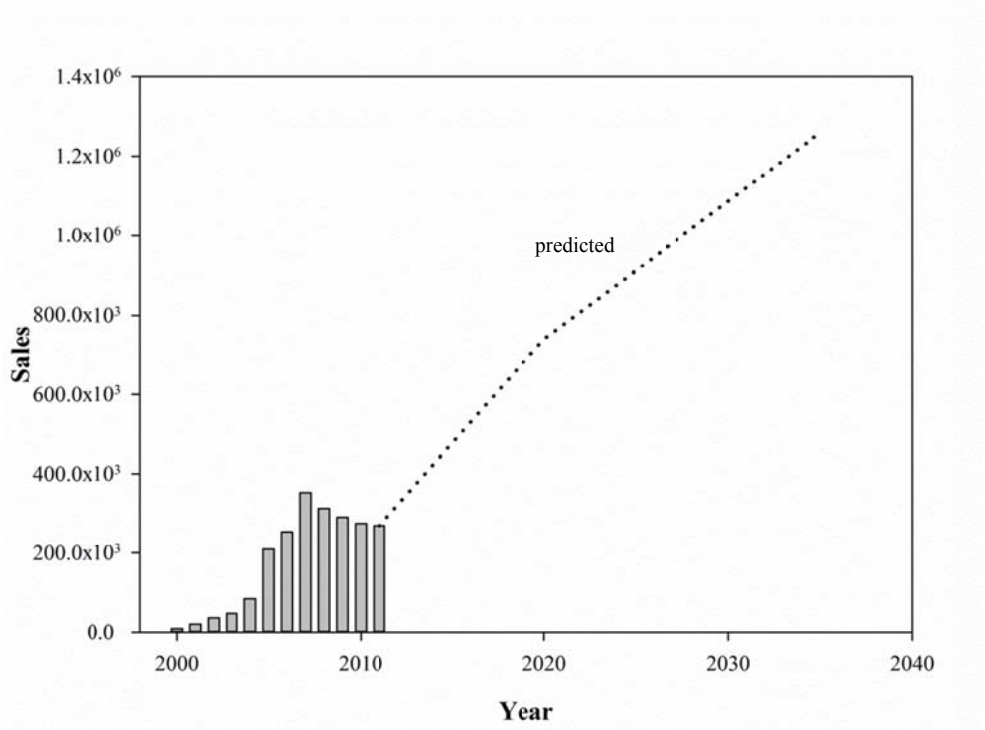

Figure 1-1. Sales and predicted sales of hybrid electric vehicles in United States.

1.2. Research objectives

Estimation methodologies of the lithium-ion battery states and control algorithm of the hybrid energy system of dual power source are suggested for this purpose. The rigorous dynamic modeling of the lithium-ion battery is developed for the estimation and control of the system. The off-white model which contains parameters is selected for lithium-ion battery modeling. The parameter estimation methodologies based on sum square error minimization approach are applied to the battery dynamic model. The SOC and SOH estimation methodologies are suggested for the accurate estimation of the battery states. The methodologies use the soft sensor methodology based on system identification for accurate and reliable estimation. The suggested model and estimation methodologies are demonstrated through comparison of the simulation result and the experimental result. The optimal and robust control methodology of the hybrid energy system applications such as FCHEVs is suggested using proposed model and estimation methodologies. The robust optimal control logic of the proton exchange membrane fuel cell (PEMFC) / lithium-ion battery hybrid energy system are developed using the battery dynamic model and state estimation methodologies. The fuzzy control logic with multi input variables and single output variable is selected for on-line control of the hybrid energy system. The control logic is applied to various operation situations for validation of the performance.

1.3. Outline of the thesis

The thesis is organized as follows. Chapter 1 suggests an explanation about motivation and objectives of the research as introduction. The dynamic battery model with the parameter estimation method based on sum square error minimization and a SOC estimation method for various operating conditions are described in Chapter 2. It followed by the development of the equivalent circuit model and parameter analysis. Chapter 3 addresses the simplified dynamic model and the methodology for SOH estimation. The soft sensor methodology based on system identification and the simplified methodologies based on the charging simulation assumption are suggested to estimate the capacity fading more rapidly, accurately and reliably. Chapter 4 deals with the control algorithm for PEMFC and lithium-ion secondary battery hybrid energy system using fuzzy control logic. The performance index of the lithium-ion rechargeable battery previously estimated SOC and SOH are selected as input variables for fuzzy logic control. Chapter 5 presents the conclusions of the thesis and the outline for future work recommendation.

CHAPTER 2 : Lithium-ion Battery Modeling and State-of-Charge Estimation*

2.1. Introduction

The SOC is equal to the fuel level in conventional vehicles for the battery pack in BEVs, HEVs, PHEVs and FCHEVs. As aforementioned, SOC is an important value to control the hybrid energy system and to estimate the maximum available power and SOH of the secondary battery.[25-26] Therefore, many studies have been researched for a last decade. Coulomb counting has been the most common method of measuring the SOC.[39] This method is easy for calculation but accumulates errors due to incorrect measurements. The open circuit voltage based method with a dynamic battery model has been suggested as an alternative. However, this method is only accurate during rest periods on low current and not during moderate or high current periods. Therefore, adaptive estimation methods such as neural networks, fuzzy logic, and extended Kalman filters have been used based on Coulomb counting and open circuit voltage based methods.[40-52]

The estimation methods described above are accurate under moderate operation conditions due to the adaptive nature of the estimator. However, these methods cannot be applied to various operating conditions. Battery operating conditions include several variables, for example, various power duty conditions occurring during current fluctuation, low and high temperatures, and varying SOC ranges.

* The partial part of this chapter is taken from the author's published paper in journal.[38]

The power duty conditions change due to power demand from the power train of the vehicle. The power duty is low for urban driving schedules but high for highway driving schedules. Power duty is extremely high in high acceleration aggressive schedules identified as the "Supplemental Federal Test Procedure (FTP)" driving schedule.[53] Existing SOC estimation methods have been applied to and demonstrated in high duty cycles, but are not sufficient to be applied to real systems.

Temperature is one of the major variables determining battery operating conditions since hybrid electric vehicles are operated under extremely hot or cold conditions. However, existing SOC estimation methods rarely take into consideration the power duty and temperature; therefore, they are not sufficient for application to real systems.[54] Battery sensor fault is another possible obstacle for battery operation. Since the SOC needs to be estimated on-line, the necessity for a reliable estimation method against transient sensor error should be emphasized for practical operations.

For SOC estimations in various operating conditions, a combination of Coulomb counting and the open circuit voltage based method is often used to overcome their individual shortcomings. The open circuit voltage based method is especially important for a dynamic battery model, which describes the battery cell in various conditions and is necessary for the SOC estimation. Dynamic battery models have been developed based on the electrochemical cell model. However, the battery models for various conditions are complicated, making them unsuitable for on-line SOC estimations. Therefore, identifying reduced complexity but rigorous models for various current and temperature conditions are important issues for the SOC

estimation. A battery model employing a parameter estimation method based on sum square error minimization from experimental data is adequate for such a purpose.

In this chapter, a dynamic battery model and SOC estimation methodology were proposed for the estimation of the SOC under various battery system operating conditions. The dynamic battery model with the parameter estimation method based on sum square error minimization is described, followed by the development of the equivalent circuit model (ECM) and parameter analysis. A SOC estimation method for various operating conditions is suggested. A combination of current integration and model based estimation is proposed. Demonstrations of the model and methodology are described under various operating conditions. Finally, Chapter 2 closes with conclusions.

2.2. Lithium-ion battery modeling by equivalent circuit model

The electrochemical cell dynamic voltage model for lithium-ion batteries is a function of current *i*, temperature *T* and voltage *V* according to Eq. 2-1.

$$f\left(i,V,T\right)=0 \tag{2-1}$$

The model is classified as follows: first principle model, equivalent circuit model, and black box model. The first principle model is a rigorous model based on electrochemistry, thermodynamics, and transport phenomena.[44, 55-59] It consists of several partial differential equations and ordinary differential equations. However, the computational load is high and the computational time required is longer than each SOC estimation interval. From some studies about computational algorithm optimization with model reformulation, the computational time was obtained equal or less than the interval of the SOC estimation – 10ms.[60-61] The computational time was equal or less than the interval of the SOC estimation. However, this result has difficulties for direct application to real battery management system (BMS). The above computation of the first principle modeling was performed at a personal computer environment. The calculation is performed at personal computer environment - 1.7 GHz processor and 1 GB RAM. On the other hand, an embedded system such as a micro control unit is used as the computation device instead of the personal computer in the battery management system environment. Therefore, the computational time is increased at the practical application.

Furthermore, the BMS takes various roles – data acquisition and storage from the system, the SOC estimation, capacity and power fade estimation, available

maximum power calculation, cooling and heating of the system with on-line control and diagnosis of the system.[62] Therefore, the battery management system does not concentrate the all source of the processing capabilities to the SOC estimation. Accordingly, the SOC estimation algorithm is more beneficial when the algorithm is simple and light. Therefore, it is not adequate for SOC estimations.

The black box model is based on measured data and statistical approaches.[63-64] It is suitable for cases in which theoretical or very complex models are difficult to solve using only existing modeling methods. It cannot be applied to interpolation and extrapolation; thus, it is not appropriate for SOC estimations.

The equivalent circuit model is a reduced model based on electrochemistry.[65-67] The model is described as a set of resistances and capacitances.[68] This model is simpler than the first principle model, and the computational runtime is extremely short. In addition, this model is based on a theoretical background. The equivalent circuit model also has disadvantages. The only monitored variables from the model are current and voltage. The behavior in the cell for the specific point could not be estimated by the model. Therefore, the equivalent circuit model is not adequate for the study of the ion transport behavior or electric potential estimation. However, the purpose of this study is estimation of the SOC and the required variables are current and voltage, fortunately. Therefore, the equivalent circuit model is reasonable for SOC estimations in spite of the disadvantages.

The infinite RC ladder circuit in the model needs to be simplified since the increase in states and parameters is the main determinant of the computational time shown in Fig. 2-1. Researchers have studied the simplification of the equivalent circuit model for several decades [68]. As a result, the circuits are simplified to a

circuit with a single resistance and a single RC ladder element shown in Fig. 2-2. Current is recognized during charging with positive terms and during discharging with negative terms. The single resistance is R_0, which signifies the lumped series resistances. A single RC ladder implies a double layer and diffusion, where R_i is the lumped interfacial resistances and C_i is the electric double layer capacitor.

The use of single resistance and a single RC ladder element have been studied.[68] Currents are balanced at each of branch in Fig. 2-2 as Eq. 2-2.

$$i = i_2 + i_3 \tag{2-2}$$

The voltages within RC ladder are summarized by circuit analysis as Eq. 2-3 and Eq. 2-4.

$$V = V_0 + iR_0 + i_3R_i \tag{2-2}$$

$$V = V_0 + iR_0 - \frac{Q_0}{C_i} \tag{2-3}$$

The capacitance in Eq. 2-3 is justified as Eq. 2-4.

$$i_2 = \frac{dQ_0}{dt} \tag{2-4}$$

These equations are summarized to Eq. 2-5 and the ECM in Fiq. 2-2 is derived as Eq. 2-5.

$$\frac{d}{dt}\left(V - V_0\right) + \frac{1}{R_iC_i}\left(V - V_0\right) = \frac{1}{C_i}\left(1 + \frac{R_0}{R_i}\right) + R_0\frac{di}{dt} \tag{2-5}$$

This ECM is integrated in time t using integrating factor by Verbrugge, according to Eq. 2-6.[65, 69]

$$V = \frac{Q_{0,0}}{C_i} e^{-t/R_i C_i} + V_0 + iR_0 + \frac{1}{C_i} \int_{\xi=0}^{\xi=t} \left(i(\xi) e^{-(t-\xi)/R_i C_i} \right) d\xi \qquad (2\text{-}6)$$

The lithium-ion battery was set to zero polarization condition at initial state. Therefore, Eq. 2-6 is expressed as Eq. 2-7.

$$V = V_0 + iR_0 + \frac{1}{C_i} \int_{\xi=0}^{\xi=t} \left(i_\xi \, e^{-(t-\xi)/R_i C_i} \right) d\xi \qquad (2\text{-}7)$$

The battery management system measured the variables in discrete time interval, Δt. The lithium-ion battery is assumed to zero current state at t≤0, and the term in the integral in Eq. 2-7 is equal to zero. Thus Eq. 2-7 could be rewritten at initial state at t=0.

$$V - V_0 - iR_0 \big|_{t=0} = 0 \qquad (2\text{-}8)$$

Eq. 2-7 could be expressed as Eq. 2-9 using al integration and Eq. 2-8 at t_1 and t_2.

$$V - V_0 - iR_0 \big|_{t=t_1} \approx \frac{e^{-t_1/R_i C_i}}{C_i} \left(i_{t_1} \Delta t \cdot e^{t_1/R_i C_i} \right) \qquad (2\text{-}9)$$

$$V - V_0 - iR_0 \big|_{t=t_2} \approx \frac{e^{-t_2/R_i C_i}}{C_i} \left[\left(i_{t_2} \Delta t \cdot e^{t_2/R_i C_i} \right) + \left(i_{t_1} \Delta t \cdot e^{t_1/R_i C_i} \right) \right] \qquad (2\text{-}10)$$

Therefore, we could summarize the Eq. 2-9 and Eq. 2-10 to Eq. 2-11 as difference between two times.

$$V - V_0 - iR_0 \big|_{t=t_2} \approx \frac{i(t_2)\Delta t}{C_i} + e^{-\Delta t/R_i C_i} \left[V - V_0 - iR_0 \big|_{t=t_1} \right] \qquad (2\text{-}11)$$

This calculation is repeated and the Eq. 2-11 could be expressed at time t as followed Eq. 2-12.

$$\hat{V}_k = V_{0,k} + i_k R_0 + \frac{1}{C_i} i_k \Delta t + \left[\exp\left(-\frac{\Delta t}{R_i C_i} \right) \right] \left(\hat{V}_{k-1} - V_{0,k-1} - i_{k-1} R_0 \right)$$

(2-12)

This battery voltage model was selected as the starting point for this study. V_0 in this model is the nominal SOC-dependent open circuit voltage. The open circuit voltage (OCV) was measured for various SOCs and temperatures. OCV rapidly increased with increasing SOC such that the relationship between SOC and OCV was linear for a SOC range of 30% to 70%. However, only slight changes were observed for different temperatures. The measured OCV is shown in Fig. 2-3.

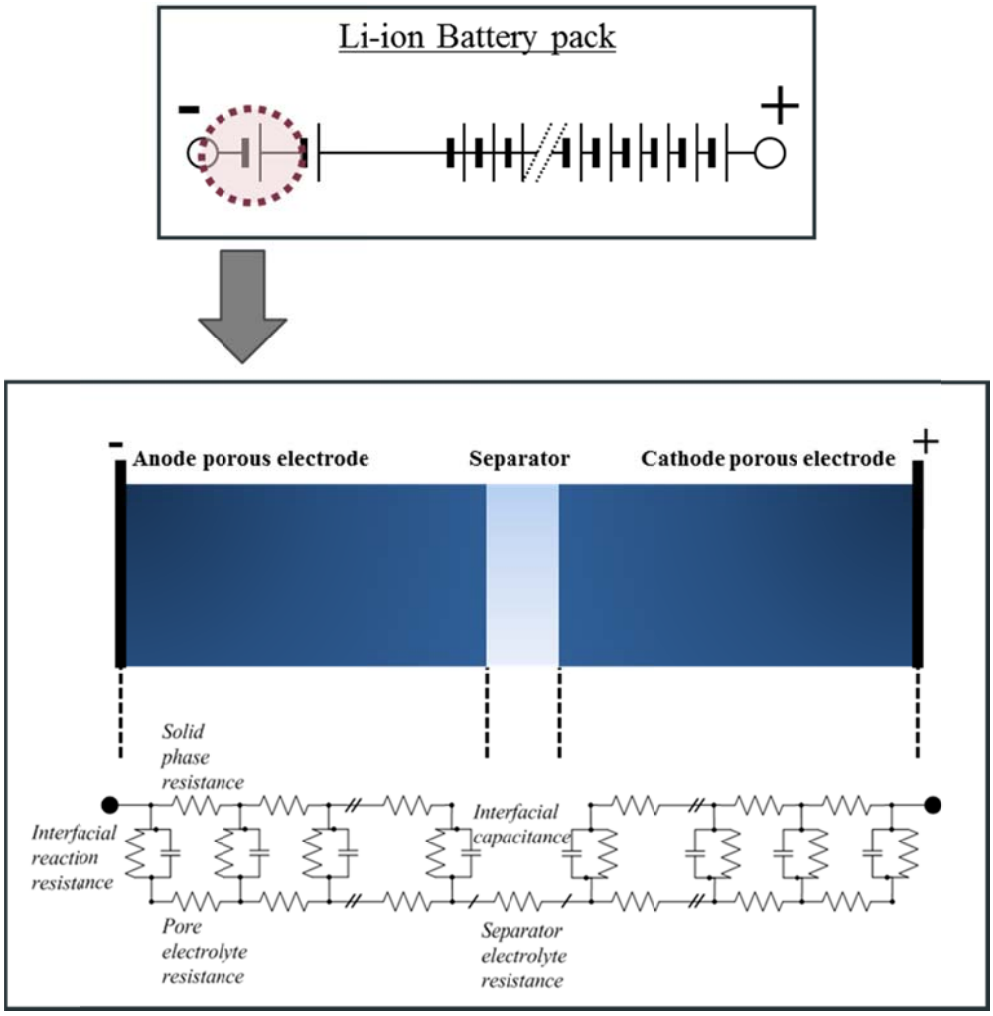

Figure 2-1. Lithium-ion battery packs and cell description by equivalent circuit model with infinite RC ladder circuit.

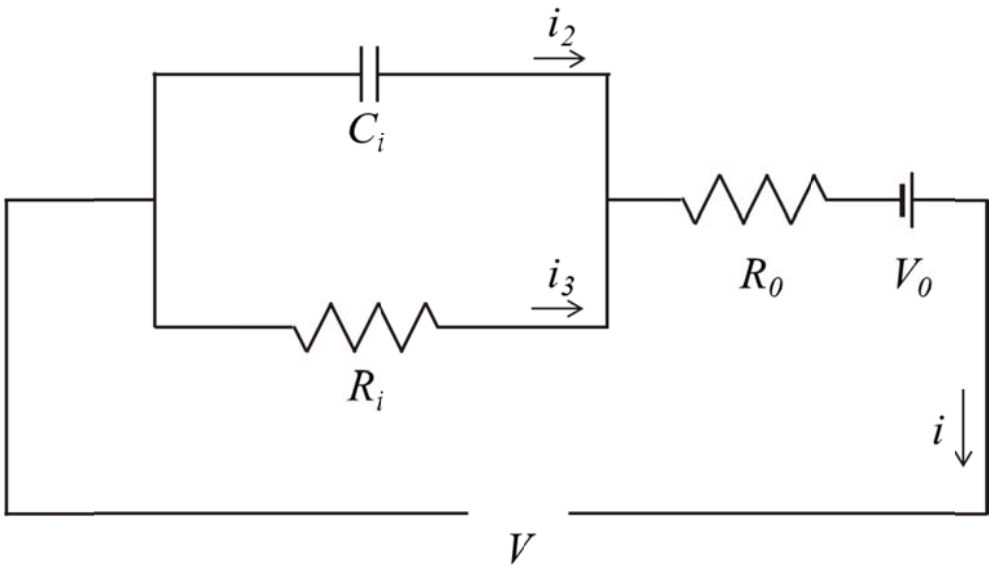

Figure 2-2. Simplified equivalent circuit battery model with a single resistance and a single RC ladder element.

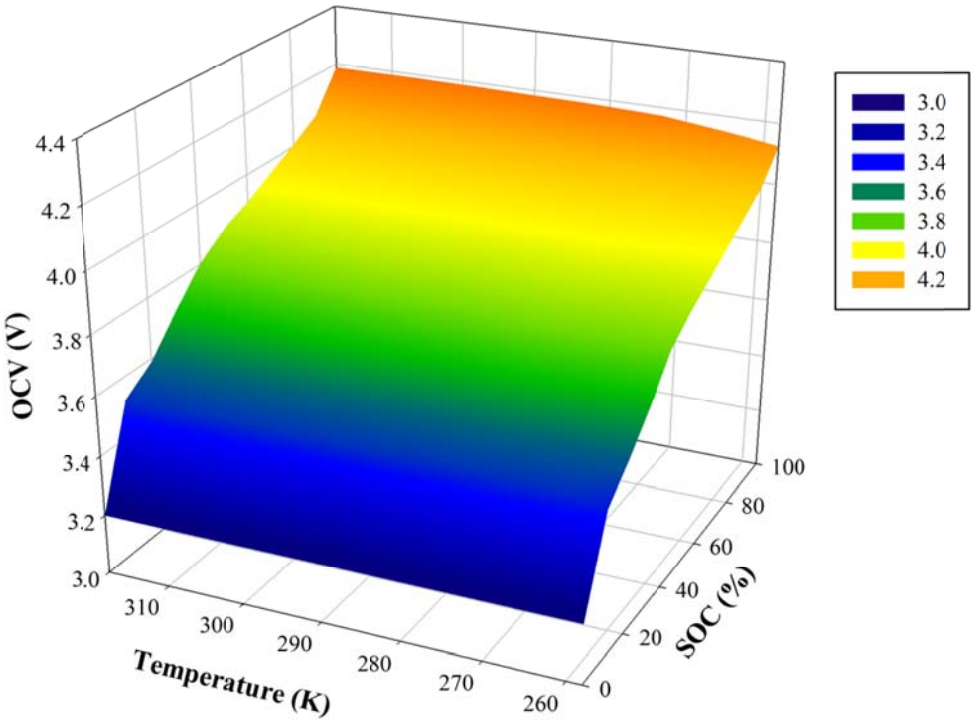

Figure 2-3. Open circuit voltage versus the SOC and temperature.

2.3. Estimation of model parameter

2.3.1. Estimation using least square estimation method

In the proposed model, the main parameters are suggested as follows: R_0, R_i, and C_i. Since these parameters depend on the charge/discharge states, current, temperature and SOC, they must be recursive as conditions change. There are many methods for recursive adaptation of parameters such as a neural network, Kalman filter and adaptive filter.[45, 51, 55, 65, 70] However, battery conditions change rapidly, and these methods have limitations in their accuracy. Therefore, a look-up table interpolation method with error minimization is adequate for these model parameters.[71-73] Look-up tables are established on experimental cell data with various pulse pattern conditions. Parameter maps are organized by interpolation and extrapolation of the look-up tables.

Lithium-ion batteries for hybrid electric vehicles were used for the experiments. These batteries were rated for 6.5Ah. Pulse pattern experiments were done at various conditions: current, temperature and SOC. The total cycle of the pulse pattern was 100s and consisted of a 10s constant pulse current period and a 90s rest period shown in Fig. 2-4. The current was varied for the mapping parameters from 6.5A to 200A, and the charge and discharge modes were separated. The temperature was varied up from 263K to 318K, and the SOC was set as 30% to 70% for nominal operating conditions. Current, voltage and temperature were measured in 1s intervals in these experiments.

From the experimental data, model parameters were set for each condition. Sum-square error (SSE) minimization was selected for parameter calculation, according

to Eq. 2-13.

$$\min \Psi = \sum_{k} \left(\hat{V}_k - V_k \right)^2 \tag{2-13}$$

The concept of a least square method for SSE is described in Fig. 2-5 and Table 2-1.[71-72, 74-75] The system model is the ECM according to Eq. 2-12 where the input variables are the current, SOC, and temperature, and the output value is the voltage. For the estimation, the first step is the selection of an initial value for a parameter, which is arbitrarily selected for the optimization. This is followed by modeling and error calculations. Here, the input variables from the experimental measurements are taken to the dynamic battery model and the output variables are calculated from the battery model using the initial parameter values. Differences between the output variables and the experimental output data are defined as errors. In such cases, the difference in voltage values from the model calculation and the experimental measurements are justified as the errors. A squared error summation for one cycle is carried out, and the SSE is calculated. The final step is determination of the optimal parameter. The parameter is regarded as an adequate value for exact phenomenon explanation when the SSE achieves a minimum value by optimization technique.

The optimal parameter is estimated using a nonlinear programming method. The method used is an interior-reflective Newton method for nonlinear programming by sequential quadratic programming in a MATLAB® simulation environment with an *fminsearch* title. This results in parameter sets for each condition, which are organized as look-up tables and parameter maps.

Measuring error and polarization phenomena were used as standards for the

valuation of the developed battery model and parameter estimation method. The error is the difference between the real voltage and estimated voltage from the model, as mentioned above. The maximum absolute value of the error was 6.75mV, which corresponds to 0.171%. Polarization phenomena are visualized by a voltage curve shown in Fig. 2-4. The polarization curve from the model is similar to real data curves; in particular, the gradient of the curve shows little difference between the real system and the model.

The confidence interval of nonlinear least square estimation is calculated to validate the reliability of the parameter estimation. Constantinides and Mostoufi suggest the confidence interval calculation for multivariable nonlinear least square estimation, according to Eq. 2-14.[76]

$$b_i - t_{(1-\alpha/2)} s\sqrt{a_{ii}} \le \beta_i \le b_i + t_{(1-\alpha/2)} s\sqrt{a_{ii}} \tag{2-14}$$

where bi means the estimated value of the parameter β_i, $t_{(1-\alpha/2)}$ means the statistic for a confidence level of (1-α) given by the Student's t-distribution, s means the standard deviation of the error and a_{ii} means the element of the parameter covariance matrix. The covariance is given by Eq. 2-15.

$$A = \left[wJ^T J \right]^{-1} \tag{2-15}$$

The Jacobian matrix J for the battery model is given by Eq. 2-16.

$$J = \begin{bmatrix} \left.\frac{\partial \hat{V}}{\partial C_i}\right|_{t=t_1} & \left.\frac{\partial \hat{V}}{\partial R_i}\right|_{t=t_1} \\ \vdots & \vdots \\ \left.\frac{\partial \hat{V}}{\partial C_i}\right|_{t=t_n} & \left.\frac{\partial \hat{V}}{\partial R_i}\right|_{t=t_n} \end{bmatrix} \tag{2-16}$$

Using the definition of Jacobian matrix J, the covariance matrix A is given by Eq. 2-17.

$$A = \begin{bmatrix} w\sum_{k=1}^{n}\left(\frac{\partial \hat{V}_k}{\partial C_i}\right)^2 & w\sum_{k=1}^{n}\left(\frac{\partial \hat{V}_k}{\partial C_i}\right)\left(\frac{\partial \hat{V}_k}{\partial R_i}\right) \\ w\sum_{k=1}^{n}\left(\frac{\partial \hat{V}_k}{\partial C_i}\right)\left(\frac{\partial \hat{V}_k}{\partial R_i}\right) & w\sum_{k=1}^{n}\left(\frac{\partial \hat{V}_k}{\partial R_i}\right)^2 \end{bmatrix}^{-1} \quad (2\text{-}17)$$

The confidence interval is calculated using these equations. The confidence level is set to 95% for the parameter estimation. The confidence range of parameter C_i is obtained about 0.414% to 1.327% of the estimated value. The confidence range of parameter R_i is also obtained about 1.082% to 2.825% of the estimated value. The results mean that the estimated parameters are reliable for use in parameter estimation. Therefore, the standards for the valuation are satisfied, and the estimated parameters are appropriate for use in practical applications.

2.3.2. Parameter map – lumped R_i and C_i

Trends for the lumped interfacial resistances R_i and electric double layer capacitor C_i are described in Fig. 2-6 to Fig. 2-9. According to Fig. 2-6 and Fig. 2-7, R_i abruptly changes with current change and has a wide gap between the charge and discharge modes. The value of R_i in the charge mode is larger than that in the discharge mode. Also, R_i decreased when the absolute current value increased, a trend that is similar to that observed in other research.[66] However, abrupt changes in intense low or high SOC regimes are not demonstrated in this model. Since the

sole purpose of the developed model is SOC estimation, and the battery is rarely operated in an extreme SOC regime, the R_i value in this regime does not have to be considered in this model and parameter estimation. The trend of C_i is the opposite of R_i, according to Fig. 2-8 and Fig. 2-9. The value of C_i is increased when the absolute current value is increased. Also, there is little difference between the charge and discharge mode.

2.3.3. Parameter map – lumped R_0

The trend of the lumped series resistance, R_0, is described in Fig. 2-10. R_0 is the ohmic resistance, which is nearly constant in isothermal conditions. It is the only temperature dependent value. A decrease in the R_0 is detected when the temperature increases. In addition, the gradient of the temperature curve decreases when the temperature increases. These phenomena are due to the deactivation of the activated layer in both electrodes. In extremely cold conditions, some freezing phenomena in electrode cells occurred, which results in a dramatic increase in the resistance of the electrode and electric double layer.

Some interesting behaviors are detected in the gradient at low temperature. First, the temperature increased by exothermic reactions in the cell electrodes. In an ambient environment, the temperature change is insufficient to change the R_0. However, at low temperatures, the R_0 is dramatically changed, especially below 273K, by small changes in temperature. The temperature of the cell increased about 0.824K for 80A discharging in 10s. At ambient conditions, the resistance increased by 0.173mΩ for a 0.824K temperature change. However, it increased by 1.97mΩ in

a low temperature environment. Under high current conditions, the temperature changes are enough to change the ohmic resistance. However, the temperature changes are small and the ohmic resistance is nearly constant in a low current regime. Therefore, differences between low and high current are significant due to the heat from the high current reaction. This implies that the estimated R_0 is dependent on current and temperature.

However, this observation disagrees with theoretical predictions. R_0, which is the ohmic resistance, is known to be a constant parameter under isothermal conditions. The low temperature compensation parameter, R_l, is suggested in Fig. 2-11 to avoid this contradiction. This parameter has a significant trend in that it is 0 under low current conditions. However, the parameter R_l increases in both the charge and discharge modes in high current conditions. R_l also increases as the temperature decreases. As a result, R_0 is independent of the current and only depends on the temperature shown in Fig. 2-10. When the parameter, R_l in Eq. 2-18 becomes a negative term, Eq. 2-12 is re-written as Eq. 2-18.

$$\begin{aligned}\hat{V}_k &= V_{0,k}(T) + i_k\left(R_0(T) - R_l\right) + \frac{1}{C_i} i_k \Delta t \\ &+ \left[\exp\left(-\frac{\Delta t}{R_i C_i}\right)\right]\left(\hat{V}_{k-1} - V_{0,k-1}(T) - i_{k-1}\left(R_0(T) - R_l\right)\right)\end{aligned} \tag{2-18}$$

Table 2-1. Procedure of the least square estimation method for parameter estimation

Step	Procedure
1	System data measurement from current pulse pattern experiment; current, voltage and temperature.
2	Voltage estimation by equivalent circuit model with initially estimated parameters.
3	Error calculation between estimated voltage and experimental measured voltage.
4	Summation of squared error for period of current pulse pattern experiment.
5	Minimization of sum square error using a nonlinear programming method.
6	Validation of estimated parameter by least square estimation method.
7	Determination of the battery model parameters.

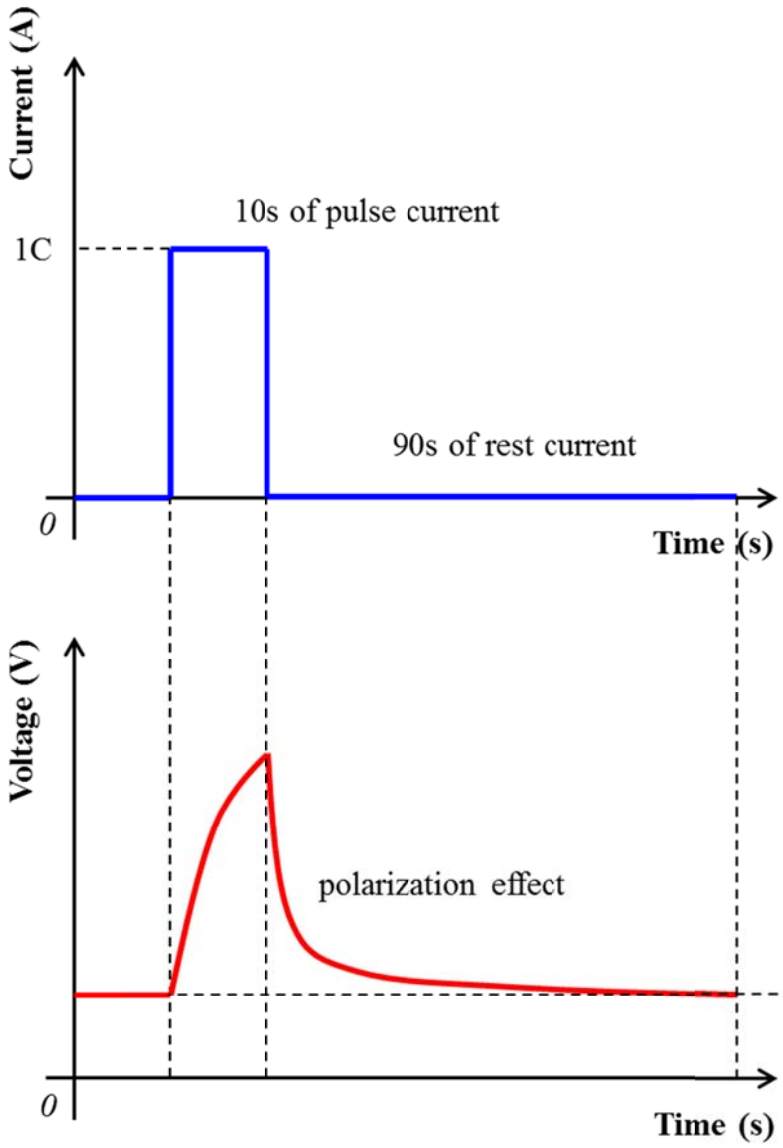

Figure 2-4. Current pulse pattern experiment for parameter estimation and polarization phenomena with the estimated voltage curve.

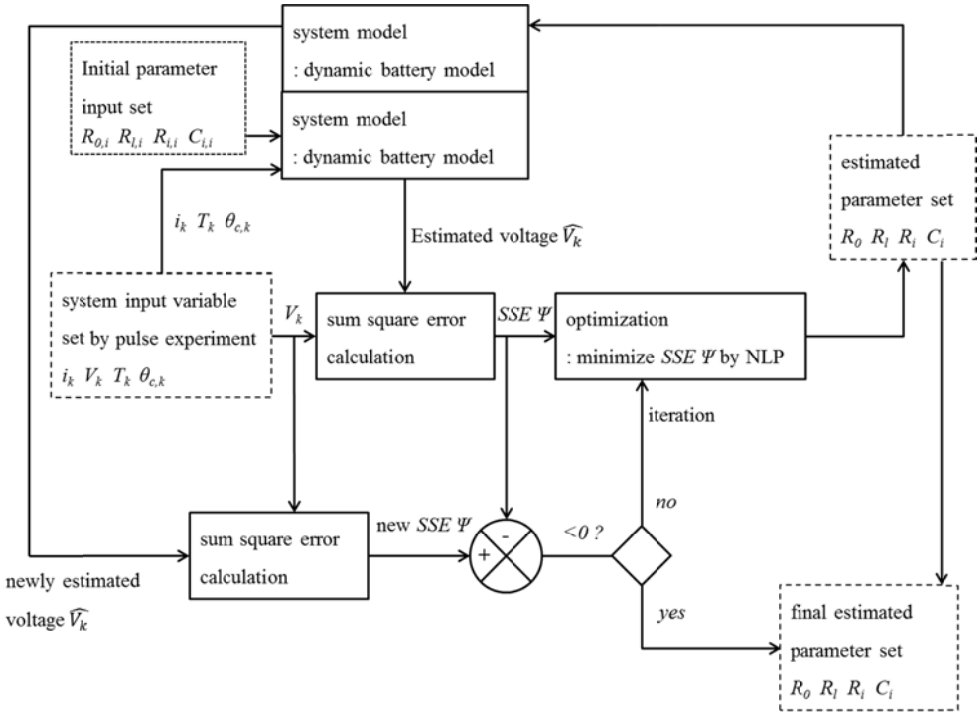

Figure 2-5. Least square estimation method for parameter estimation.

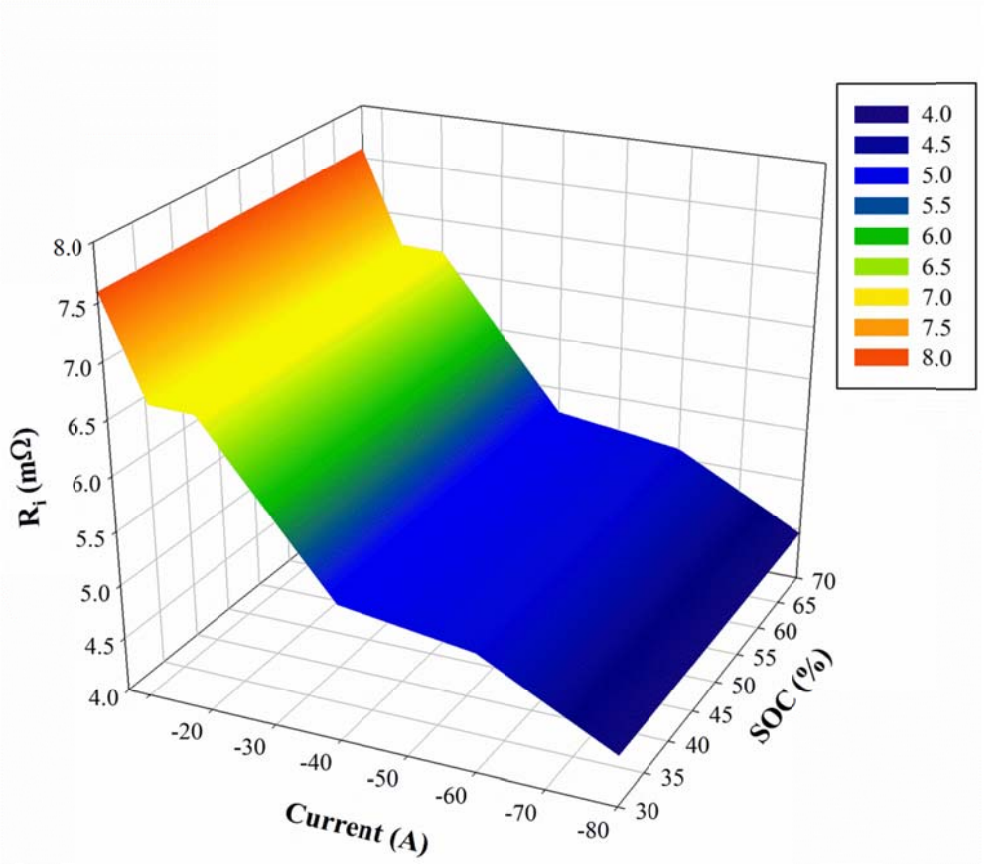

Figure 2-6. Trend of the lumped interfacial resistances R_i versus the current and SOC in discharge mode.

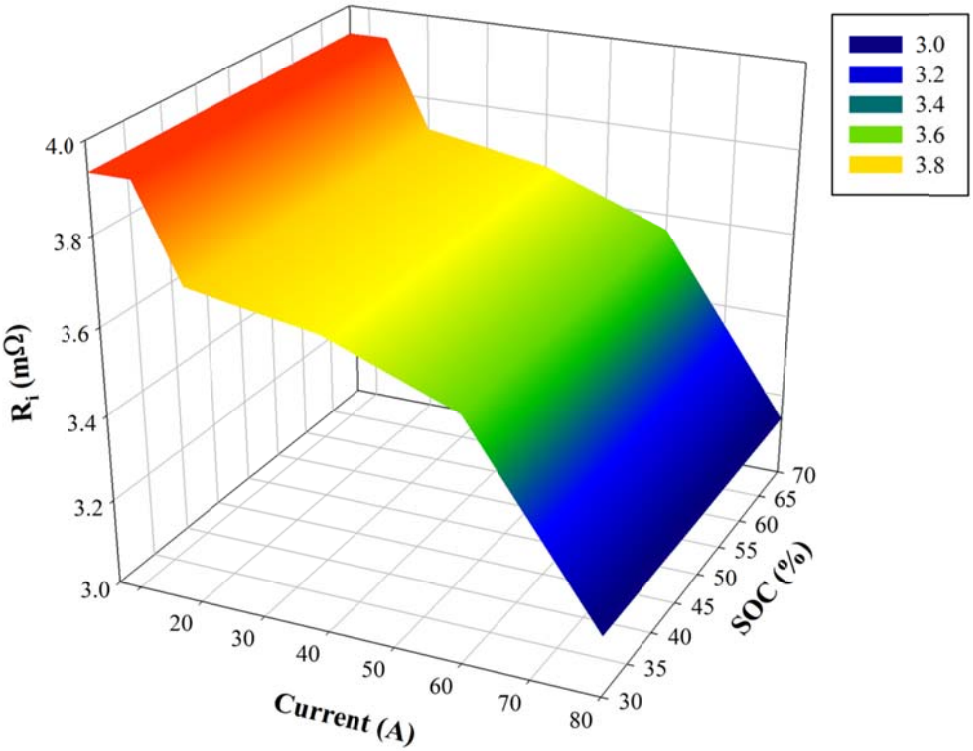

Figure 2-7. Trend of the lumped interfacial resistances R_i versus the current and SOC in charge mode.

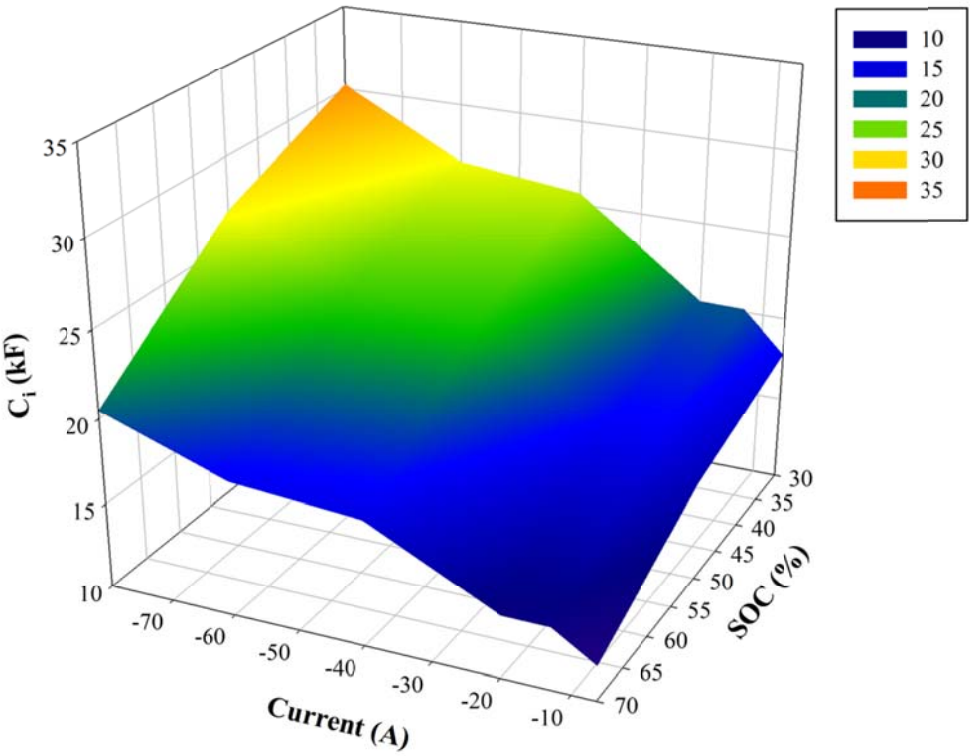

Figure 2-8. Trend of the electric double layer capacitor C_i versus the current and SOC in discharge mode.

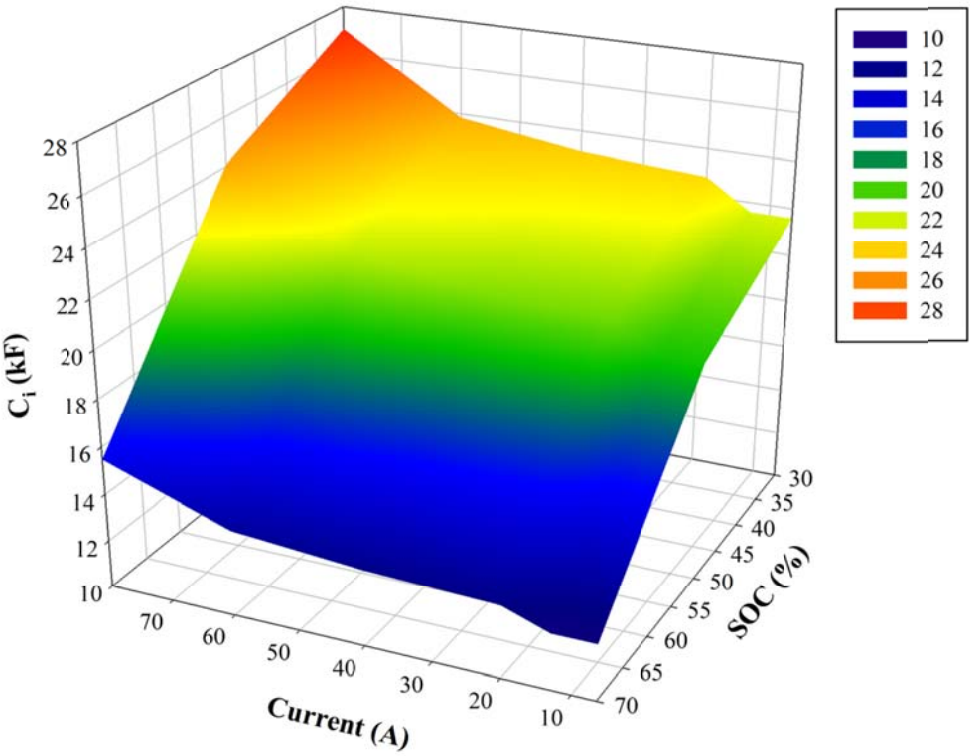

Figure 2-9. Trend of the electric double layer capacitor C_i versus the current and SOC in charge mode.

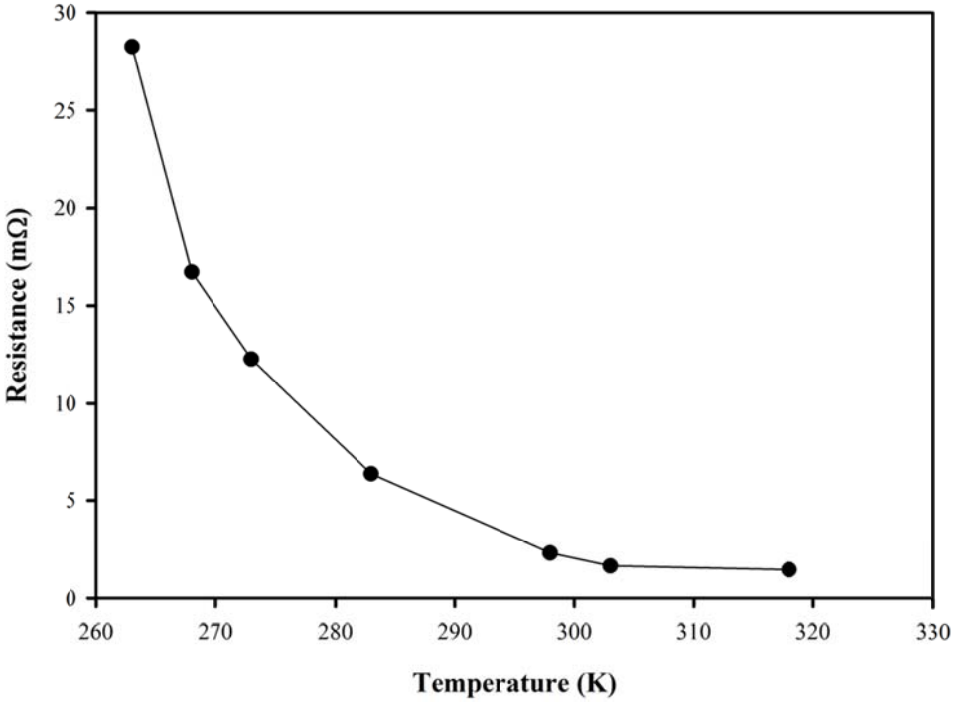

Figure 2-10. Ohmic resistance R_0 versus temperature.

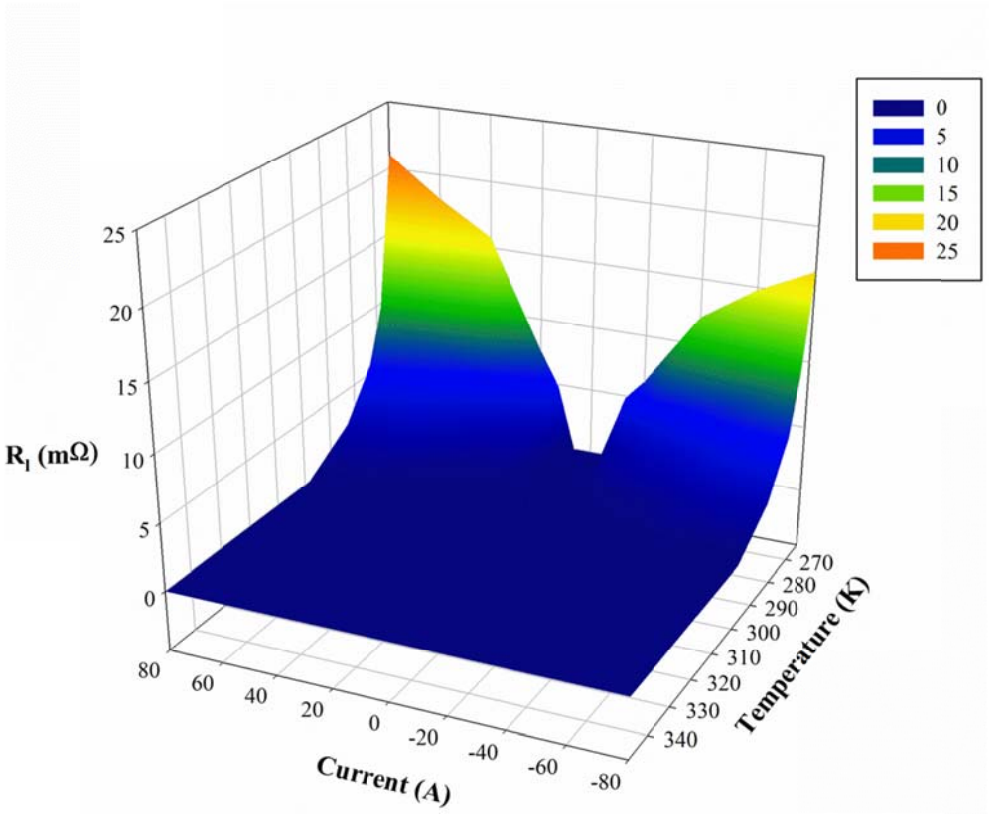

Figure 2-11. Low temperature compensation parameter R_l versus the temperature and current.

2.4. Methodology for State-of-Charge estimation

The SOC estimation was done using a recursive estimator, which is based on a combination of current integration and battery model based estimations: θ_i and θ_v, respectively.[77] These two SOC values are combined to the final estimated SOC value, θ_c. The methodology is related to the SOC based on the least-squares recursive identification techniques with a low pass filter and an adaptive filter for credibility. The equivalent circuit shown in Fig. 2-2 should be used to represent the main features of the lithium-ion battery system for OCV estimation by the voltage, current, and temperature data. The entire methodology of combining θ_i and θ_v is described on Fig. 2-12 and Table 2-2.[78]

The first step is data measurement. BMS data consist of current, voltage, and temperature values at 1s intervals. The data set is pre-processed by a low pass filter, and then, the θ_i is estimated using Coulomb counting. Next, current integration is done to estimate the θ_i, which is estimated from the current, i_k, and previously estimated SOC values, $\theta_{c,k-1}$, according to Eq. 2-19.

$$\theta_{i,k} = \theta_{c,k-1} + \frac{\Delta t}{Q_{0,\max}} i_k \tag{2-19}$$

The following step is the estimation of θ_v based on a battery model. In the second section, OCV was shown to be the nominal SOC-dependent voltage. Therefore, θ_v is estimated based on the value of the OCV and the measured temperature. Experimental data reflecting the relationship among the temperature, OCV, and SOC are shown in Fig. 2-3. From the data, the parameter maps are applied to the θ_v estimation.

$$\theta_{v,k} = \theta_{v,k}\left(V_{0,k}, T_k\right) = \theta_{v,k}\left(V_k, i_k, T_k\right) \quad (2\text{-}20)$$

The temperature is measured at the first step while OCV is not directly measured from the sensor; rather, it is estimated from the battery model. The ECM given in Eq. 2-18 requires some variables and parameters. Variables such as current, voltage, and temperature are measured in the first step, whereas the parameters in the model are estimated from the measured variables. Therefore, the degree of freedom is equal to zero, and the OCV is estimated from the battery model.

The final step is the final estimated SOC, θ_c, estimation. The current based SOC θ_i is a reliable value, but it is not reliable when an error occurs due to sensor fault in the battery system. Error accumulation becomes huge, and θ_i is not estimated accurately. On the other hand, the value of θ_v is an absolute value, but it is inaccurate at high current and dynamic states. Thus, θ_v is adequate for most battery rest states such as low current operations. The combinatorial methodology is based on the characteristics of the two SOC values. θ_i is used at most operating conditions, and in these cases, θ_i is selected as the final estimated SOC. However, θ_v is introduced during the rest state to eliminate the accumulated error. The main criteria for the definition of the rest state are the absolute current value and the duration of the low current: *a* and *d*. Furthermore, the battery is operated at an absolute value of a – from -aA to aA – and this state is continued for ds, until the state of the battery breaks into the rest state. In this state, θ_v is selected as the final estimated SOC, θ_c.

Table 2-2. Procedure of the SOC estimation methodology

Step	Procedure
1	Data measurement from BMS at 1s intervals; current, voltage, temperature and previously estimated SOC value.
2	Low pass filtering
3	θ_i estimation by Coulomb counting
4	θ_v estimation based on a battery model
5	θ_c estimation with combination of θ_i and θ_v

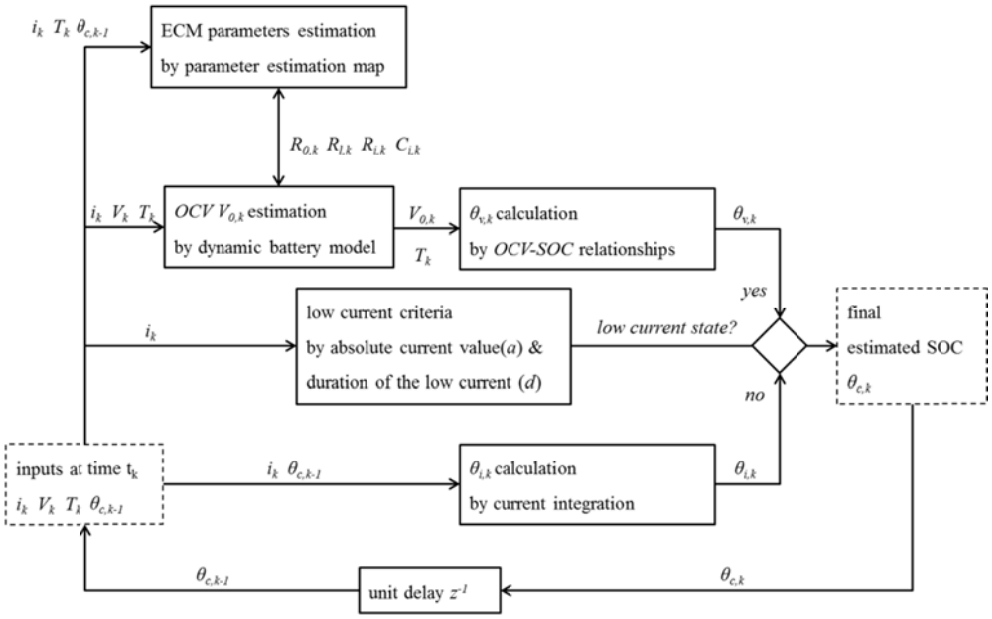

Figure 2-12. Schematic overview of the estimation methodology procedure.

2.5. Results and analysis

2.5.1. Dynamic battery modeling

The dynamic battery model is described as an ECM with parameter estimation using SSE minimization. The model was demonstrated with experimental data from different cycle patterns using various temperatures and SOC conditions. Cycle types were light duty in an urban driving schedule mode and heavy duty in a highway driving schedule mode. Temperature conditions were varied from ambient to high and low and fluctuating temperatures. Model input variables were the current and the temperatures, which were inputted as a time series in the experiment. The output variable was voltage, which was compared to real measured voltages from the experiment. The parameters in the model were updated with changes in the battery conditions, e.g., current, temperature, and SOC.

Validation of the battery model and parameter estimation for ambient conditions at 298K is described in Fig. 2-13 and Fig. 2-14. Fig. 2-13 is for the light duty mode for the urban driving pattern. Power demand from the battery was stable; thus, the current behavior was stable. The average absolute value of error was 3.220mV with 0.083% accuracy. Fig. 2-14 is for the heavy duty mode for the highway driving pattern, where the power from the battery was large and pitching; thus, the current behavior was rapidly changing. In this case, the average absolute value of error was 6.501mV with 0.167% accuracy. Both of the validation results are accurate since the average error was below 0.5%. This implies that the battery model is robust for ambient conditions, regardless of the current patterns.

Validation for high and low temperature operations is described in Fig. 2-15 and

Fig. 2-16. Operation at a high temperature condition of 313K was done in light duty mode, in Fig. 2-15. The average absolute value of the error was 2.910mV with 0.075% accuracy. This accuracy is similar to the ambient condition results. Operation at a low temperature of 263K was done in a light duty mode, in Fig. 2-16. In this case, the average absolute value of error was 16.35mV with 0.419% accuracy. The error was larger than the ambient or high temperature conditions. However, the accuracy is still sufficient for the application of the model where the average error was below 0.5%.

As previously described, this model is adequate for fixed temperature conditions. Thus, validation with fluctuating temperatures was done in Fig. 2-17 and Fig. 2-18. Operation of the battery was done from 263K to 298K in a light duty mode at Fig. 2-17. Here, the average absolute value of error was 6.916mV with 0.177% accuracy. The maximum value of the absolute error was below 20mV with 0.513%. In this case, the accuracy of the model increased as the temperature increased.

2.5.2. State-of-Charge estimation methodology

A validation study of the suggested SOC estimation methodology in ambient conditions was conducted. The driving schedules were varied from light duty to extremely heavy duty. The urban driving schedule represented light duty, and the highway schedule represented heavy duty. The SOC estimation results for each driving schedule are described in Fig. 2-19 and Fig. 2-20. θ_i represents the final SOC in most cases, except for when θ_v was substituted for the final SOC in the rest state. θ_v was estimated accurately due to the developed battery model with the parameter estimation method described above. Thus, the estimation error increased

when the power duty was intensified with heavy fluctuations in the current with not much of a rest state. However, the errors under ambient conditions were very low, such that the suggested methodology is sufficiently accurate to apply to ambient battery systems.

A validation study of the suggested methodology was conducted under harsh conditions such as low temperatures. The developed methodology was applied to an urban driving schedule in high and low temperature conditions: 318K and 263K, respectively. The SOC estimation results for each temperature condition are described in Fig. 2-21 and Fig. 2-22. In high temperature conditions, the accuracy was higher than under ambient conditions. However, the accuracy in low temperature conditions was lower than in any other conditions. These results are due to the developed battery model, in which accuracy at high temperatures is greater than for the other conditions, and the accuracy is poor at low temperature conditions. The dynamic battery model affects the estimation of the θ_v. Thus, the accuracy of the estimation methodology is dependent on temperature. However, errors for various conditions are low enough that the methodology is sufficiently accurate to apply to harsh condition systems.

The reliability against transient errors in sensor measured data of the suggested SOC estimation methodology was demonstrated according to current sensor fault. Here, the experimental condition was chosen as an urban driving schedule with ambient conditions, and a 40% to 60% SOC range. A current sensor fault was assumed and the inaccurate data from the malfunctioned sensors were classified into two types: fixed offset and unknown random disturbances. The fixed offset data were obtained by the sum of the normally measured current data and 1A.

Apparently, error accumulation in θ_i was expected due to the current integration. However, the SOC estimation result is so that the accuracy is sufficiently low to apply to real systems. According to Fig. 2-23, the average value of the SOC error was -1.415%, and the maximum value of the error was -2.343%. In the methodology, θ_v, the absolute estimated value, is selected during the rest state for the elimination of error accumulation. The final SOC was estimated accurately by the θ_v compensation.

Unknown random disturbance data included the sum of the measured data and random white noise. The random white noise was a zero mean Gaussian random variable.[79] The SOC estimation result is such that the average value of the SOC error was -0.315% and the maximum value of the error was -1.343%, according to Fig. 2-24. The accuracy of the methodology is ensured by θ_v compensation. The results of the validation with the current sensor fault are that the suggested SOC estimation methodology has sufficient reliability against transient errors in sensor measured data for application to practical systems.

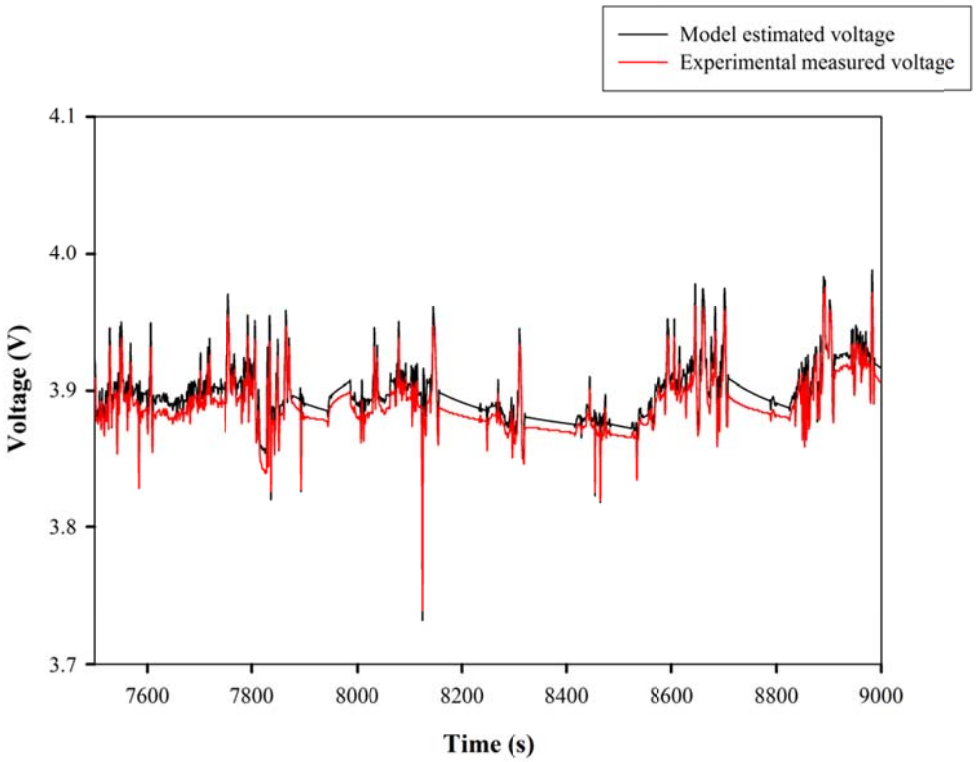

Figure 2-13. Validation of the battery model and parameter estimation for ambient conditions at 298K for 25min; simulation result for the urban driving pattern: model and real voltage.

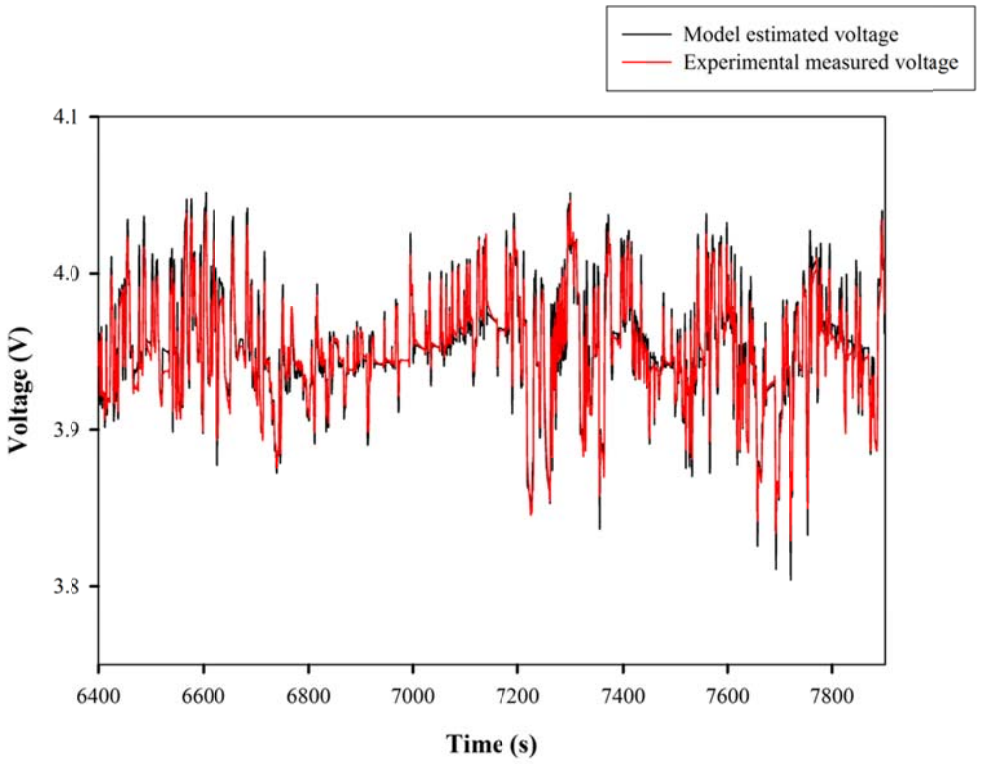

Figure 2-14. Validation of the battery model and parameter estimation for ambient conditions at 298K for 25min; simulation result for the highway driving pattern: model and real voltage.

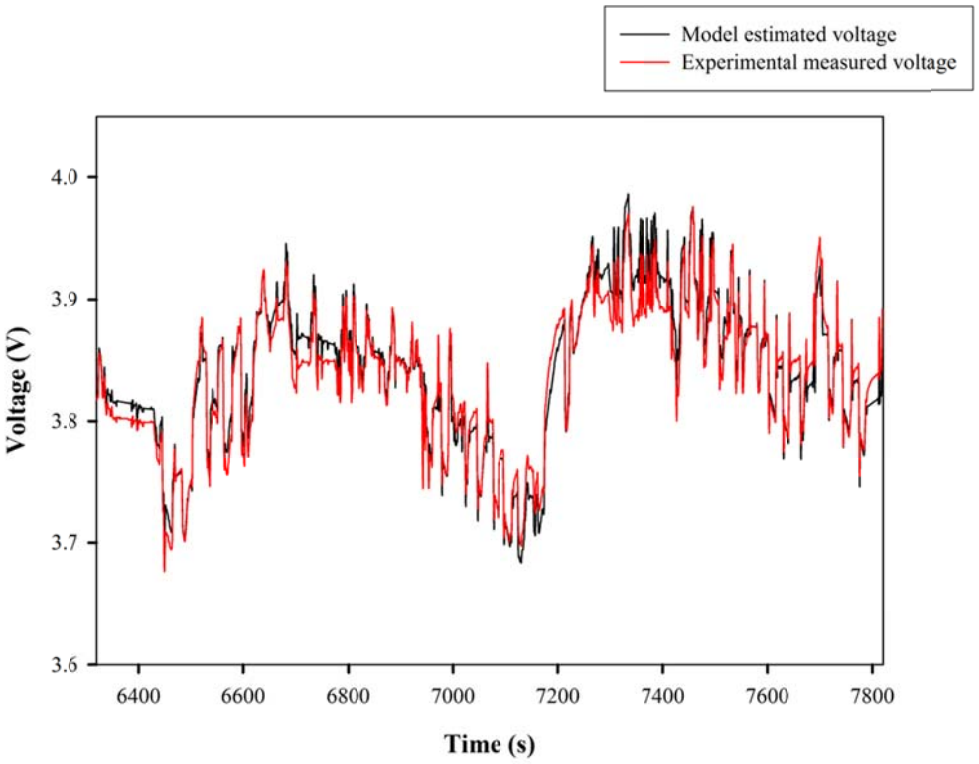

Figure 2-15. Validation of the battery model and parameter estimation for high temperature operations of 313K with urban driving pattern for 25min: model and real voltage.

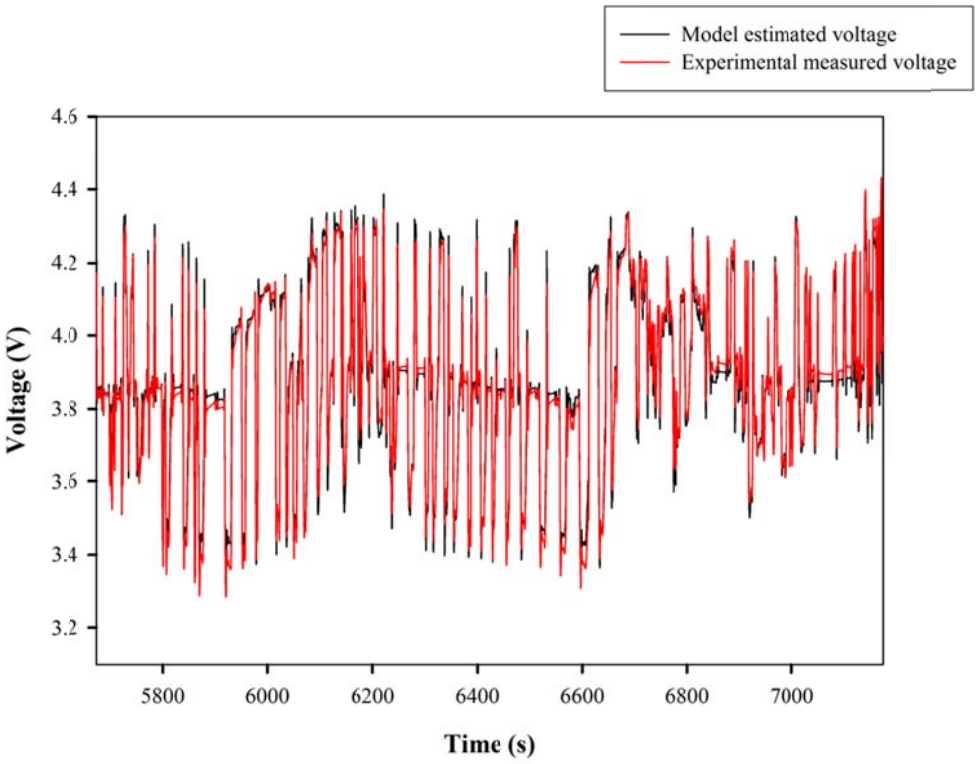

Figure 2-16. Validation of the battery model and parameter estimation for low temperature operations of 263K with urban driving pattern for 25min: model and real voltage.

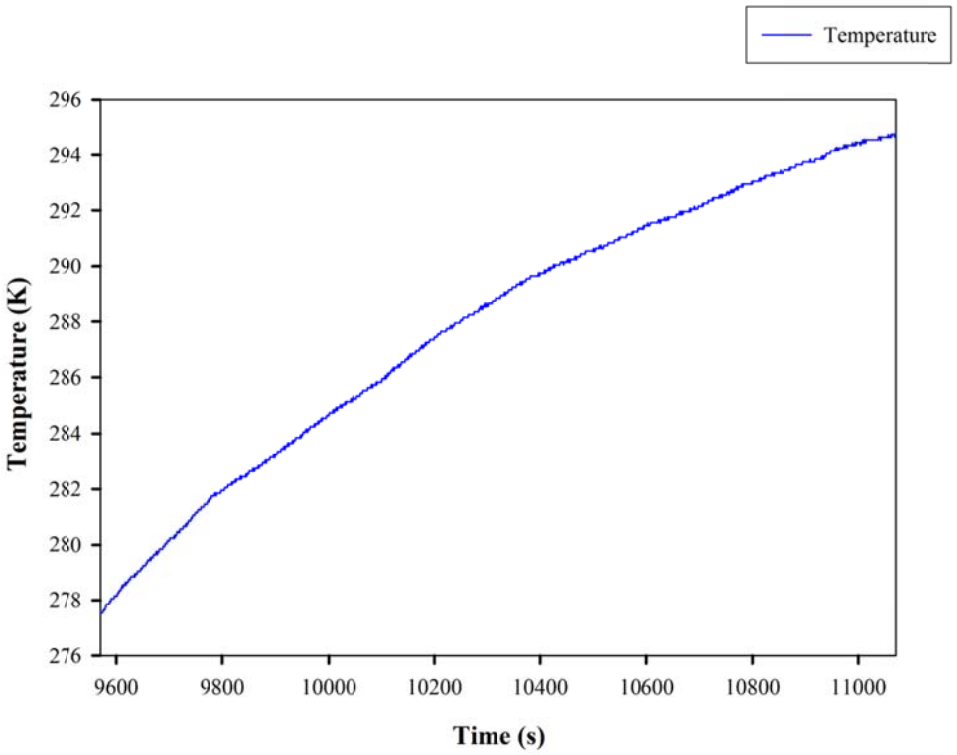

Figure 2-17. Fluctuating temperature operations from 277K to 294K with an urban driving pattern for 25min.

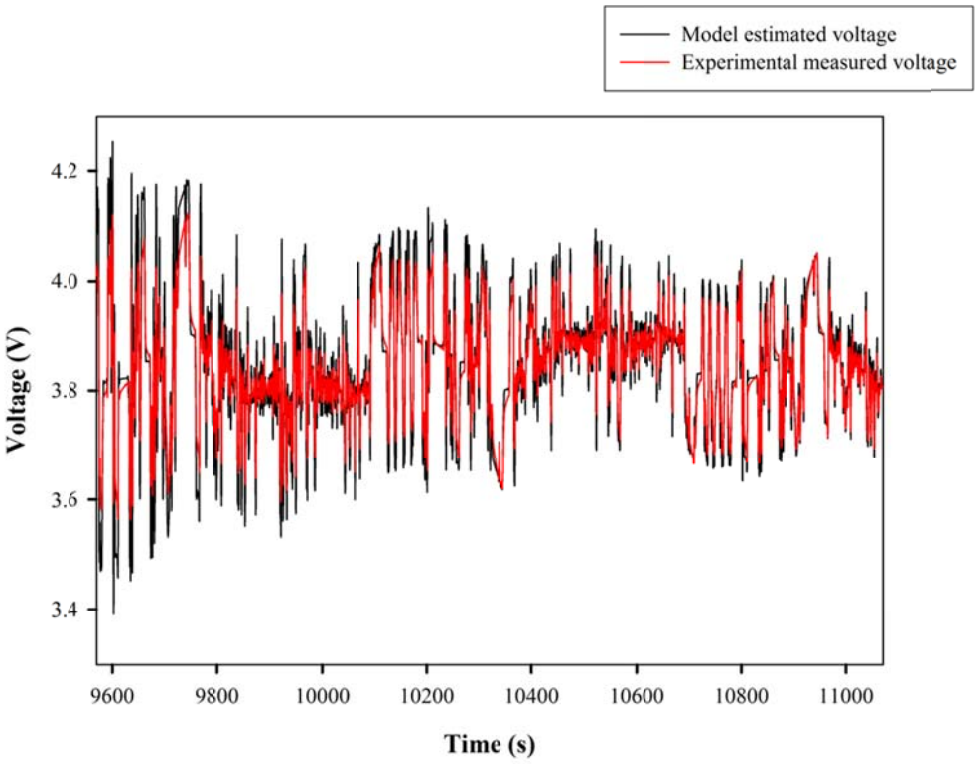

Figure 2-18. Validation of the battery model and parameter estimation with fluctuating temperature operations from 277K to 294K with an urban driving pattern for 25 min: model and real voltage.

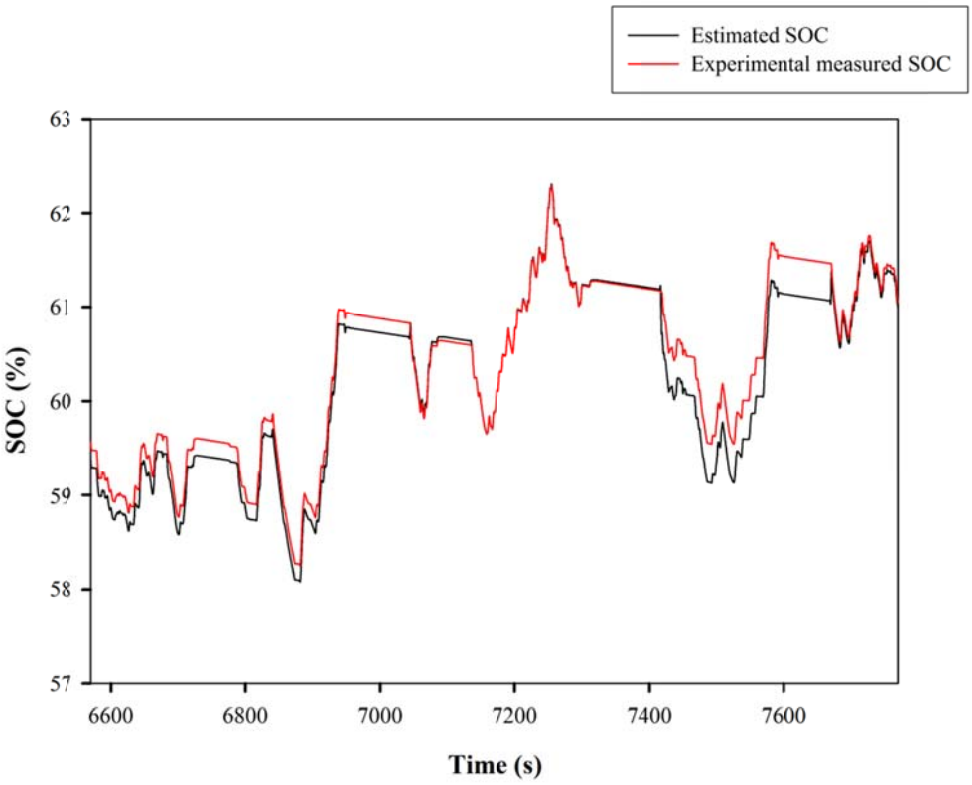

Figure 2-19. Validation of the SOC estimation methodology for ambient conditions at 298 K for an urban driving pattern of 20min.

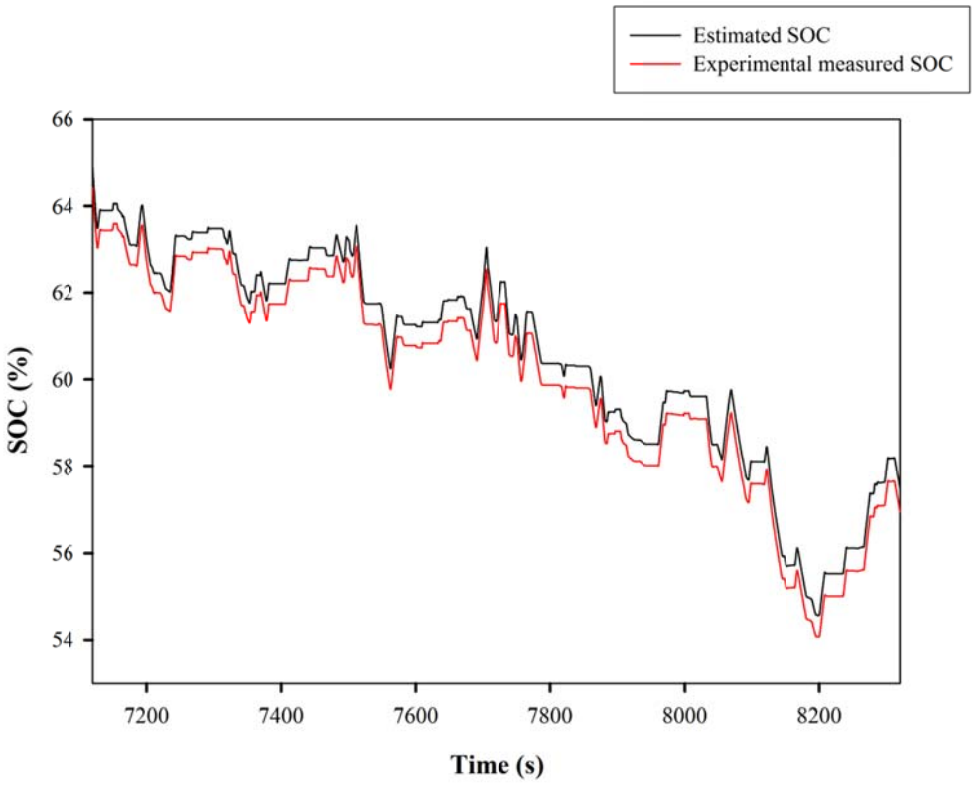

Figure 2-20. Validation of the SOC estimation methodology for ambient conditions at 298 K for a highway driving pattern of 20min.

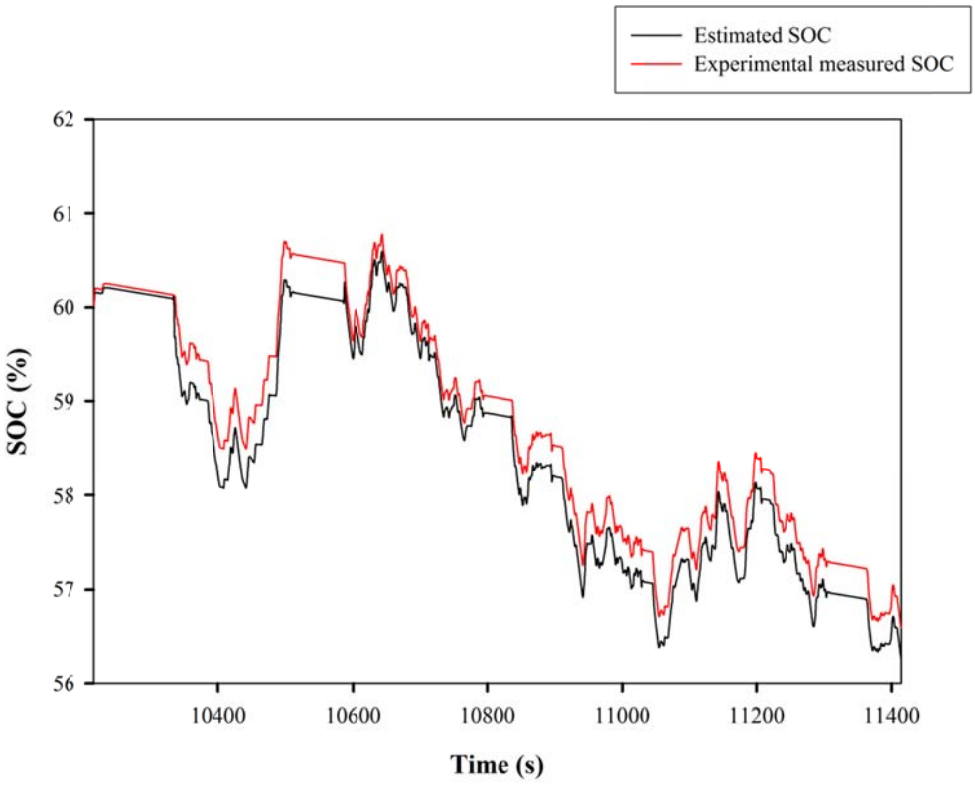

Figure 2-21. Validation of the SOC estimation methodology for high temperature operations of 313K with an urban driving pattern for 20 min.

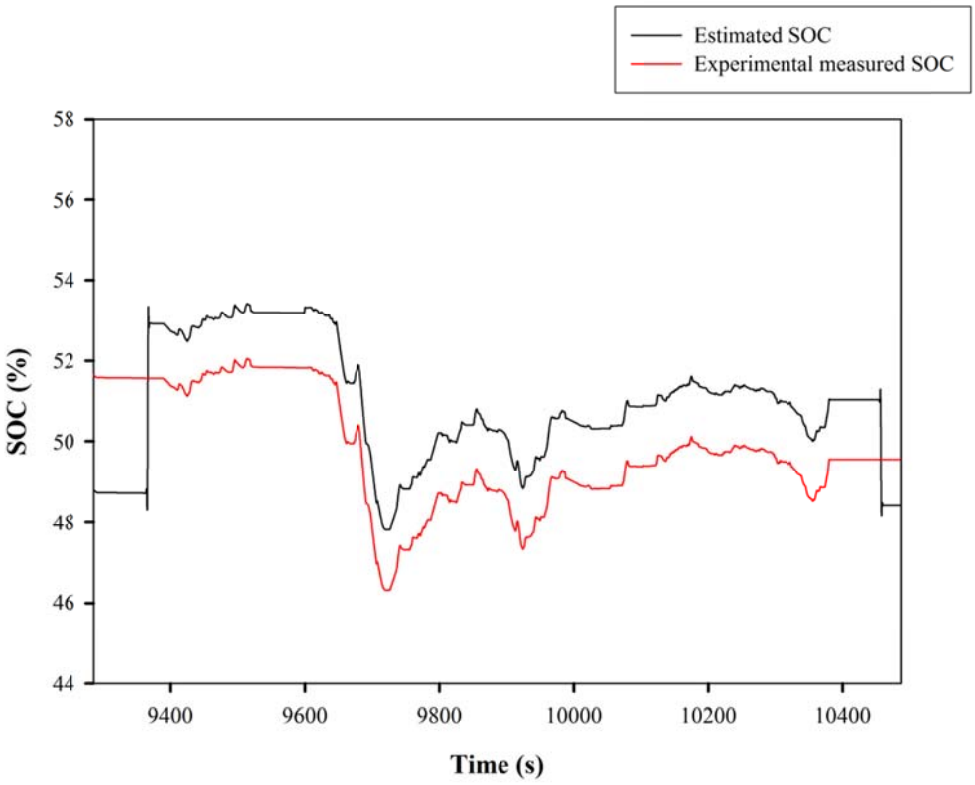

Figure 2-22. Validation of the SOC estimation methodology for low temperature operations of 268K with an urban driving pattern for 20 min.

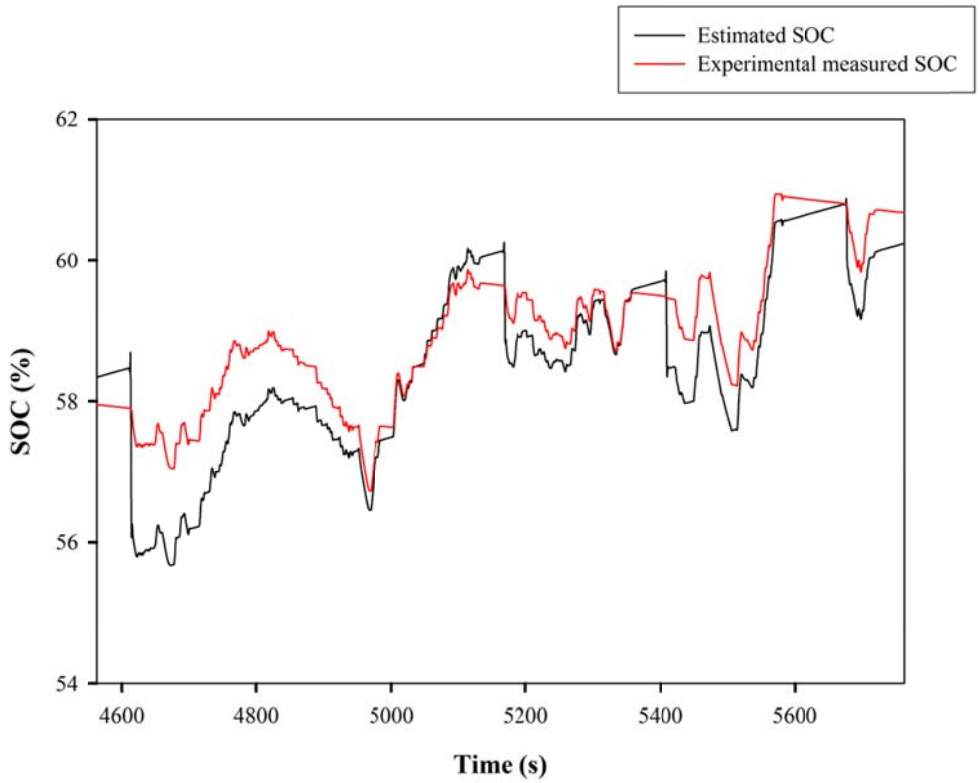

Figure 2-23. Validation of the reliability against sensor error of the SOC estimation methodology according versus current sensor fault with fixed offset for urban driving pattern at 298 K for 20 min.

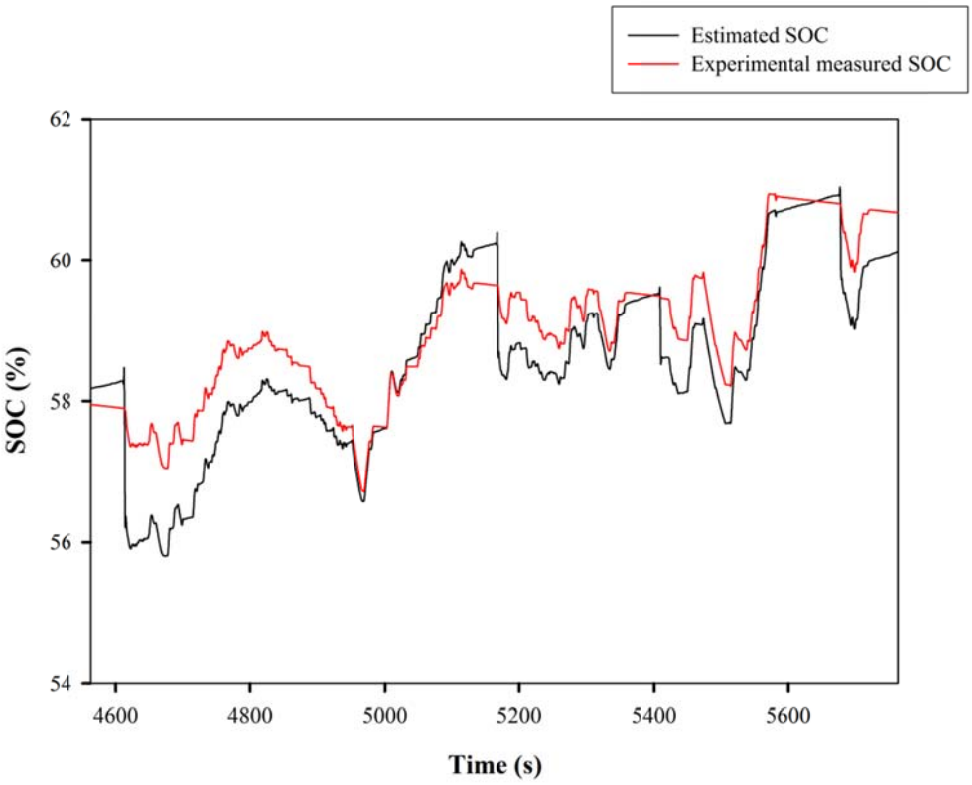

Figure 2-24. Validation of the reliability against sensor error of the SOC estimation methodology according versus current sensor fault with random disturbance for urban driving pattern at 298 K for 20 min.

2.6. Conclusions

This chapter describes the dynamic battery model and the SOC estimation methodology for lithium-ion batteries. The model and the methodology were developed for applications under various conditions: fluctuating currents, SOC ranges, and temperatures. The battery model originally suggested by Verbrugge is enhanced and refined by the parameter estimation. The conventional methodologies of the process systems engineering are successfully applied to lithium-ion battery applications. Especially, the parameter estimation method based on a parameter map with error minimization from experimental data is effectively applied for the battery model. The SOC estimation methodology is a combination of the current integration and model based estimation for θ_i and θ_v. Both of the SOCs are combined and their shortcomings are overcome using our developed battery model. Case studies of various conditions were demonstrated for current fluctuations, temperature changes and sensor faults. We applied our methodology for the estimation of SOC under various conditions successfully with good accuracy and reliability against transient errors in the sensor measured data. The developed model and methodology are expected to be valuable in lithium-ion battery applications such as BMS in hybrid electric vehicles or plug-in hybrid electric vehicles. Furthermore, suggested battery dynamic model and SOC estimation methodology are applied to SOH estimation methodologies in Chapter 3 and optimal control of FCHEV in Chapter 4.

CHAPTER 3 : State-of-Health Estimation[†]

3.1. Introduction

Performance of the lithium-ion batteries deteriorates over time. State-of-health (SOH) is the main parameter used to express the performance state. For example, SOH is defined as the ratio of the capacity of the aged battery to the capacity of the fresh battery.[81] In other cases, SOH is defined using power instead of capacity. If the SOH value drops below 80%, the battery is typically predicted to reach its end-of-life (EOL) and needs to be.[82] Therefore, estimation of the SOH as capacity and power fading is an important issue to measure the actual battery performance, to determine the EOL, and to predict the precise time to change the battery. The on-line estimation of actual battery performance is especially highlighted in real world applications of eco-friendly vehicles.[32-33]

Given the importance of the performance estimation for a battery system in eco-friendly vehicles, some researchers have developed an estimation methodology for capacity and power fading. The measured variables in the monitoring system of BMS are voltage, current, and temperature.[67] However, the target variables for the estimations are the capacity and power of the cell. Thus, direct measurement of the performance with a BMS sensor was a difficult problem. Therefore, researchers have been focused on estimating the performance using a battery model instead of direct measurements. However, these researches have some limitations such as destructive techniques and optimized techniques to specific scenarios.

[†] The partial part of this chapter is taken from the author's published paper in journal.[80]

In this chapter, capacity and power estimation methodologies are suggested for on-line estimation of actual battery performance. A soft sensor methodology based on system identification was developed to estimate the capacity and power fading more accurately and robustly. A dynamic battery model was applied to the soft sensor method.[83] In addition, a simplified methodology based on the simulation assumption was developed to estimate capacity and power fading more quickly.[84] Moreover, the two algorithms were combined to complement each other, to compensate for each other's faults and finally, to form a hybridized algorithm. These methodologies were demonstrated under various levels of SOH with various types of batteries.

3.2. Research background

3.2.1. State-of-Health estimation techniques

Some researchers have developed the SOH estimation methodology for last decade. Two major estimation methodologies have been suggested: the empirical method and semi-empirical method. The empirical method has put emphasis on impedance experiments based on electrochemistry and instrumental analysis.[85-87] These studies have resulted in highly accurate measurements of the capacity but been based on invasive and destructive techniques. The battery had to be disassembled from the vehicle for the impedance experiments. Therefore, this method has focused on the development and validation of new materials for electrodes and electrolytes in batteries and on further studies for the estimation of capacity and power fading. The results from previous works have been used in the semi-empirical method.

The semi-empirical method has put emphasis on the empirical model based on the first principle model and experimental data.[88-92] The cycle and calendar life curve are deducted from the model and experimental data.[93-97] These semi-empirical models have been developed under tightly controlled conditions. Therefore, the developed model only matches to the corresponding cycles, which is not applicable to the real world. As a result, when the model is confronted with an unexpected cycle or unknown disturbance and/or phenomenon in real world application, the estimated and actual performance value diverge from each other.

Therefore, some researches have suggested the compensative model as a semi-empirical model for application to the real world.[98] Real life scenarios, which intensify capacity and power fading, were applied to the compensative model with

updated weighting parameters. However, the mechanism for the cause and effect relationship on capacity fading is not sufficiently clear for real world applications. Therefore, a model that considers undefined phenomena and unexpected disturbances is urgently necessary in eco-friendly vehicle applications. A reclusive model such as Kalman filter and digital filtering in other studies has been investigated for use in on-line estimation of actual battery performance.[42-43, 99-104] However, the recursive algorithms had to update the sample data and were inadequate for the on-line estimation of capacity and power fading.

3.2.2. Research objectives

An estimation methodology for capacity and power fading with on-line estimation is necessary to measure the actual battery performance. This methodology would have some qualifying conditions. It would have to be a non-invasive, non-destructive technique for on-line estimation under various conditions of battery operations. Therefore, a model-based estimation method using a reduced electrochemical cell model was developed for such purposes.[105-107] The soft sensor methodology based on system identification was the representative methodology to consider undefined phenomena and unexpected disturbances.[71, 108] The unknown variables such as capacity and power could be estimated by known variables and appropriate models. A general model to explain dynamic behavior was necessary for this methodology. Nevertheless, this methodology had a limitation regarding its computational load. A simple methodology is necessary for on-line estimation. Therefore, a compensation methodology with a reduced computational load is necessary for the purpose of this chapter.

Capacity and power fading estimation algorithms were developed to measure the slow phenomenon of capacity and power deterioration accurately. These algorithms were proposed for the application to on-line estimation. Therefore, the on-line estimation algorithm with soft sensor technique, hereafter referred to as the principal algorithm, was applied to the experimental system during each cycle. Moreover, the principal algorithm has a heavy computational load due to optimization calculation. Therefore, a simplified estimation algorithm, hereafter referred to as the supplementary algorithm, was applied to the same system. Finally, the principal and the supplementary algorithm were combined to complement each other and form a hybridized algorithm.

3.2.3. Experiments

Lithium ion batteries for HEVs and PHEVs applications were used to collect the measured data over multiple cycles. The batteries for the HEVs were rated at 6.5Ah, and the batteries for the PHEVs were rated at 15.5Ah. Moreover, various levels of capacity and power-faded lithium-ion batteries, from the 100% level of SOH to the 75% level of SOH, were used in the experimental system. The experimental cycle included three patterns: two constant charging and discharging patterns and one driving pattern. The constant charging and discharging pattern was as follows: the batteries were discharged at a rate of -1C for 25 minutes, and then charged at a rate of 1C for 30 minutes, and the current dropped to 0A for 30 minutes. After the constant charging and discharging pattern, the driving pattern was as follows: the supplemental FTP driving schedule was applied for 1 hour, and then, the current dropped to 0A for 30 minutes for rest of the battery system[53].

After the driving pattern, the constant charging and discharging pattern as aforementioned was applied again. These three cycles were included in one cycle. Moreover, the PHEV application had repeated charging patterns for several hours with a sinusoidal input pattern. The charging patterns were considered as the experimental cycles. The data set was collected from the experimental system in 1s interval. The measured data from experimental system was used to validate the developed estimation algorithms for capacity and power fading.

3.3. Principal algorithm

3.3.1. Model description

The principal algorithm for the estimation of capacity fading is based on the soft sensor technique. This technique is based on the system identification methodology. This methodology is suggested for the estimation of unknown system variables in a dynamic system.[100, 108] The mathematical models for a dynamic system are built based on measured data for modeling, simulation, parameter estimation and system state identification.

The system identification loop is suggested to construct model from observed data in Fig. 3-1. The methodology to determine a model parameter of a dynamical system from observed input-output data involves three ingredients: the input-output data, candidates for the dynamic model structure and a criterion to select a particular model from among the set based on the information in the data. The experiments are designed with prior knowledge and input-output data from the process to be identified are collected. The input-output data is examined to remove trends and outliers, and select useful portions of the original data with filtering to enhance important frequency ranges. The model is selected and defined for objectives. The off-white model which contains parameters that have unknown or uncertain numerical values are selected for SOH estimation. After the selection of the model, differences between the observed output data and calculated data from the model, referred to as the error, is then calculated. The error is adjusted by the unknown system variables. The specific values with minimum error estimation are determined for the unknown system variables as parameters. Optimization

techniques to minimize each error are applied in the system identification technique.

It is necessary to define the model for the principal algorithm, which uses the soft sensor technique. A battery cell model is classified for the first principle model as the white model, the ECM as the off-white model, and the statistical model as the black box model. The off-white model is appropriate for the estimation of unknown system variables. Due to a low level of complexity and a high level of accuracy, the ECM is adequate for an on-line monitoring system in BMS. Therefore, ECM was selected as the dynamic model for the estimation of capacity fading as the off-white model.

Some researchers have developed various types of ECMs with different properties and objectives. A general ECM has a single resistance and one ladder for the resistance and capacitance in Fig. 2-2. The general ECM is appropriate for the dynamic cell model to investigate short-term phenomena.[109] However, the purpose of our model is to estimate the SOH with capacity and power fading. The time order of the capacity and power fading mechanism is 10^6s.[95] Since the time order of the polarization is 10^{-1}s to 1s, the deviation of the polarization effect is neglected in this study. Therefore, the target ECM model substitutes a single resistance for the ohmic resistance and the RC ladder. The simplified ECM with only a single resistance was selected in this study shown in Fig. 3-2. Calculations for the equivalent circuit model were done according to Eq. 3-1.

$$\hat{V}_k = V_{0,k} + i_k R_t \tag{3-1}$$

The current i is set to positive terms at charging and during negative terms at

discharging. The V_0 in the model is the nominal open circuit voltage. As aforementioned, the open circuit voltage is dependent on the SOC and temperature. Therefore, the OCV is calculated as a function of the SOC and temperature shown in Eq. 3-2.

$$V_{0,k} = \alpha_0(T)_k + \alpha_1(T_k)\theta_k + \alpha_2(T_k)\theta_k^2 + \alpha_3(T_k)\theta_k^3 + \alpha_4(T_k)\theta_k^4 \tag{3-2}$$

The SOC is estimated by Coulomb counting, which is the calculation of the current integration shown in Eq. 3-3.

$$\theta_k = \theta_0 + \frac{100}{3600Q}\int i_k dt = \theta_0 + \frac{1}{36Q}\sum_k i_k \tag{3-3}$$

In these model equations, the input variable is the current and the output variable is the cell voltage. The capacity, Q, in Eq. 3-3 and the total resistance, R_t, in Eq. 3-1 are defined as the model parameters. Using the least squared parameter estimation method for the soft sensor technique, Q and R_t are determined with each experimental set. The degraded Q estimation explains the capacity fading and the increased R_t estimation explains the power fading. The battery model was simulated in MATLAB® and SIMULINK® environments for implementation.

3.3.2. Soft sensor estimation methodology

The parameter estimation using the least squared error method was used to determine the capacity fading and power fading. For the parameter estimation, the observed input-output data were specified. In this case, 200 data sets at 1s intervals were selected as the observed variables. As mentioned above, the input variables

were the current and temperature. The output variables were the voltage, and the error was defined as the difference between the measured voltage data and the calculated data from the ECM. The parameters that were the unknown system variables, which should be determined by the estimation algorithms, were the capacity and resistance. The error was passed to optimization routine to determine the optimized parameter values for the target cycle.

The optimization objective function consisted of the error calculation term and variance inhibiting term shown in Eq. 3-4.

$$\Phi(Q_j, R_{t,j}) = \sum_k (\hat{V}_k - V_k)^2 + \left[w_Q (Q_j - Q_{j-1})^2 + w_R (R_{t,j} - R_{t,j-1})^2 \right] \tag{3-4}$$

The error calculation term, in the first part of the equation, serves as an error minimization role for the battery model. The error minimization method in this algorithm was the SSE. In previous research, the mean-squared error (MSE) was used to estimate capacity fading. Due to the time difference term, MSE is more nonlinear than SSE. When the sample data set is not fixed, MSE is more appropriate for an accurate optimization. However, the sample data set length was fixed at 200 for every sample data. Therefore, SSE is adequate in this case.

The variance inhibiting term, in the second part of the equation, serves the role of preventing the rapid deviation of the parameters between estimation runs. This term is based on a moving horizon-based approach.[75, 100, 110-111] The capacity and power are slow decreasing variables in a battery system. As previously mentioned, the time order of the capacity and power fading mechanism is 10^6s. However, the capacity and power estimation is done every day at about 10^4s. Moreover, the

capacity and power decreases as slow drifts enough such that the performance values remain a constant value during a single run of the estimation. Therefore, the inhibition of variable variance term to prevent rapid change is required in the capacity and power fading algorithm. In the variance inhibiting term, differences between the present parameters estimated in this run and the previous parameters estimated in the last run are needed.

The sum squared differences are minimized with weighting factors, w_Q and w_R. The weighting factors are adjustable parameters using the standard deviation of the current during the 200 data set. If the weighting factor is large, the variance inhibiting term is more important than the error calculation term. It means that the parameters are estimated conservatively although there is a large deviation in the current. If the standard deviation is larger than 1.5, the current pattern is recognized as the driving pattern. Therefore, the weighting factors are set to large values. The weighting factors are set to small values in the case in which the reverse is occurred. In this case, the current pattern is recognized as the rest pattern.

The weighting factors are also adjustable parameters based on the measurement conditions. If the weighting factors are large, the deviation between the target parameters dwindles. Therefore, larger weighting factors are adequate for the difficult conditions of capacity and power fading such as room temperature conditions, short-term run for measuring the capacity and power, and the battery system at rest conditions. However, smaller weighting factors are more appropriate to the prone conditions of capacity and power fading such as high or low temperature conditions, long-term run for measuring the capacity and the power, and the battery system at overcharge conditions. Therefore, the weighting factors

are a function of the standard deviation of the current, temperature, time interval between estimation runs, and any events of intensified capacity and power fading.

The unconstrained optimization routine is solved by the nonlinear programming technique. The optimization algorithm known as an *lsqnonlin* is provided by MATLAB®. This algorithm is based on interior-reflective Newton methods for nonlinear programming and interior trust region approach for nonlinear programming.

Based on the model and optimization algorithm mentioned above, the principal algorithm to estimate capacity and power fading was developed for application to the HEV and PHEV.[83] The principal algorithm has three steps, described in Fig. 3-3 and Table 3-1. The first step of the principal algorithm is to measure the voltage, current, and temperature data. The 200 data set is collected from the battery management system at 1s intervals. The selection of weighting factors in the variance inhibiting term is the second step. The selection is based on the standard deviation of the current data set, temperature history of the operating battery, time interval between estimation runs, and any events of intensified capacity and power fading. The third step is calculating the capacity and power with the soft sensor technique using the simplified ECM and parameter estimation method based on nonlinear programming. The capacity fading and power fading are measured after completion of these steps. The capacity fading is indicated by estimated capacity Q value, and the power fading is indicated by estimated lumped resistance for simplified equivalent circuit model R_t value using Ohm's law.

Table 3-1. Procedure of the principal algorithm for SOH estimation

Step	Procedure
1	System data measurement from current pulse pattern experiment; current, voltage and temperature.
2	Selection of weighting factors in the variance inhibiting term.
3	Calculation the capacity and power with the soft sensor technique.
4	Determination of the SOH level of the lithium-ion battery.

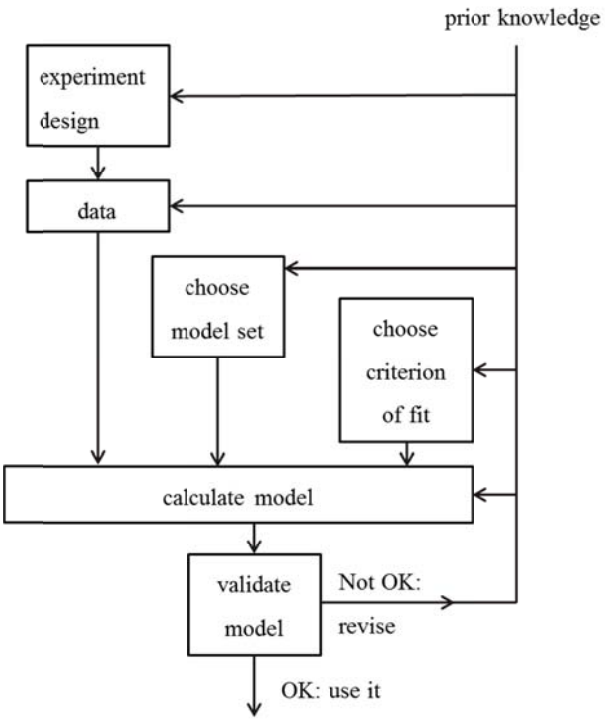

Figure 3-1. System identification loop for SOH estimation

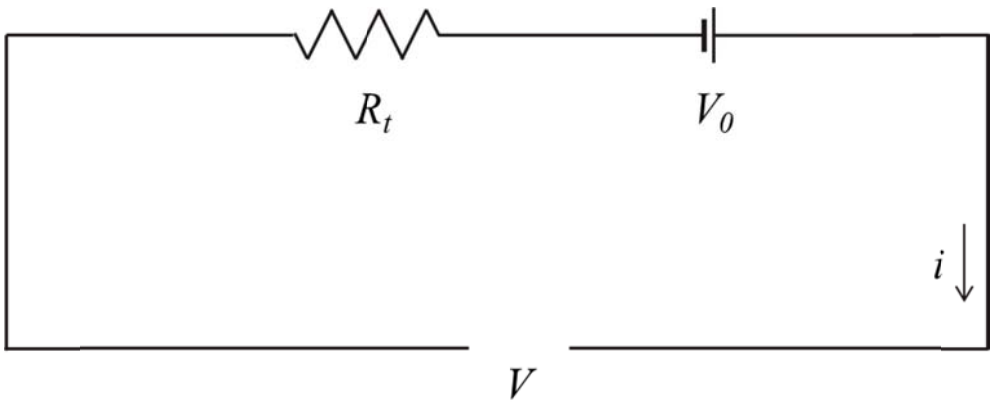

Figure 3-2. Simplified Equivalent circuit battery model with a single resistance.

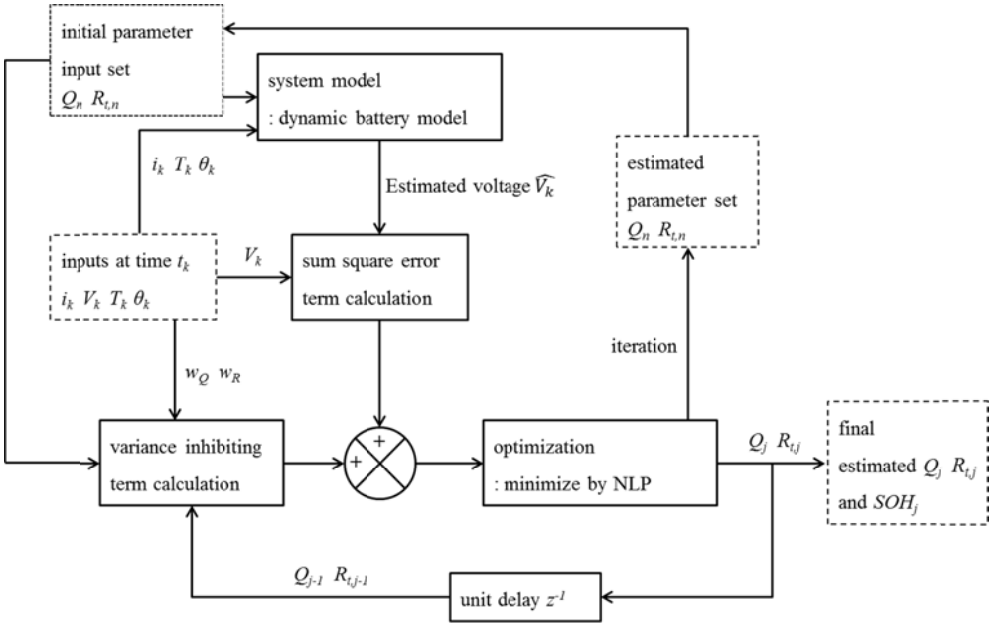

Figure 3-3. Schematic overview of the principal algorithm procedure.

3.4. Supplementary algorithm

The principal algorithm which is described above is an accurate and robust algorithm for estimating capacity and power fading. However, the algorithm has a computational load to be reckoned with due to the nonlinear programming for the SSE and variance inhibiting term calculations. The algorithm is too heavy to monitor the capacity and power fading in real time. Therefore, a supplementary algorithm for on-line monitoring of capacity fading is suggested. The supplementary algorithm is less accurate than the principal algorithm but has less of a computational load.

The supplementary algorithm is a kind of compact modeling with analytical method. The algorithm is based on the simple ECM as aforementioned and described in Fig. 3-2. The algorithm has two assumptions for the simple modeling of a lithium-ion battery cell. The first assumption is the linear relationship of SOC and OCV. In moderate SOC conditions from 30% to 80%, the SOC increases linearly with the change in OCV described in Fig. 3-4. The R^2 of the linear regression was 0.9852. In HEV and PHEV applications, the SOC operating range is limited to 30% to 80% to prevent battery ageing.[82] Therefore, the first assumption is acceptable in HEV and PHEV applications. For the second assumption, the overall resistance in Fig. 3-2 is constant in the same measurement sequence. The resistance changes considerably with changes in temperature and power fading. However, the same measurement sequence is about a few minutes and enough short to neglect the change in resistance.[100] Therefore, the second assumption is acceptable in the estimation algorithm.

The formula for Eq. 3-1 is selected as the starting point of the supplementary

algorithm. In the sequential current and voltage data, two main points are selected as the starting and closing points for the estimation algorithm. The qualification of the two points is simple: the current value is equal to the two points. Between the two points, however, these conditions are not necessary. For point 1 and 2, Eq. 3-1 is expressed as follows:

$$\hat{V}_1 = V_{0,1} + i_1 R_t \tag{3-5}$$

$$\hat{V}_2 = V_{0,2} + i_2 R_t \tag{3-6}$$

The difference between two equations is expressed as follows.

$$\Delta\hat{V} = \Delta V_0 + \left(i_2 R_t - i_1 R_t\right) \tag{3-7}$$

In this equation, i_1 and i_2 are equal due to the qualification of the two points. Moreover, the resistance is equal based on the second assumption. Therefore, Eq. 3-7 is modified to become Eq. 3-8.

$$\Delta\hat{V} = \Delta V_0 \tag{3-8}$$

The equation means that the difference between the voltages is equal to the difference between the OCVs under the measuring conditions. The OCV is the linear function of SOC based on the first assumption as follows in Eq. 3-9.

$$V_{0,k} = \gamma_0 + \gamma_1 \theta_k \tag{3-9}$$

The parameters γ_1 and γ_2 are dependent on the temperature and cell characteristics. Eq. 3-9 is expressed with point 1 and 2. The difference between the two points is obtained with Eq. 3-10 and is substituted to Eq. 3-8 as follows.

$$\Delta V_0 = \gamma_1 \Delta\theta \tag{3-10}$$

$$\Delta V = \gamma_1 \Delta\theta \tag{3-11}$$

The SOC is estimated by current integration based on Coulomb counting as follows in Eq. 3-3. By combining Eq. 3-3 and Eq. 3-11, the capacity Q is defined as the function of the current and voltage.

$$Q = \frac{\gamma_1}{36\Delta\hat{V}} \sum_k i_k \tag{3-12}$$

The calculated Q represents the capacity fading phenomenon. The equation is acceptable for capacity estimation by simple calculation. The necessary values for the calculation are the voltage and current, which are measured in a BMS. The slope of the SOC-OCV linear regression is obtained for the SOC-OCV relationship experimentally.

Since the capacity fading mechanism is a long-term phenomenon, the estimated Q is equal in the same day measurement. Therefore, repetitions of the Q measurement are necessary for an accurate estimation. The repeated measurements are set to the representative capacity value by the moving average estimation methodology described by Eq. 3-13.

$$\bar{Q}_j = \sum_{l=0}^{m} w_{m,l} Q_{j-l} \tag{3-13}$$

For elimination of the noise from the measurements, the maximum and minimum values are negligible in the average calculation. Moreover, the old measurement value has a low weighting factor and the present measurement value has a high weighting factor. The summation of weighting factors $w_{m,k}$ is equal to 1 for average calculation.

Fig. 3-5 and Table 3-2 shows the organization of the supplementary algorithm, which used Eq. 3-12 to calculate the capacity and Eq. 3-13 for the moving average

estimation. The supplementary algorithm has four steps.[84] The first step of the supplementary algorithm is to gather the voltage, current, and temperature data. The data set is collected from the battery management system in 1s intervals. The selection of two main points is the second step with the current integrated between the two points. The third step is to calculate the capacity with Eq. 3-12 and the last step is to estimate the capacity using the moving average estimation.

Table 3-2. Procedure of the supplementary algorithm for SOH estimation

Step	Procedure
1	System data measurement from current pulse pattern experiment; current, voltage and temperature.
2	Selection of two concurrent points with the current integration.
3	Calculation the capacity with the simplified equation.
4	Determination of the SOH level of the lithium-ion battery.

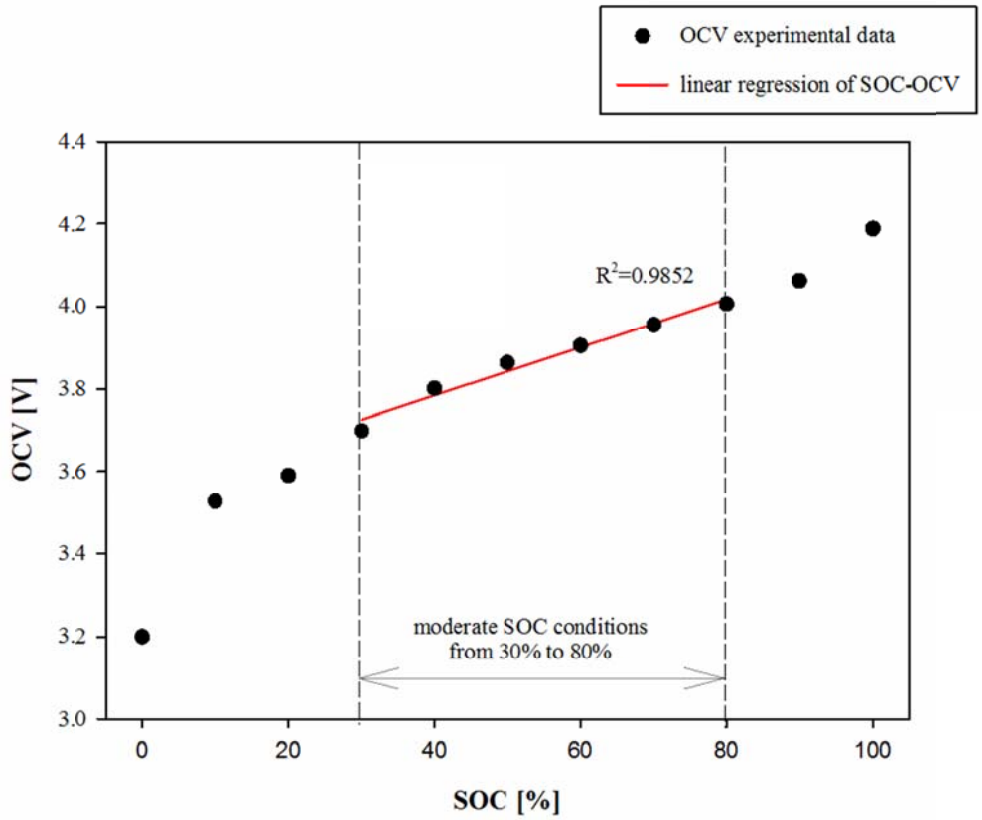

Figure 3-4. Open circuit voltage versus the SOC for linear regression.

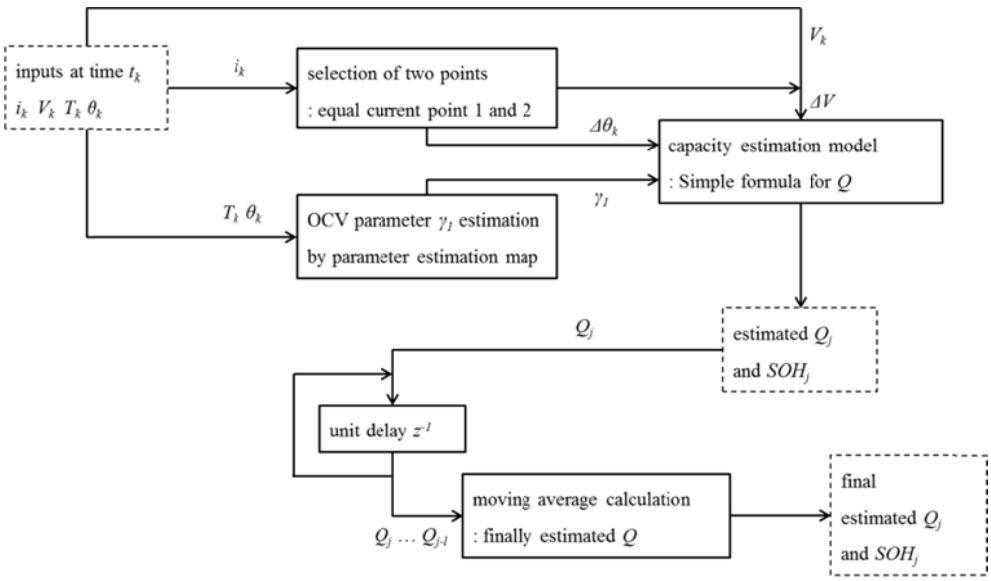

Figure 3-5. Schematic overview of the supplementary algorithm procedure.

3.5. Hybridized algorithm

As mentioned earlier, a principal algorithm and supplementary algorithm to estimate capacity and power fading were developed. The developed algorithms each have their merits and faults. The principal algorithm has high strengths and weaknesses but also a high computational load. However, the supplementary algorithm is less accurate but has a lower computational load. To develop the complementary algorithm, the principal and supplementary algorithms were combined shown in Fig. 3-6. The combined algorithm is called the hybridized algorithm.

The hybridized algorithm consists of three main steps. Batch estimation data are collected at the first step. The data are transferred to the estimation algorithm, which includes the principal algorithm and the supplementary algorithm. The proper estimation method from the two algorithms is selected based on a selection criterion that included the calculation frequency and the degree of capacity and power fading.

The supplementary algorithm frequently estimates the capacity fading to check the progress of the level of fading. SOH, which represents the level of the actual battery performance, is estimated less accurately by the supplementary algorithm than by the principal algorithm. Nevertheless, this algorithm is used for frequent estimations due to its low computational load and simple progression. The principal algorithm runs according to a fixed period such as a week. An accurate level of capacity and power fading is estimated at this run. However, the principal algorithm could run abruptly according to prescribed cases. The capacity and power deteriorates rapidly compared to normal conditions due to unknown

disturbances or unexpected causes. This phenomenon could be observed by the estimation result of the supplementary algorithm between one run of the principal algorithm. If the differences between the results are larger than the predetermined values, then unexpected fading has occurred. Therefore, the principal algorithm runs unexpectedly when the results are larger than the predetermined value.

The previous value of capacity is needed to calculate the variance inhibiting term in the principal algorithm. The values of the supplementary algorithm, which are located between the runs of the principal algorithm, are used as the previous value in the hybridized algorithm. The intermediate values are the more recent values for the capacity; these values are more adequate than the values from the previous principal algorithm. The weighting factors are established under the previous criterion of the principal algorithm.

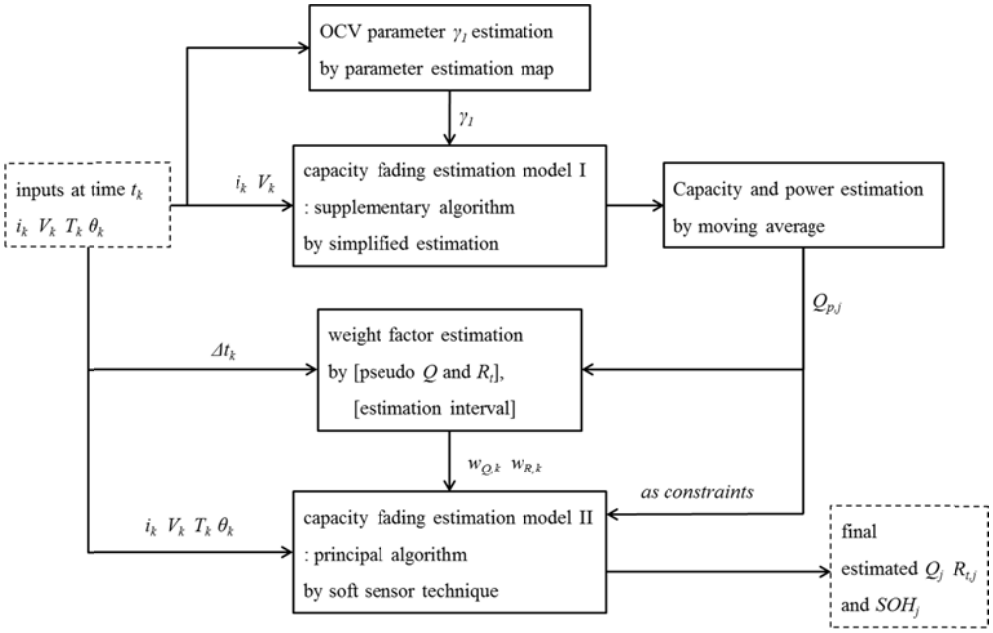

Figure 3-6. Schematic overview of the hybridized algorithm procedure.

3.6. Results and analysis

Several case studies were used to demonstrate the developed algorithms. The case studies were categorized into two different groups: the HEV application and PHEV application. The capacity and power of the HEV application were lower than that of the PHEV application. Therefore, the results had different implications for real-world applications. Each group included different types of battery operation patterns and SOH levels. The principal algorithm was validated by different groups, and the parameters were optimized under various conditions. Sensitivity analysis of the weighting factors was done to evaluate the performance of the algorithm and to determine the optimized value for an accurate estimation. The supplementary algorithm and the hybridized algorithm were validated under the same conditions as the validation of the principal algorithm. These results were compared to the experimentally measured data obtained from the impedance experimentswith various state lithium-ion cells.[112]

3.6.1. Estimation results of the principal algorithm

Cycle experiments for the battery from the HEV application were done to estimate the battery performance and to demonstrate the performance of the principal algorithm. The error between the actual and the estimated values were analyzed with the standard deviation of the current variation, shown in Fig. 3-7 to Fig. 3-10. The accuracy decreased when the standard deviation of the current increased with equal weighting factors. Therefore, the weighting factors needed to be optimized for each case. The at rest cycle experiments for the battery of the HEV application

were done with various weighting factors. The results are shown in Fig. 3-11 and Fig. 3-12 with various values for the weighting factors. The capacity was estimated accurately with various values of the actual SOH. The standard deviation of the current was less than 1.5; the current was stable and unknown disturbances were predicted to have a negligible value. Therefore, smaller weighting factors were adequate for the rest of the cycle due to less error in the error calculation terms in Fig. 3-11. Nevertheless, the zero weighting factors resulted in inaccurate estimated values about -6.23% errors. The larger values were less accurate than the smaller values, and the slope of the estimation is stable at smaller values. Therefore, the appropriate sizes of the weighting factors were optimized to 0.01 and 0.005 in the rest mode.

The driving cycle experiments were done with various weighting factors, shown in Fig. 3-12. The capacity was also estimated with an equal SOH value from the at rest cycle experiments. The standard deviation of the current was larger than 1.5. Therefore, larger values of the weighting factors were more stable than that of the at rest cycle cases. The estimated values were inaccurate in smaller weighting factor value than 0.5. Therefore, the adequate values of weighting factors were 10 and 5 in the driving mode.

Cycle experiments for the battery from the PHEV application were done to validate the algorithms with a high size for the capacity case. The results are shown in Fig. 3-13 with a high accuracy for the estimation of the battery performance. The standard deviations of the current were almost constant when the PHEV batteries were charged with a sinusoidal input current pattern. Therefore, the weighting factors were fixed with 0.04 and 0.02. The weighting factors were newly optimized

with the deviations of the previous changes in values. The weighting factors were larger than the HEV applications due to the absolute size of the capacity.

Cycle experiments with various previous estimated values were done to validate the reliability against inaccurate previous estimated values of the algorithm. The errors were less than the deviations between the previous value and actual value, shown in Fig. 3-14. The algorithm functioned accurately in estimating the exact value of the battery performance. Nevertheless, the error decreased when the deviations decreased. Therefore, the weighting factors were optimized for deviations between the previous value and actual value. The deviations were translated to the intervals of the operation runs with the assumption that capacity fading occurred smoothly and gradually. The optimized weighting factors were applied to each case and shown in Fig. 3-14 with high accuracies. However, the assumption is undefined when capacity fading is accelerated by the promotion events. Therefore, the remedy for the weakness of the algorithms was presented at the results of hybridized algorithms.

3.6.2. Estimation results of the supplementary algorithm

Cycle experiments for batteries from HEV and PHEV applications were done to demonstrate the performance of the supplementary algorithm. The algorithm results were confirmed to be in agreement with the assumptions for the algorithm. The overall resistance maintained an almost constant value during the single runs for data acquisition. The R-squared values of the linear regression of the SOC-OCV relationship in Fig. 3-4 were more than 0.98. Consequently, the assumptions were reliable for each estimation case.

The results of the estimations are shown in Fig. 3-15 for the HEV application. The errors were larger than the results of the principal algorithm. Nevertheless, the results were low enough to estimate the battery performance accurately. The results were different when the standard deviations of the current changed. However, errors at the highest standard deviation were low enough to have a high confidence in the performance of the algorithm. The results of the PHEV application are shown in Fig. 3-16. The standard deviations were almost constant for the charging cycle. The results were accurate for the varying ranges of SOH except for cases that were less than 80%. The error was larger than 3%, but the batteries were rarely operated at these conditions. Therefore, the accuracy of the supplementary algorithms was compensated for normal conditions of the SOH, from 80% to 100% ranges.

3.6.3. Estimation results of the hybridized algorithm

The hybridized algorithm was validated with experiments on batteries from HEV and PHEV applications. The previous estimated values as the variance inhibiting term of the principal algorithm were substituted with the values of the intermediate estimated values by the supplementary algorithm. The results of the application of the algorithm are shown in Fig. 3-17 and Fig. 3-18 with high accuracy. The errors were lower than that of the supplementary algorithm and comparable to the results of the principal algorithm. The weighting factors for the principle algorithms were optimized to improve performance. The results of the substitution to the optimized value were precise with various SOH values. Moreover, the computational load decreased due to the reduction of nonlinear programming calculations. In

conclusion, the accuracy was maintained at the level of the principal algorithm and the computational speed improved compared to the principal algorithm.

3.6.4. Analysis and discussion

In this study, on-line battery performance estimation algorithms were suggested and validated. The capacity and the power of the battery identify the actual battery performance. The accuracy and reliability of the algorithms were demonstrated through cycle experiments. Previously studied algorithms for on-line estimations focused on recursive estimations such as the Kalman filter.[42-43, 99-104] The recursive algorithms take into consideration the unknown variables of a model accurately.[113] The Kalman filter was used as on-line estimation method, but was not appropriate due to lack of observability.[114] The battery system model was not observable in the traditional dynamic system context. In addition, sample data and model updates are needed for recursive estimation. The sampling frequency is 10^{-1}s to 1s and the time order of the capacity and power fading mechanism is 10^{6}s.[95] Therefore, update benefit by computational load is not sufficient to deal with time scale differences.

Moreover, the linearization of a nonlinear target system with noise measurements has heavy computational loads. Therefore, the previous methods are adequate to study undefined phenomena and unknown variables in laboratory conditions. However, the developed algorithms in this study have the advantages of on-line calculations and target variable estimation such as capacity. The index for the actual battery performance was represented as the capacity and the power. As a result, the developed algorithms were more than adequate to accurately estimate the actual battery performance in real time. However, the three algorithms have

different characteristics and they were appraised for their appropriateness to different purposes.

The accuracy of the principal algorithm varied with the weighting factors. The current pattern influenced the accuracy of the error accuracy term; the estimated capacity and the estimated power with the smallest weighting factors fluctuated without a downfall in the tendency. Therefore, the weighting factors have an important role in the variance inhibiting term in a highly fluctuating current pattern. The weighting factors varied with the standard deviation of the current pattern and the accuracy of the algorithm was preserved as the current pattern changed. Nevertheless, the principal algorithm is more accurate than the supplementary algorithm for both HEV and PHEV applications. The error from the supplementary algorithm was higher several times than the error of the principal algorithm. However, the maximum measured error was below to 2% and the confidence of the algorithm was maintained when applying the algorithm.

The computational time and load are other major criteria to validate an algorithm's performance. The principal algorithm had a high computational load due to the optimization routine. The optimization objective function consisted of nonlinear formulas in which it took over 20s to compute a solution [100]. The problems are impossible to solve during the interval of gathering data, which is about 1s. The algorithm is inadaptable to on-line estimation of the capacity and the power. Therefore, running the principal algorithm by itself is problematic for the purpose of this study.

The supplementary algorithm has the advantage of a lower computational load. The equations of the supplementary algorithm, which consists of four linear

fundamental arithmetic operations, are simple enough to be applied to a real BMS. The computational load by the algorithm is so small that the overall computational time is less than 0.1s. The generation interval of the sample data from the BMS is assumed to be 1s but the sampling time of the BMS could decrease to approximately 0.1s for an accurate measurement of the battery status. The supplementary algorithm is adequate for this case even if the sampling data increased about ten times with a 10-fold reduction in the interval time 1s to 0.1s. The quantity of the data is not a crucial problem for the supplementary algorithm since the setting of the two main points and summation of the current are the only parameters necessary for the algorithm to run. Therefore, the supplementary algorithm is adequate for application to on-line estimation of the actual battery performance.

The advantages and faults of the two developed algorithms are significant and complementary. Consequently, the principal algorithm and supplementary algorithm were combined to the hybridized algorithm to maximize the advantages and minimize the disadvantages. On-line estimation is possible by frequently running the supplementary algorithm. Moreover, accurate estimation is accomplished by the regular running of the principal algorithm. The combination of the two algorithms has the advantage of reliability against the inaccurate previous estimated values as well. If the estimated capacity and the estimated power are significantly abnormal, the principal algorithm is run to estimate the precise value. If the previously estimated capacity and power is significantly different from the actual value, the SSE and variance inhibiting term help to estimate the capacity and the power correctly. The optimized weighting factors,

which reflect the running interval of the algorithm, provide the reliability against the inaccurate previous estimated values of the algorithm. In other words, the hybridized algorithm has both accuracy as reliability and computational convenience by successive combination.

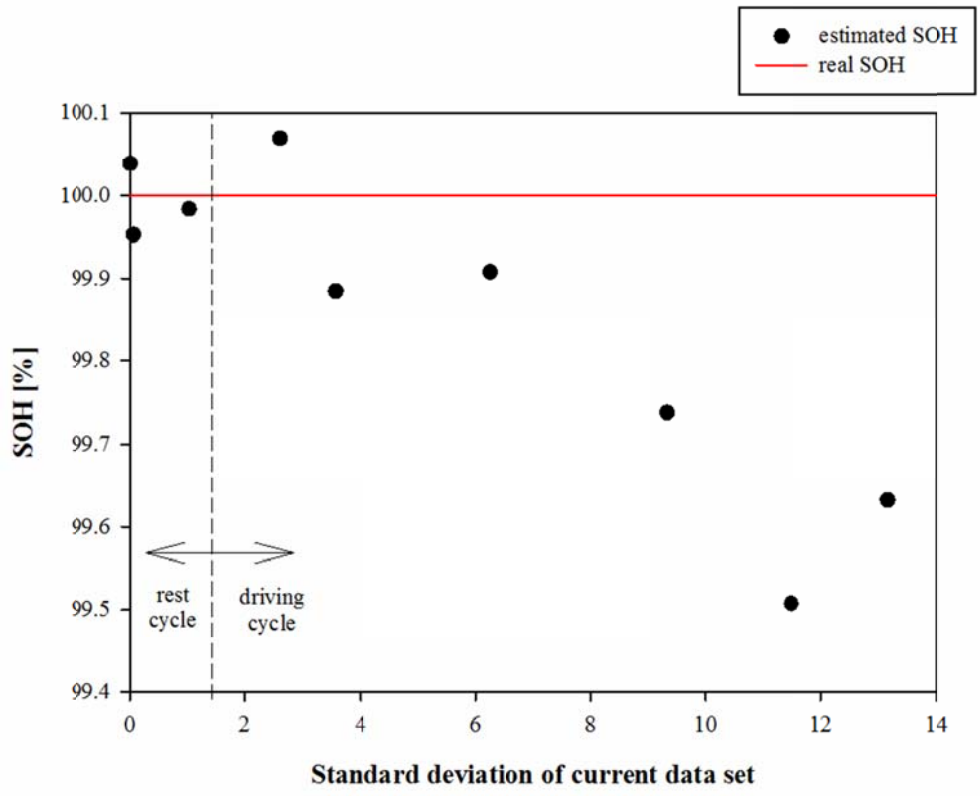

Figure 3-7. Validation of the principal algorithm for HEV application with various current variations at SOH 100%.

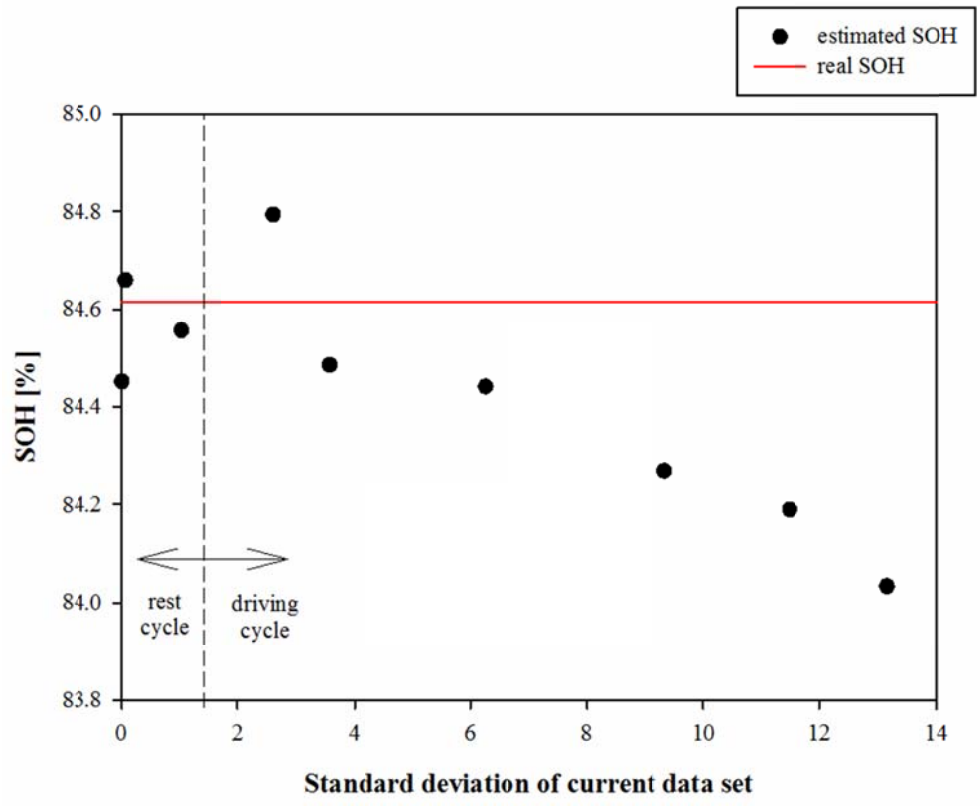

Figure 3-8. Validation of the principal algorithm for HEV application with various current variations at SOH 84.62%.

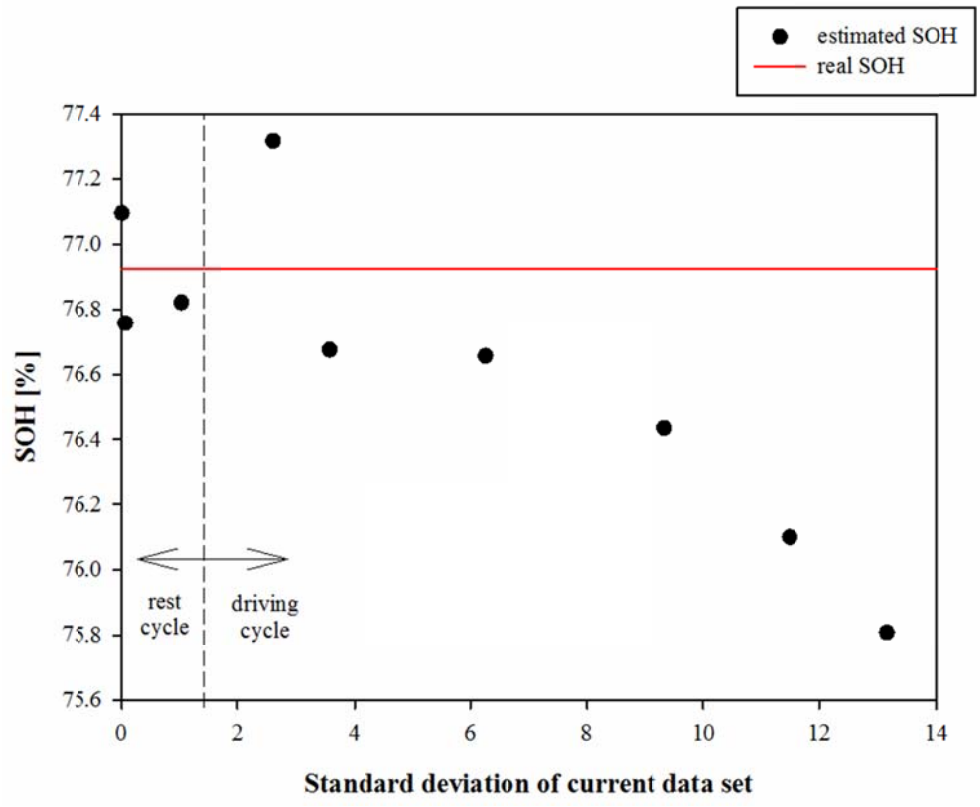

Figure 3-9. Validation of the principal algorithm for HEV application with various current variations at SOH 76.92%.

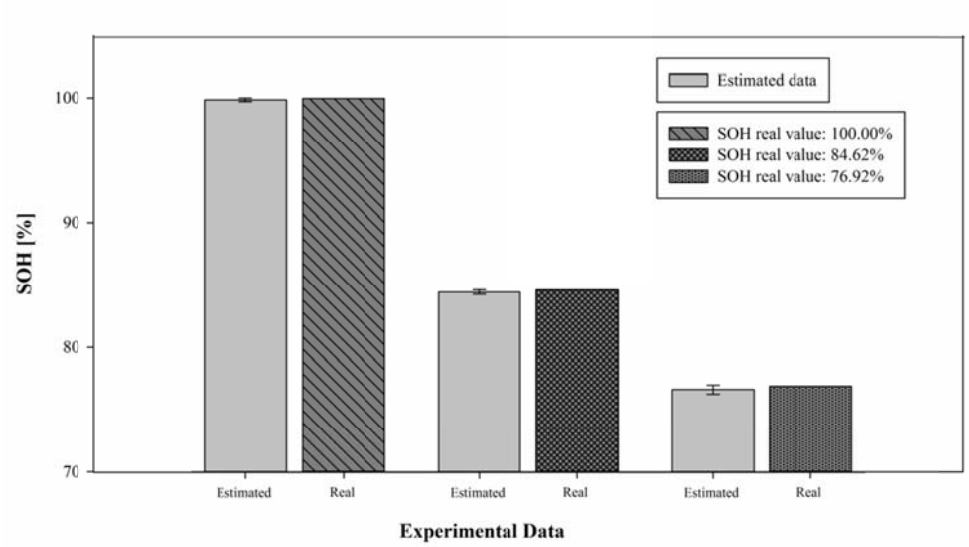

Figure 3-10. Validation of the principal algorithm for HEV application with various current variations with varied SOH levels.

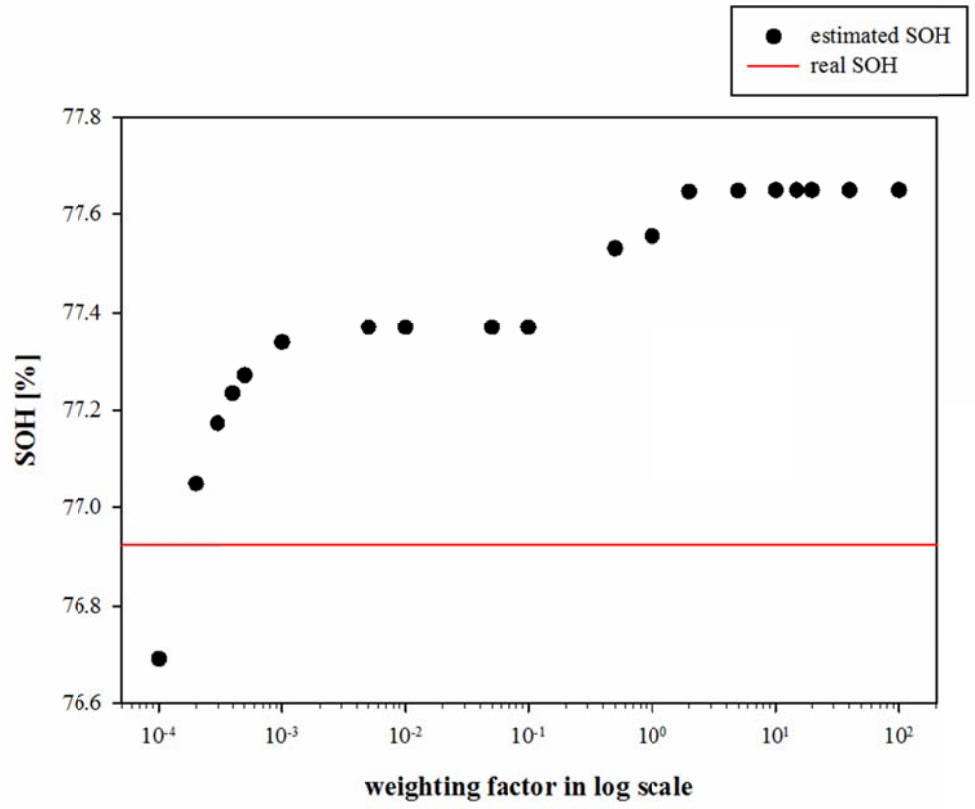

Figure 3-11. Validation of the principal algorithm for HEV application with various values for the weighting factors at rest cycle.

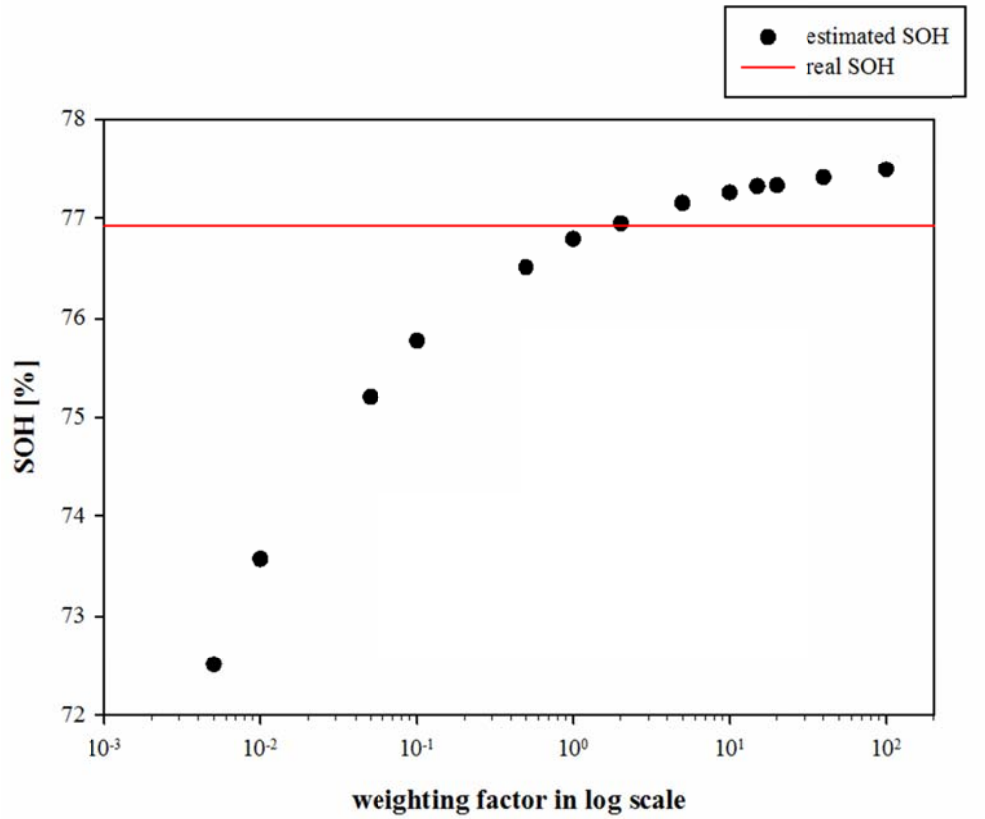

Figure 3-12. Validation of the principal algorithm for HEV application with various values for the weighting factors at driving cycle.

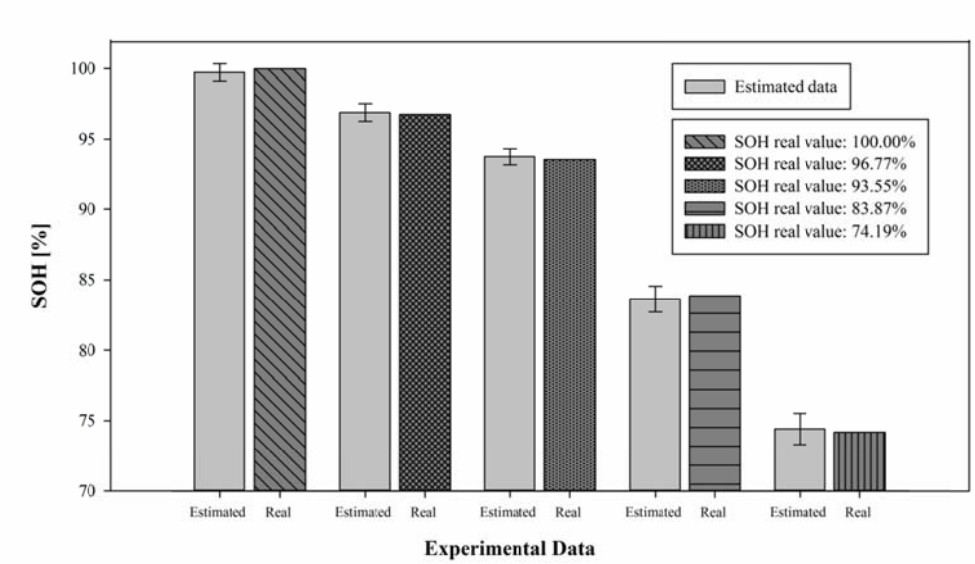

Figure 3-13. Validation of the principal algorithm for PHEV application estimation result for optimized weighting factor.

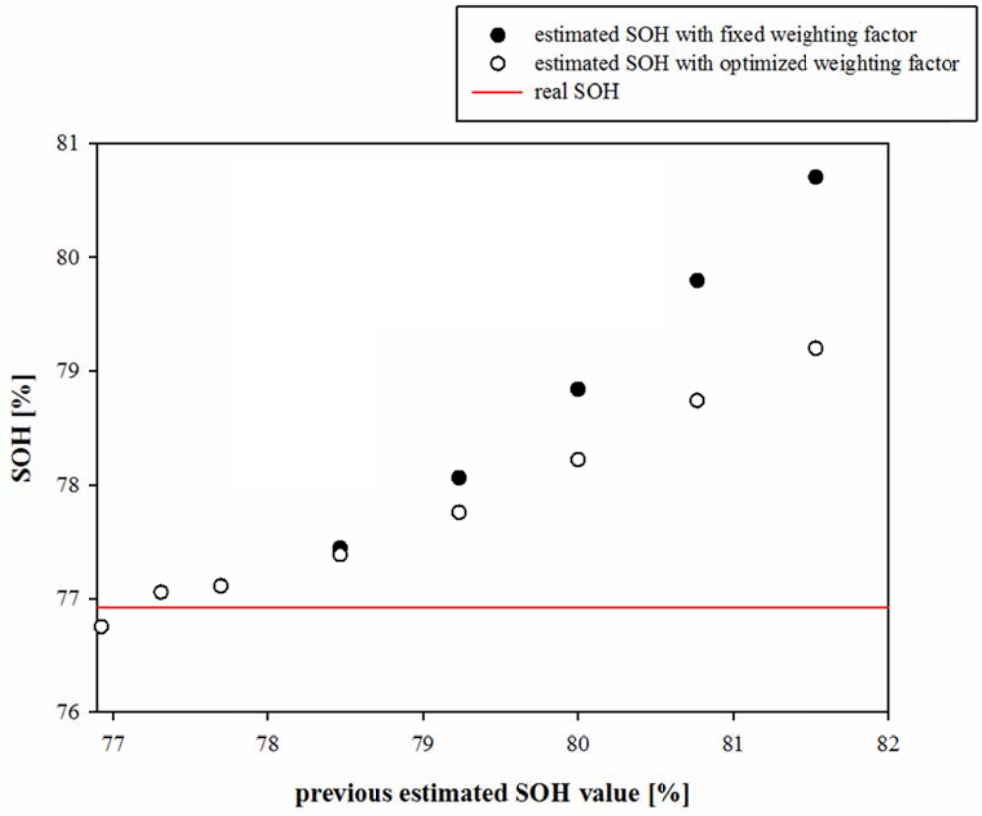

Figure 3-14. Validation of the reliability against the inaccurate previous estimated values of the principal algorithm with various previous estimated values.

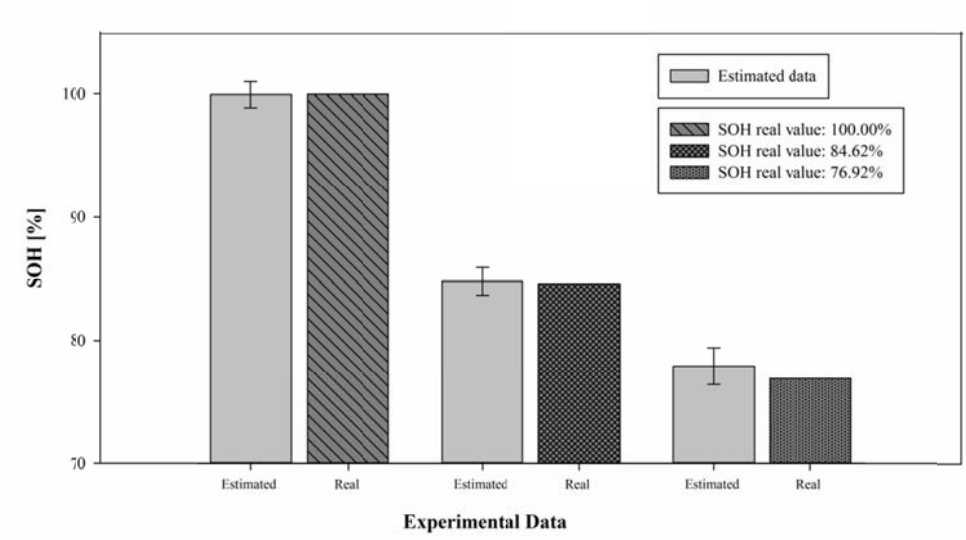

Figure 3-15. Validation of the supplementary algorithm for HEV application estimation result.

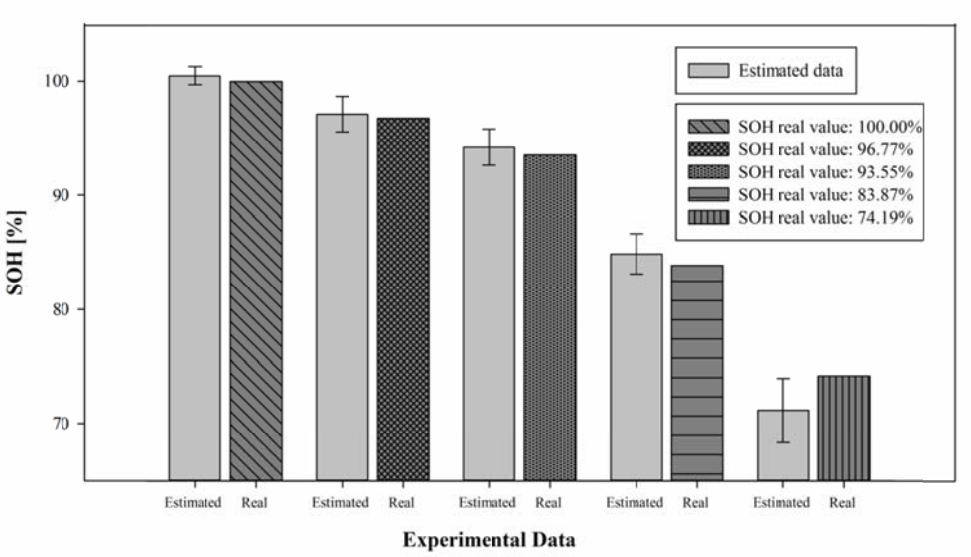

Figure 3-16. Validation of the supplementary algorithm for PHEV application estimation result.

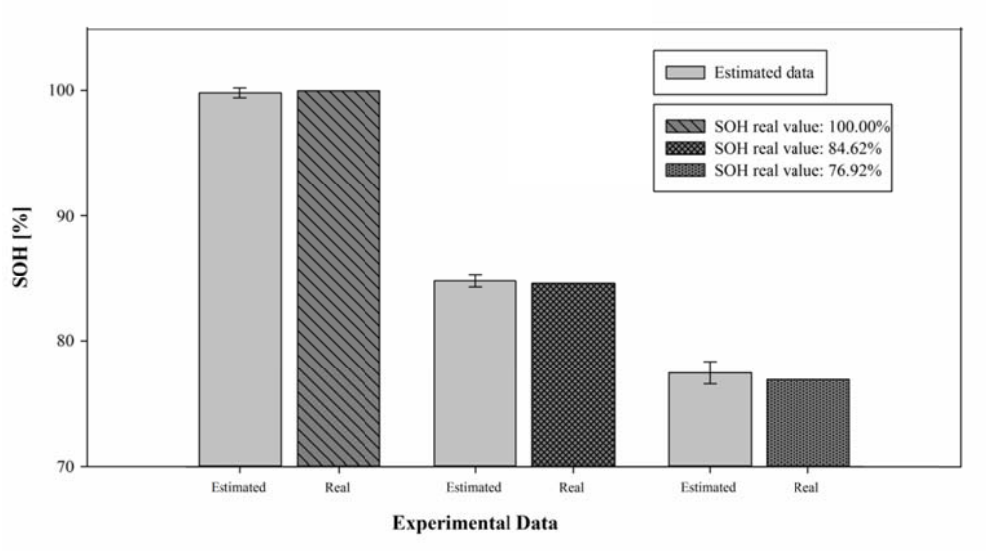

Figure 3-17. Validation of the hybridized algorithm for HEV application estimation result.

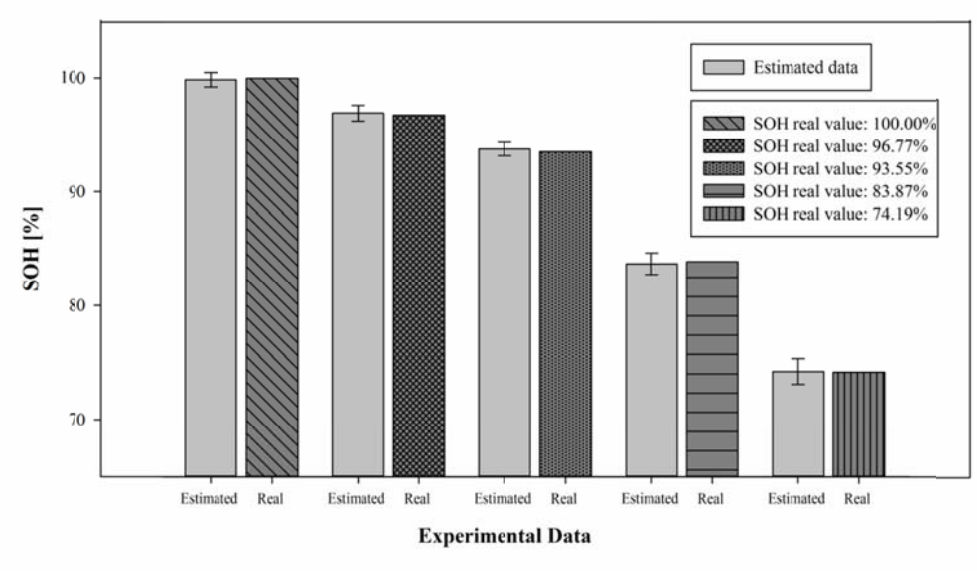

Figure 3-18. Validation of the hybridized algorithm for PHEV application estimation result.

3.7. Conclusions

Three estimation algorithms have been suggested to estimate the actual battery performance of HEV and PHEV applications in Chapter 3. Both the principal and the supplementary algorithms achieved accuracy in estimating the capacity and power fading. However, the principal algorithm has a heavy computational load for each step of data acquisition even if the capacity and the power are estimated correctly. On the other hand, the supplementary algorithm has the advantage of on-line computation but has a lower accuracy than that of the principal algorithm. Therefore, the two algorithms were combined to form the hybridized algorithm for on-line estimation with high accuracy. The results from various cycle experiments for HEV and PHEV applications demonstrate the congruence of the accuracy, reliability against the inaccurate previous estimated values and computational load. Consequently, the hybridized algorithm is more than adequate for accurate on-line estimation of the actual battery performance as quantitative values of capacity and power in real time. Furthermore, suggested SOH estimation methodologies are applied to battery dynamic model and SOC estimation methodology in Chapter 2 and optimal control of FCHEV in Chapter 4.

CHAPTER 4 : Optimal Control of Hybrid Energy System

4.1. Introduction

FCHEVs have been gaining traction as an ultimate technology of the eco-friendly vehicles.[115-116] The vehicle uses fuel cell system to generate power. The fuel cell system generates on-board motive power of the vehicle as a substitute for conventional internal combustion engine. The fuel cell system uses the hydrogen or reformed hydrogen from hydrocarbons as fuel instead of fossil fuels such as gasoline or diesel. Therefore, FCHEVs rarely generate polluted exhaust gas than conventional vehicle and even HEVs and PHEVs.[8-13, 117-119]

However, the fuel cell system has limitation to commercialization. The fuel cell system could not respond to peak demand power. Moreover, vehicle starting has some problems at low temperature. The secondary battery could enhance traction power during starting of the fuel cell system. Therefore, auxiliary power supply system is needed to solve these demerits. The FCHEVs generally use dual power sources, the fuel cell as well as the secondary battery as though the conventional HEVs or PHEVs use the secondary battery as auxiliary power supply source.[120] The secondary battery with intended role for hybridization gets some merits. As aforementioned, the secondary battery could help the starting and shut-down of the fuel cell system. Furthermore, the stack size of the fuel cell could be downsized by increased capacity of the battery. Therefore, the cost of the fuel cell system and FCHEVs could be decreased. Moreover, the FCHEVs respond faster to high peak

demanded power than the single fuel cell system. Acceleration performance of the vehicle is guaranteed of high performance level. In addition, the secondary battery could assist the on-board motive power during drive cycle, and recapture the superabundant energy during regenerative breaking. Therefore, it is able to be operated more profitable than single fuel cell system.[121-123]

Consequently, power management control strategy is required to operate the hybrid energy system efficiently. Development of the power distribution control system is important for the efficiency and the stability of the hybrid energy system. The control system is developed to achieve maximum system's efficiency to minimize the fuel consumption. In addition, the SOC of the battery have to be maintained in moderated range while operating the system by the control logic. The secondary battery deteriorates when the battery is operated at very low or high SOC level. As a result, the power and capacity of the secondary battery is reduced and the life of the battery is shortened than expected life length. Consequently, maintaining SOC of the battery is necessary to prevent frequent replacement of the battery and to maintain the stability of the hybrid energy system.[124]

The power management control strategy for FCHEV is divided into two main topics.[18] The first strategy is based on optimization methodologies.[11, 125] The strategy is based on dynamic programming, stochastic programming and model predictive control with predicted driving schedules. The other strategy is based on deterministic or fuzzy rules.[124] The rules are suggested based on heuristics, intuition, experience and mathematical model of FCHEV system. Especially, the fuzzy rule based methodology has been widely used to control of various vehicles.[126-128] Therefore, the fuzzy based control logic is appropriate to on-line

control of FCHEVs.[129]

In this chapter, the controller using fuzzy logic and the rigorous model of the secondary battery and the PEMFC system is suggested for this control problem. The secondary battery model which was suggested on Chapter 2 and Chapter 3 was applied to simulate the battery of the FCHEVs. In addition, the PEMFC system was suggested with rigorous zero dimensional process model. The fuzzy rule was suggested with rule-base membership function. The control strategy was demonstrated under various driving schedule from Environmental Protection Agency (EPA) of USA, operating condition and battery states.

4.2. Hybrid energy system modeling

4.2.1. Target system configuration

The target system is the fuel cell hybrid city bus. The maximum speed of the bus is 100km h^{-1} and the maximum power of the electric motor is 90kW.[25, 127] The fuel cell system applied to FCHEV is PEMFC. Most of the fuel cell systems for FCHEVs are PEMFC due to operation temperature, fuel characteristics and degree of commercialization. The secondary battery system consists of 30kW and 6.5Ah lithium-ion battery. The specification of the target FCHEV is summarized in Table 4-1.

The FCHEVs has various types according to variation of power source type, vehicle size and specification, topology of power source organization and the degree of hybridization.[18, 128] In this chapter, the target system is a parallel hybrid type of vehicle. Fig. 4-1 is the configuration of the fuel cell-battery hybrid energy system. The fuel cell system generates power from hydrogen fuel. The fuel cell supplies power to the secondary battery and/or DC/DC converter. This electric power is amplified by DC/DC converter and passes to the vehicle motor. The secondary battery is coupled in this path, in parallel system. The power from the fuel cell and the battery is going to DC/AC converter and motor. This electric power is converted to mechanical force, and the vehicle is able to move. The series system could be applied to hybrid system, but these contents are out of scope of this thesis.

The power distribution strategy is important in this path. Both the fuel cell and the battery generate power when the peak on-board motive power is demanded, such

as accelerating of the vehicle. Moreover, the secondary battery is only discharged and the fuel cell system switches over to standby mode during start-up and shut-down of the vehicle. The secondary battery is discharged and the SOC of the battery is decreased. On the other hand, the fuel cell generates power and it is split to the motor and the battery while the SOC of the battery is low. In addition, the battery could be charged during regenerative breaking. The battery is charged and the SOC of the battery is increased.

The instantaneous available maximum powers from the battery and the fuel cell have to be measured for dedicated control. Moreover, the SOC of the battery would have to be measured for criteria of the control. But these variables could not be directly measured by on-line sensor. They are measured directly by off-line method in the lab-invasive and destructive technique. Consequently, the estimation of these variables is needed with the rigorous model. Therefore, the rigorous model of the secondary lithium-ion battery and the proton exchange membrane fuel cell system is developed in the first place.

4.2.2. Lithium-ion battery modeling

The secondary battery in FCHEVs is anticipated as the similar characteristics of that of the HEVs. The secondary battery is required to equivalent charge capacity and power density to assist the FCHEVs on the same plane as HEVs.[123] Consequently, equivalent battery model to battery of HEVs would be applied to the optimal control configuration.

The lithium-ion secondary battery model in Chapter 2.2 and 2.3 is used as the battery model of the FCHEVs. The dynamic battery model is suggested as Fig. 2-2

and Eq. 2-7.

$$V = V_0 + iR_0 + \frac{1}{C_i}\int_{\xi=0}^{\xi=t}\left(i_\xi\, e^{-(t-\xi)/R_iC_i}\right)d\xi \tag{2-7}$$

The BMS measured voltage, current and temperature variables in discrete time interval, *Δt*. Thus the differential terms are rewritten as finite difference method form with Taylor series expansion.

$$\frac{d\xi}{dt} = \frac{\xi_k - \xi_{k-1}}{\Delta t} + \Theta'\left(\Delta t\right) \tag{4-1}$$

Eq. 2-7 is solved by Eq. 4-1 in first order backward accuracy. Thus the battery model could be expressed as follows.

$$\hat{V}_k = V_{0,k} + h\left(\hat{V}_{k-1} - V_{0,k-1}\right) + \left[\left(1-h\right)\left(R_0 + R_i\right) + hR_0\right]i_k - hR_0 i_{k-1} \tag{4-2}$$

where $h = \frac{R_iC_i}{\Delta t + R_iC_i}$. The Eq. 4-2 is selected as a main solving equation for dynamic battery modeling.

The OCV is calculated as a function of the SOC and temperature shown in Eq. 3-2 at Chapter 3.3.

$$V_{0,k} = \alpha_0\left(T\right)_k + \alpha_1\left(T_k\right)\theta_k + \alpha_2\left(T_k\right)\theta_k^{\,2} + \alpha_3\left(T_k\right)\theta_k^{\,3} + \alpha_4\left(T_k\right)\theta_k^{\,4} \tag{3-2}$$

The lumped ohmic resistance R_0 in Eq. 4-2 means the available maximum power of the lithium-ion battery. The lumped ohmic resistance increases within temperature decreasing. The power of the system would be calculated using Ohm's law and be inverse proportion to the ohmic resistance. Therefore, the power of the

lithium-ion battery system increases within temperature increasing till 318K as shown in Fig. 4-2. Furthermore, the power of the battery would decrease over 323K in experimental environment. However, the hot temperature condition over 318K is not the target of the vehicle simulation. Therefore, the power of the lithium-ion battery is considered limitedly at ambient and low temperature in Fig 4-2.

The developed parameter estimation algorithm in Chapter 2 is applied to the battery model in Chapter 4 in Eq. 4-3.

$$\Psi\left(R_i, C_i\right) = \left[\sum_k \hat{V}_k \hat{V}_k^T\right]^{-1} \left[\sum_k \hat{V}_k e_k\right] \tag{4-3}$$

Moreover, SOC of the lithium-ion battery is the key variable for optimal control. Therefore, the developed SOC estimation methodology in Chapter 2.4 is combined to the dynamic battery model as Eq. 2-19 and Eq. 2-20.

$$\theta_{i,k} = \theta_{c,k-1} + \frac{\Delta t}{Q_{0,\max}} i_k \tag{2-19}$$

$$\theta_{v,k} = \theta_{v,k}\left(V_{0,k}, T_k\right) = \theta_{v,k}\left(V_k, i_k, T_k\right) \tag{2-20}$$

In addition, the charge capacity and power of the battery has a role of main boundary conditions for optimal control. The instantaneous available maximum power is an upper boundary condition of the battery performance. Also, the capacity is a main variable to calculate the SOC level. However, the capacity and the power of the lithium-ion battery could deteriorate over continuous usage. The capacity and power fading might include in the battery model. Therefore, the SOH estimation methodology in Chapter 3.5 is applied to the dynamic battery model.

In other words, the developed models and methodologies for HEVs and PHEVs applications are applied to the battery simulation model for the optimal control algorithm. The dynamic battery model with state estimation algorithm is developed and simulated in MATLAB® and SIMULINK® simulation environment.

4.2.3. Proton exchange membrane fuel cell modeling

The PEMFC model is suggested to the optimal control configuration. The model requirements are as follows. The model is lumped zero-dimensional model for fuel-to-electricity efficiency calculation, fuel as hydrogen consumption estimation and generating power from the stack calculation.[130] Fig. 4-3 shows the PEMFC systems for FCHEVs. The system includes hydrogen recirculation and cathode humidifier model. The fuel cell stack has a lot of cell connection in series. In this case, each cell has uniform characteristics about cell voltage and current. Therefore, the stack voltage is the summation of the voltage of the entire cell.

The main reaction is reaction with hydrogen and oxygen. It is modeled as Eq. 4-4 with voltage model.

$$\hat{V} = V_0 - \eta_{act} - \eta_{ohm} - \eta_{conc} \tag{4-4}$$

V_0 is the open circuit voltage of the PEMFC unit cell but voltage is decreased by overpotential. η_{act} is the activation overpotential by reaction kinetics, η_{ohm} is the ohmic overpotential by ionic conduction resistance and electronic ohmic resistance, and η_{conc} is the concentration overpotential by mass transfer limitation. Each term is defined as following equations.

$$V_0 = -\frac{\Delta g(T)}{2F} + \frac{RT}{2F}\ln\left(\frac{a_{H_2} a_{O_2}{}^{0.5}}{a_{H_2O}}\right) \tag{4-5}$$

$$\eta_{act} = \frac{RT}{\alpha^{cat} F}\ln\left(\frac{i}{i_{ocat}}\right) + \frac{RT}{\alpha^{an} F}\ln\left(\frac{i}{i_{oan}}\right) \tag{4-6}$$

$$\eta_{ohm} = i\left(R_{el} + R_{ion}\right) \tag{4-7}$$

$$\eta_{conc} = -\frac{RT}{4F}\ln\left(1 - \frac{i}{i_{lcat}}\right) - \frac{RT}{2F}\ln\left(1 - \frac{i}{i_{lan}}\right) \tag{4-8}$$

The activities in Eq. 4-5 are equal to concentration of each component. In addition, overpotential is modeled with cathode and anode overvoltage. The power of the PEMFC system could be calculated using the Eq. 4-4 with Eq. 4-5 to 4-8. The voltage and current density are multiplied to calculate the power of the unit cell. The performance curves with current density change are shown in Fig. 4-4. As shown in the Fig. 4-4, the PEMFC model is accurate to apply to FCHEV control problem.

The current of the PEMFC system is determined by the developed model with respect to PEMFC output power. The hydrogen fuel consumption is determined by the current density with mass balance model. The mass balance model is required to calculate the hydrogen consumption.

$$v_{in,H_2,an} = \left(\frac{RT_{air}}{p_{atm}}\right)\left(\frac{i}{n_{H_2} F}\right) \tag{4-9}$$

$$v_{in,air,cat} = 2\left(\frac{RT_{air}}{p_{atm}}\right)\left(\frac{i}{n_{O_2} F}\right) \tag{4-10}$$

$$p_{vapor,an} = \frac{RH_{an,in}}{100} p_{sat,cell} \tag{4-11}$$

$$p_{vapor,cat} = \frac{RH_{cat,in}}{100} p_{sat,cell} \tag{4-12}$$

$$F_{in,fc} = \left(\frac{RT_{air}}{p_{atm}} \right) \times \frac{P_{fc}}{V} \times 2 \tag{4-13}$$

The stoichiometry of hydrogen gas and air are calculated with partial pressure of hydrogen and oxygen. The pressure of each gas is estimated by relative humidity due to cathode humidifier model. The efficiency is considered in Eq. 4-13 to calculate the fuel consumption flow rate using demanded power and low heating value of hydrogen.

The PEMFC model combined with stack cell model and mass balance model is developed by Excel with VBA. The input of the model is the demand power and environment of the system and the output variable is hydrogen consumption rate with efficiency.

4.2.4. Vehicle modeling

The required on-board motive power of the vehicle is calculated with vehicle speed with respect to the driving schedule given by EPA. The input variables are mass, acceleration and aerodynamic drag coefficient of the vehicle given by Eq. 4-14.

$$P_{veh} = \frac{\delta M_{veh}}{2t_a} \left(v_f^{\,2} + v_v^{\,2} \right) + \frac{2}{3} M_{veh} g f_r v_f + \frac{1}{5} \rho_{air} C_D A_f V_f^{\,3} \tag{4-14}$$

Three power requirement terms are located in Eq. 4-14. The first term is accelerating power regarding mass of the vehicle. The second and third terms are

representative power to overcome the rolling resistances of the tires and the aerodynamic drag. Each parameter is described in Table 4-1. The supplied power from the two power sources are calculated by required power from the vehicle P_{veh} with the efficiency of the traction motor and transmission of the vehicle. The output power from two power sources are calculated by Eq. 4-15.[1]

$$P_{ps} = \frac{P_{veh}}{1000 eff_m eff_t} \tag{4-15}$$

Table 4-1. Specification of the target FCHEV

Specification		
Fuel cell system	Type	PEMFC
	Output power	65 kW
Battery system	Type	Lithium-ion battery
	Capacity	6.5 Ah
	Output power	30 kW
Vehicle	Mass	1,500 kg
	Rolling resistance coefficient	0.01
	Aerodynamic drag coefficient	0.3
	Front area of the vehicle covers	2.0 m^2
	Transmission efficiency	0.9
	Motor efficiency	0.85
	Maximum speed	160 km h^{-1}

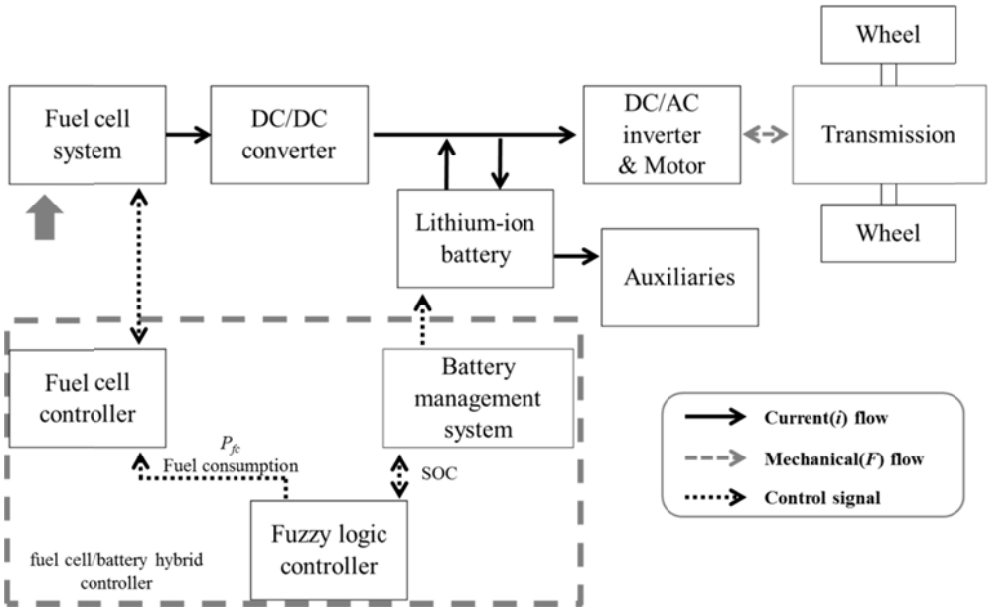

Figure 4-1. Configuration of PEMFC / lithium-ion battery hybrid energy system.

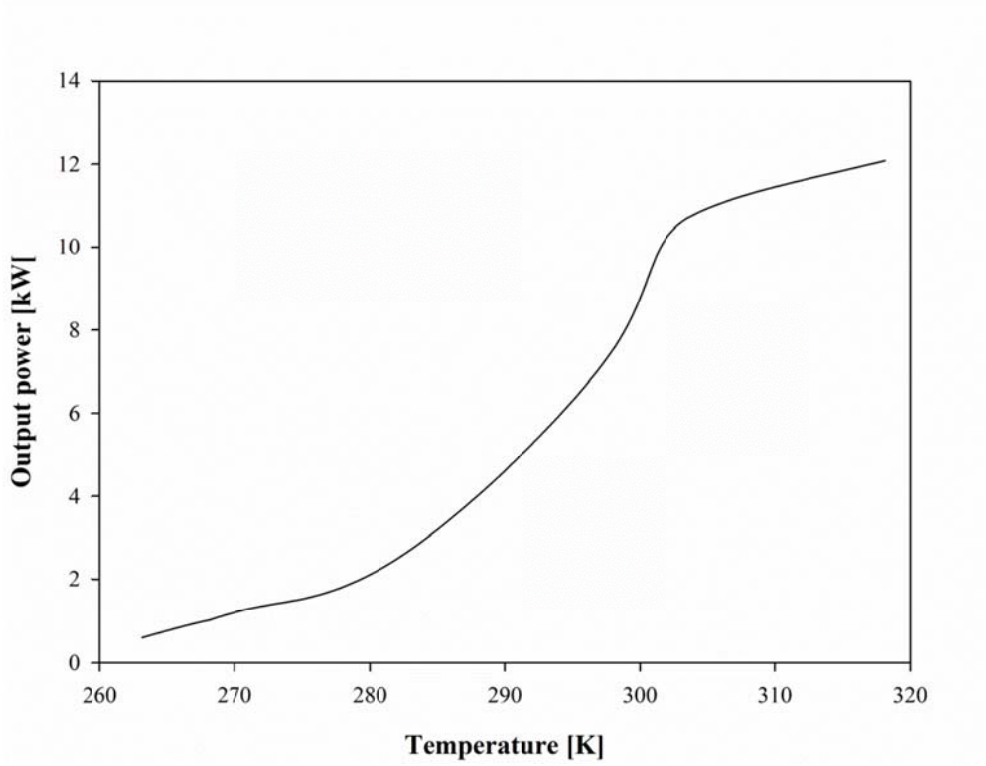

Figure 4-2. Power curve versus the temperature of the lithium-ion battery unit pack.

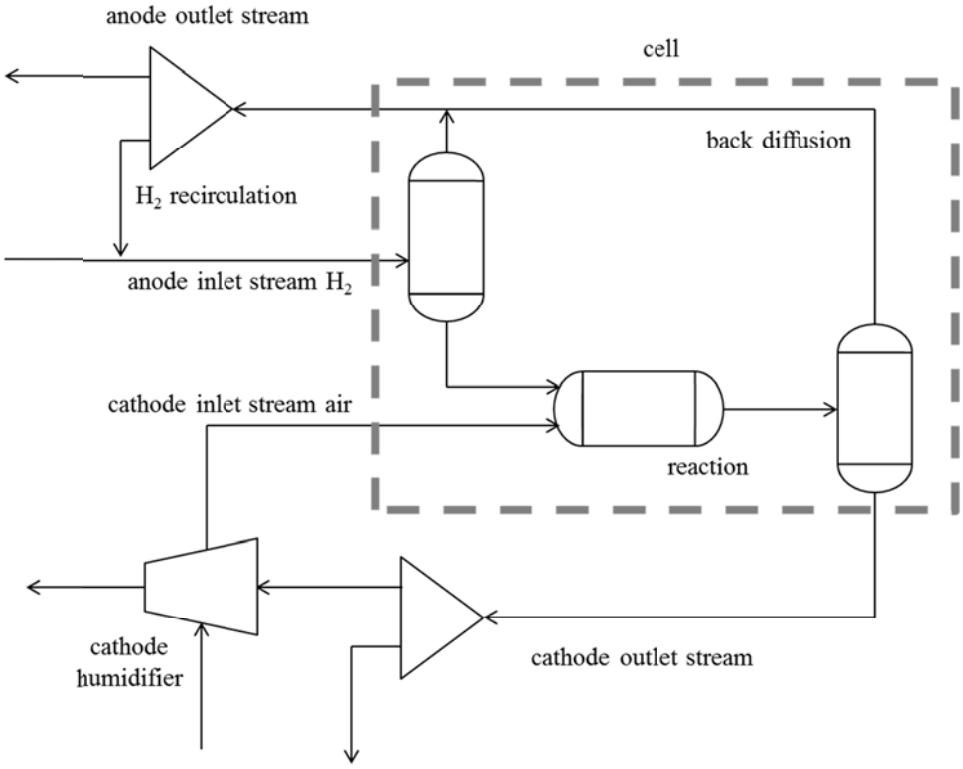

Figure 4-3. Configuration of PEMFC system model with hydrogen recirculation and cathode humidifier.

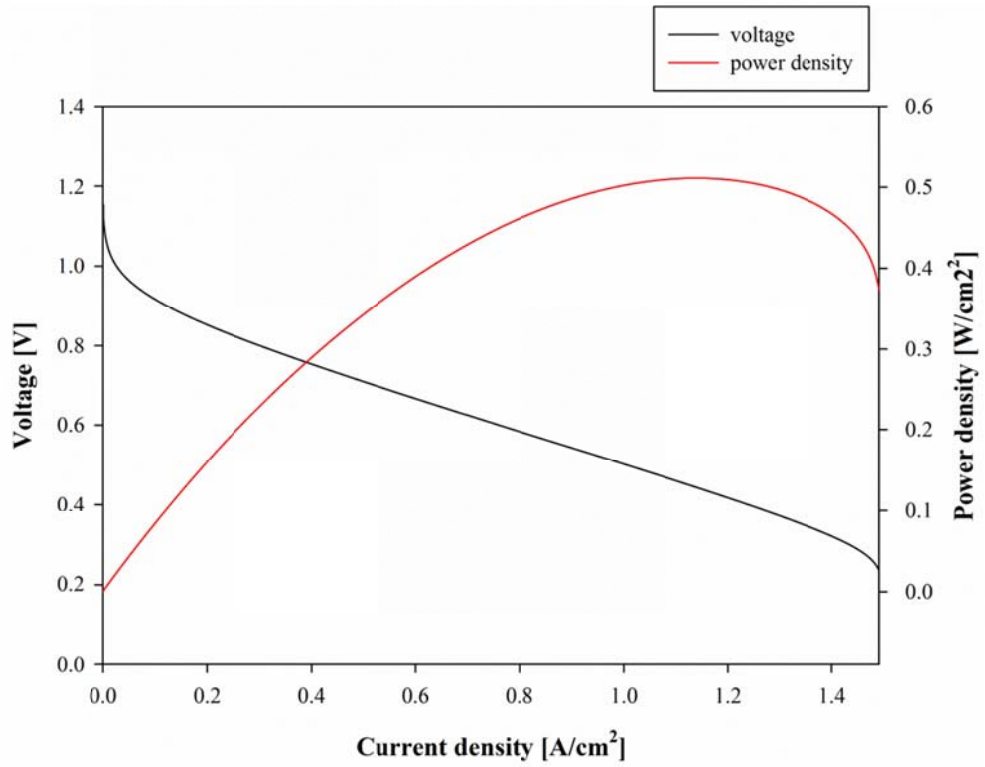

Figure 4-4. Polarization curve for the IV performance and power of the fuel cell unit cell.

4.3. Fuzzy control logic

4.3.1. Background theory

The power management control strategies for HEV, PHEC and FCHEV are classified into two main topics in Table 4-2.[18, 131] The first strategy is optimization based control strategies.[11, 125] The optimization based control strategies are divided into two topics: global optimization based method and real time optimization based method. The global optimization based strategies are based on linear programming, nonlinear programming, dynamic programming, stochastic dynamic programming, control theory approach, game theory and genetic algorithm.[132-136] The control strategies are based on maximization of the powertrain efficiency with minimization of power loss on the basis of Bellman optimality principles.[137] The optimization based strategy is performed in fixed driving pattern. The global optimum solution could be found using the optimization procedure. However, the situations in roads are not typical and it changed momentarily and unpredictably. Thus the control is not truly optimal or it is optimal in its sub-class.

The real time optimization based methods are based on model predictive control with predicted driving schedules, decoupling control, robust control approach and real time control based on equivalent fuel consumption.[138-140] The strategies are suitable for real time control but the computational load is beyond the capacity of embedded system in BMS. Therefore, the strategies could not be directly applied to on-line power management system. This strategy has been developed to a basis of a design rule of FCHEV manufacturing, on-line implementation and validation rule of other control logics.[131]

The other strategy is rule-based control strategy. The rule-based control strategy is divided into two topics: fuzzy rule based control method and deterministic rule based control method.[124, 131] The strategy has merit on on-line supervisory control. The rules are suggested based on heuristics, intuition, experience and mathematical model of FCHEV system. Furthermore, knowledge about priori defined driving cycles is not required for rule based control. The deterministic rule based control method is based on heuristics about power flow analysis, efficiency of vehicle, emission map of the ICE and human experiences via lookup table.[141-142] However, the lookup table based method is not suitable in multi-domain, nonlinear and time varying system approach. The deterministic method could not be adopted in real time and obtained suboptimal.

Therefore, the fuzzy rule based methodology has been widely used to control of various vehicles.[126-128] The fuzzy rule based methodology has advantages on robustness and adaptation. The control strategy is tolerant to variation, especially unpredictable driving situation. In addition, the fuzzy control logic is able to be tuned easily than other control logics.[143-144] Therefore, the fuzzy based control logic is appropriate to on-line control of FCHEVs in this thesis.[129]

The fuzzy logic controller is selected for the optimal control of the hybrid energy system. The fuzzy control logic has been widely used as intelligent controller of complex dynamic system and decision maker.[145] The fuzzy control logic has some merits on robustness and adaptation. Consequently, fuzzy logic is selected as controller of target system in this chapter. The fuzzy logic was based on rule-based heuristic method which implements intuitions, experiences and preferences through membership functions and rules.[146] The membership functions represented logical

inference as the universe of discourse. The membership function substituted the linguistic input variables and output variables with smooth curve of mathematical expressions. Triangular, trapezoidal or quadratic functions were usually selected for continuous variables. The fuzzy rules were expressed as matrix format using if-then rules. The number of the fuzzy rules was calculated by multiplication of fuzzy set number of each input variable. Therefore, hierarchy controllers have been used to reduce number of the rules for multivariable fuzzy control.[147]

The fuzzy control system was designed involving five steps. The input variables and output variables were identified with ranges and names. The variables were fuzzified by degree of membership functions. The fuzzy rules were determined by knowledge and experiences and classified by assigning of the weights of the rules. At last, the rules were combined and the output variables were defuzzified. The complex dynamic system was intelligently controlled using the designed fuzzy control system. The general step of fuzzy control had three steps, shown in Fig. 4-5. The input variables and output variables were fuzzified by fuzzy operator. The implementation method was applied by decision making logic based on knowledge and experiences. Finally, the output variables were defuzzified to real space for practical control.

4.3.2. Control problem formulation

The control problem is described in this chapter. The variables for control problems are classified into manipulated variable, controlled variable and state variable in Table 4-3.[148] The demanded power from the vehicle P_{ps} and the SOC value of the lithium-ion battery system are generally selected as input variables in

the previous researches.[13, 127, 139, 149] However, the lithium-ion battery deteriorates over time and the capacity and power of the battery is decreased to 80% over two years.[95] Therefore, consideration about capacity and power fading is required to practical application to FCHEVs. In this study, the input variables include three variables – SOC θ_c, demanded power from the vehicle P_{ps} and SOH. The SOC is estimated by suggested methodology in Chapter 2 and SOH is calculated by developed methodologies in Chapter 3. The demanded power from the vehicle P_{ps} and SOC could be easily adjusted by distribution of power between the fuel cell and the battery. Therefore, the manipulated variables are the demanded power from the vehicle P_{ps} and the battery SOC that affect the fuel cell power and the battery power rapidly. The state variable is SOH that determines the state of the system. The output variable is output power of the fuel cell system P_{fc}. Fuel cell power and battery power are measured on-line and affect the fuel consumption rate that represents a product quality. Therefore, both the output power of the fuel cell system P_{fc} and the output power of the rechargeable battery P_{rb} are classified as controlled variables in this control problem.

The objective of fuzzy control problem is to minimize the fuel consumption of the FCHEV in Eq. 4-13. Therefore, the control problem can be expressed as follows with optimization formula:[150]

$$\text{Minimize: } F_{in,fc} = \left(\frac{RT_{air}}{p_{atm}} \right) \times \frac{P_{fc}}{V} \times 2$$

$$\textit{s.t.} \quad \max SOC(k) \le 80$$

$$\min SOC(k) \ge 40$$

$$\max P_{fc}(k) \le P_{fc\max}$$

80% of the SOC is the upper bound of SOC and 40% of the SOC is the lower bound of SOC as a conservative target. The fuel cell maximum power is determined by specification of the FCHEV in Table 4-1. The control problem with variable selection is applied to fuzzy logic control with three input variables and one output variable in next section.

4.3.3. Design of fuzzy controller

The fuzzy controller with three input variables and one output variable is developed to optimal control of the hybrid energy system shown in Fig. 4-6. The linguistic input variables associated with SOC are low (L), medium (M) and high (H) shown in Fig. 4-7. The appropriate operation condition of SOC is from 40% to 80%. Therefore, the medium range is set to 40% to 80%. The linguistic input variables associated with demanded power from the vehicle are very low (VL), low (L), medium (M) and high (H) shown in Fig. 4-7. The very low conditions are under 10kW which means nearly idle condition or regenerating breaking condition. Finally, the linguistic input variables associated with SOH are low (L), medium (M) and high (H) shown in Fig. 4-7. The SOH value below 80% is typically predicted to reach its end-of-life (EOL) of the lithium-ion battery.[82] Therefore, target operation condition is from 80% to 100% for nominal operation of the rechargeable battery. The linguistic output variables associated with output power of the fuel cell are very low (VL), little low (LL), medium (ME), little high (LH) and very high (VH) shown in Fig. 4-8.

Table 4-4 shows the fuzzy conditional rules with Fig. 4-9 to 4-11. Totally 36 possible rules existed in the rule base. The first rule is interpreted as if “SOC is high”, “demanded power from the vehicle is very low” and “SOH is high”, then output power of the fuel cell is very low. The output power index, if very low, means that the fuel cell system generates very low power for on-board motive power. The SOC is very high and the SOH is high with no fading of the power and capacity. Thus, the battery is ready to be discharged with generating power. The demanded power from the vehicle is very low and the massive power is not needed in this situation. Consequently, very low power is needed to generate by the fuel cell system.

If the SOC level is low, the battery might be charged to maintain the battery SOC range and the fuel cell would generate more power to the powertrain. On the other hand, the SOC level is high, the battery might be discharged to maintain the battery SOC range and the fuel cell would generate less power to the powertrain. The battery would generate power to the powertrain. If the required power from the vehicle is high, both of the fuel cell system and the battery system would generate power to meet the massive power. Thus the fuel cell system generates more power than normal operation condition. On the contrary, the required power from the vehicle is low or very low as idle or regenerate braking condition; the fuel cell system would generate less power. If SOH of the battery is high, the battery would generate more power and store more charges. However, if SOH of the battery is low, the battery would generate less power and store more charges. Therefore, the fuel sell system would generate more power than fresh battery condition. These strategy help avoid abrupt increase in the power generating from the fuel cell and

beyond the range of SOC normal operation.

The output power from the fuel cell system is determined by developed fuzzy logic controller. The input/output power of the battery is determined by difference between the demanded power from the vehicle and the output power from the fuel cell system. The developed fuzzy controller is set by MATLAB® and SIMULINK® environments for implementation.

Table 4-2. Classification of power distribution control problem

Type	Rule based		Optimization based	
	Fuzzy rule based	Deterministic rule based	Global optimization	Real time optimization
Advantages	robustness and adaptation	using heuristics with simple lookup table	global optimum solution	real time control
Disadvantages	suboptimal case	not adopted in real time sub optimal	requirement for predetermined driving cycle	high computational load
Usage	on-line control of FCHEV	degree of hybridization selection	basis of a design rule	basis of a design rule
Method	Conventional fuzzy strategy/ Fuzzy adaptive strategy/ Fuzzy predictive strategy	State machine/ Power follower baseline control/ Modified power follower baseline control/ Thermostat control	Linear programming/ Nonlinear programming/ Dynamic programming/ Stochastic dynamic programming/ Game theory/ Genetic algorithm	Model predictive control/ Decoupling control/ Robust control approach/ Real time control based on equivalent fuel consumption

Table 4-3. Classification of process variables for design control system

Classification	Variables
Manipulated variables	demanded power from the vehicle P_{ps}
	SOC θ_c
State variable	SOH
Controlled variables	output power of the fuel cell system P_{fc}
	output power of the rechargeable battery P_{rb}

Table 4-4. Fuzzy rule base

SOH: H

P_{ps} \ SOC	L	M	H
VL	LL	VL	VL
LL	M	LL	VL
M	LH	M	M
H	VH	LH	LH

SOH: M

P_{ps} \ SOC	L	M	H
VL	LL	LL	VL
LL	M	M	VL
M	LH	LH	M
H	VH	VH	LH

SOH: L

P_{ps} \ SOC	L	M	H
VL	M	LL	LL
LL	LH	M	LL
M	VH	LH	LH
H	VH	VH	VH

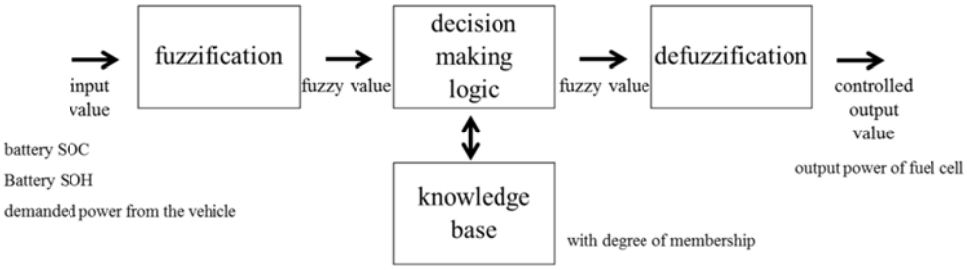

Figure 4-5. Block diagram of fuzzy logic controller.

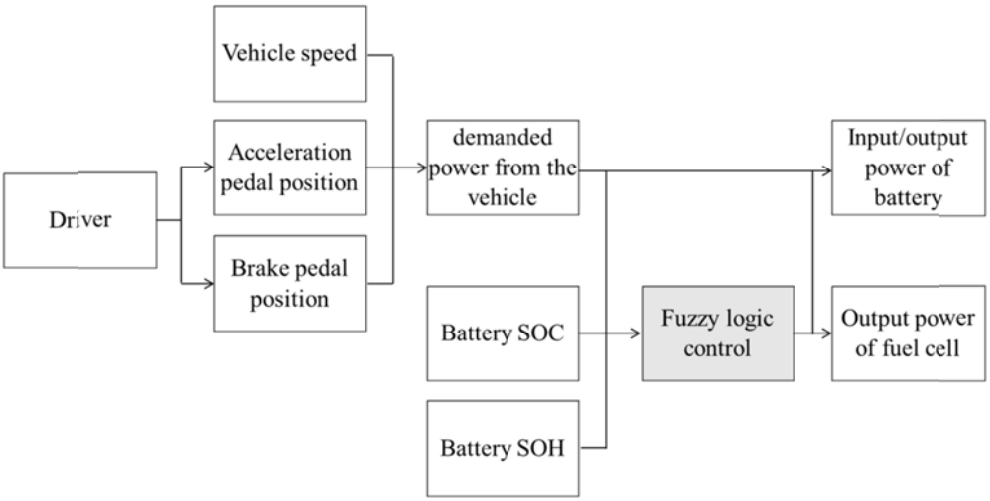

Figure 4-6. Basic control structure of the FCHEVs.

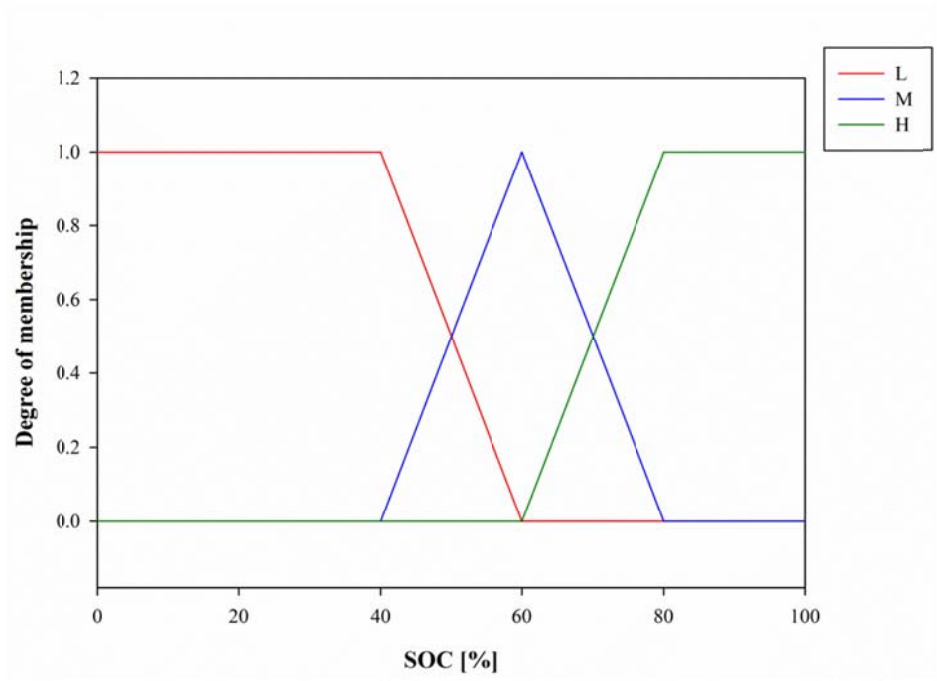
L
M
H
Degree of membership
1.2
1.0
0.8
0.6
0.4
0.2
0.0
0
20
40
60
80
100
SOC [%]

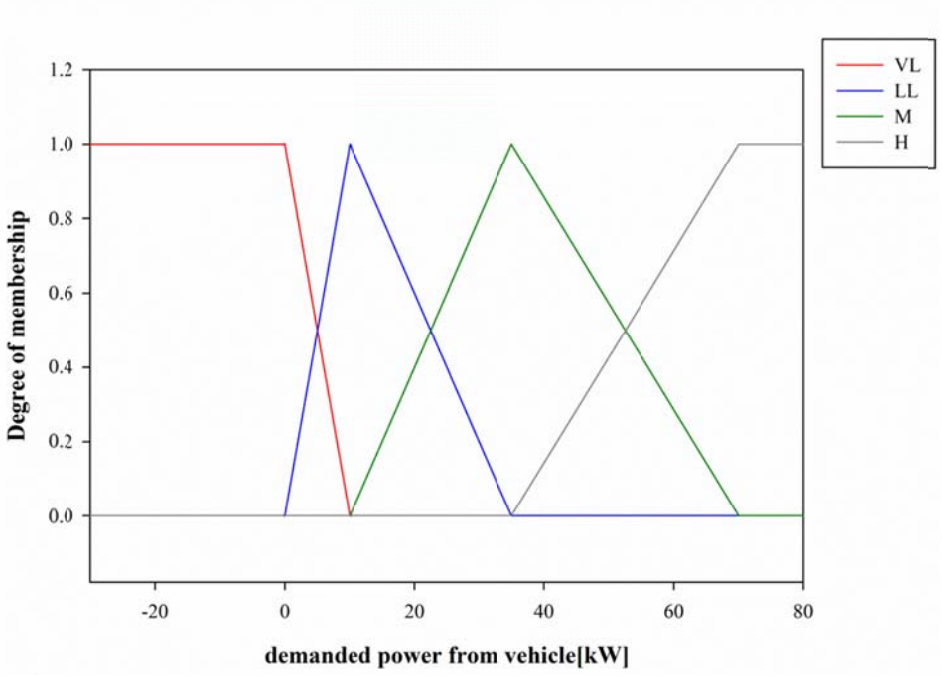
VL
LL
M
H
Degree of membership
1.2
1.0
0.8
0.6
0.4
0.2
0.0
-20
0
20
40
60
80
demanded power from vehicle[kW]

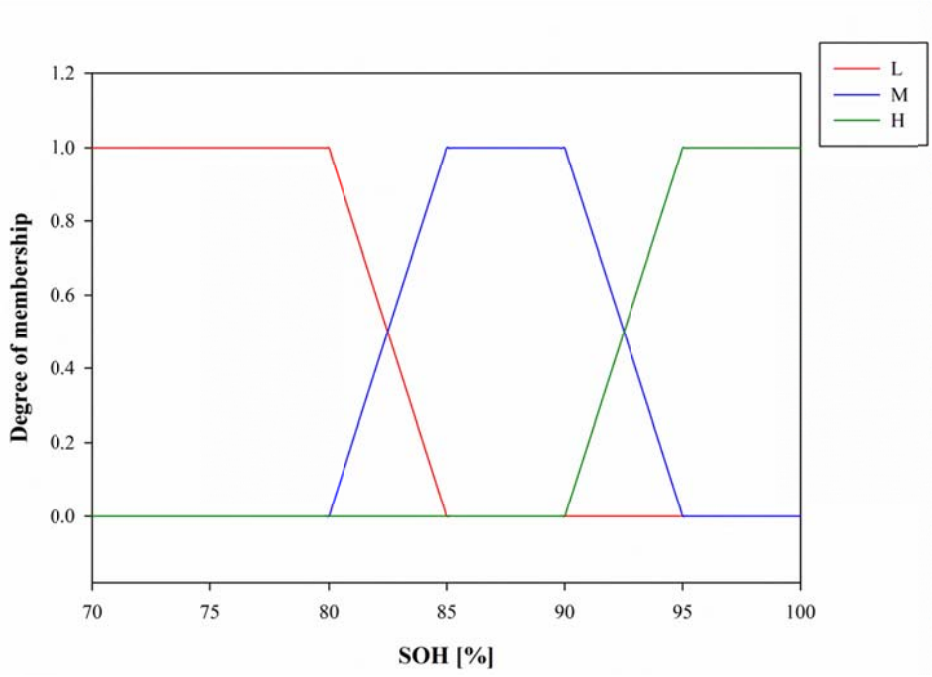

Figure 4-7. Membership functions of input variables.

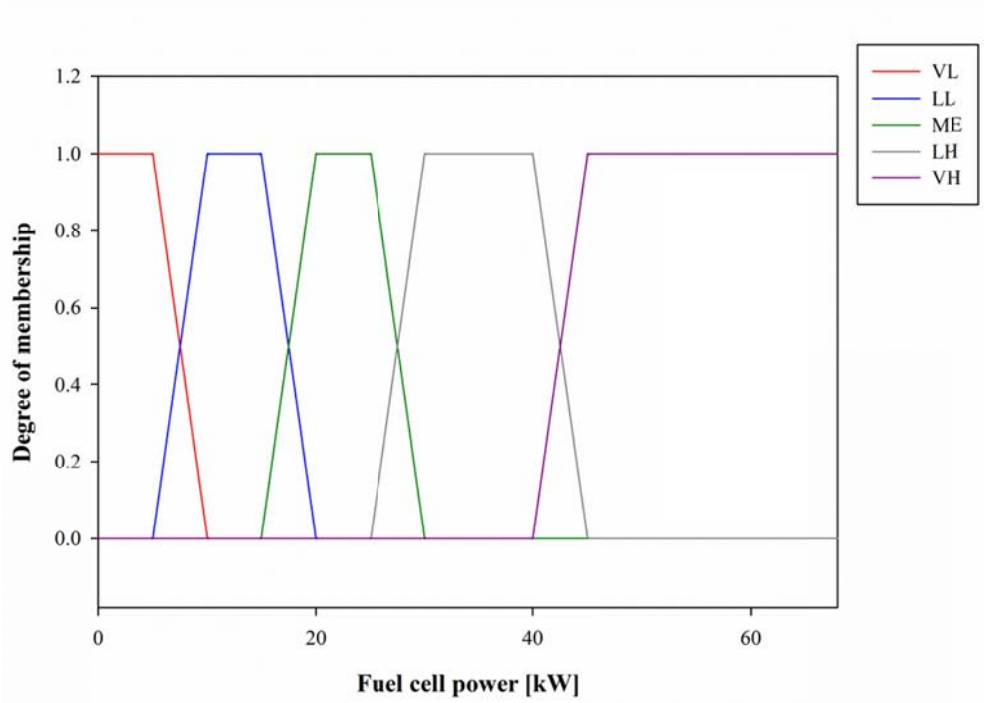

Figure 4-8. Membership functions of output variables.

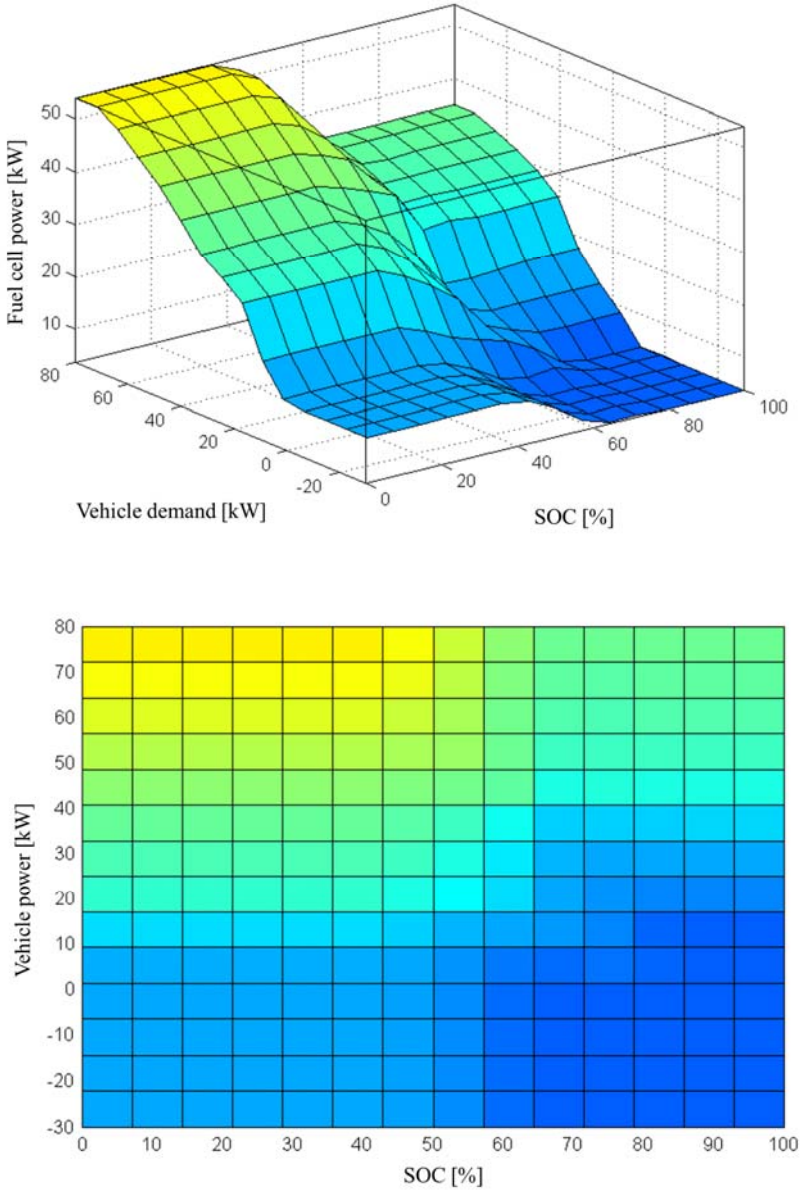

Figure 4-9. Rule base of the fuzzy logic controller at 100% SOH level (H).

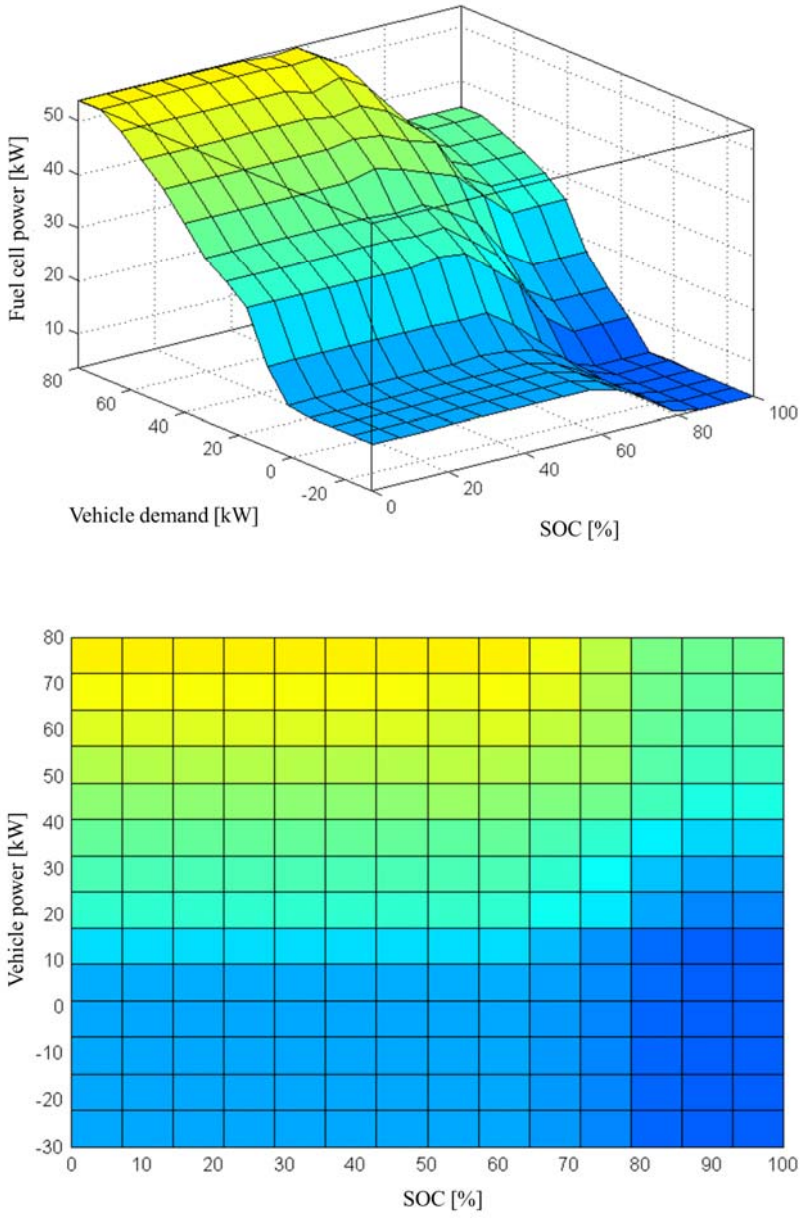

Figure 4-10. Rule base of the fuzzy logic controller at 87.5% SOH level (M).

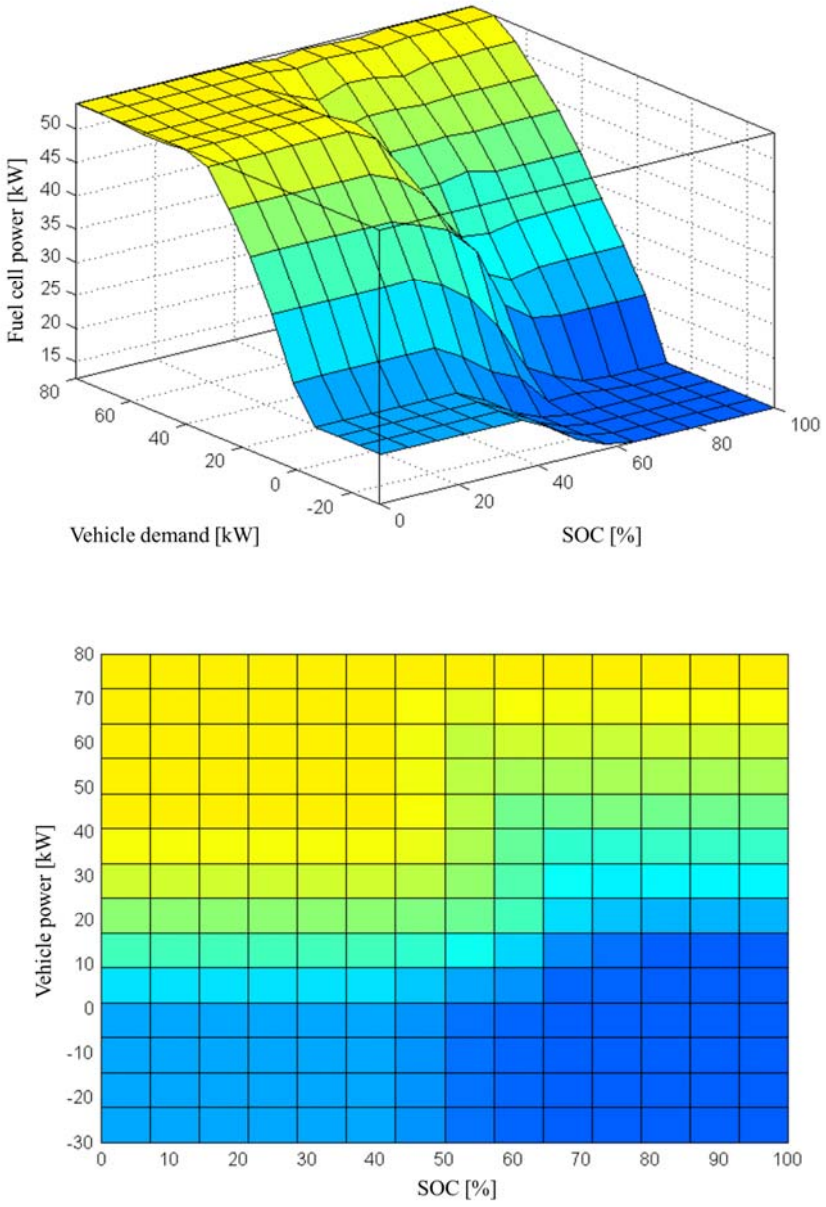

Figure 4-11. Rule base of the fuzzy logic controller at 80% SOH level (L).

4.4. Results and analysis

4.4.1. Vehicle driving schedule

Simulation of the vehicle and hybrid energy system is carried out using above-mentioned model of the PEMFC / lithium-ion battery hybrid energy system and vehicle. The dynamic battery model is modeled by MATLAB® and SIMULINK® environment. The PEMFC system model and vehicle are modeled by Excel with VBA. The simulation schedules are provided to test fuel economy of renewedly developed vehicle by EPA.[128] Two schedules are applied to simulate the vehicle operation – a city driving schedule and a highway driving schedule. The characteristics of two driving schedules are explained in Table 4-5.

The city driving schedule known as urban dynamometer driving schedule (UDDS), U.S. FTP-72 cycle or LA-4 cycle represents city driving schedule for light duty testing. The profile of speed and required power are shown in Fig. 4-12. The speed of the vehicle is widely varied and idle states such as start-up and shut-down repeatedly occurs. Consequently, the battery system is frequently charged and discharged to improve the fuel economy of the vehicle.

The highway driving schedule known as highway fuel economy driving schedule (HWFET) represents highway driving schedule for heavy duty testing. The profile of speed and required power are shown in Fig. 4-13. The peak power demand is infrequently presented according to few speed variation of the vehicle. Furthermore, idle states occur at starting and ending of the schedule. Therefore, the battery system is almost steady to improve the fuel economy.

The objective of optimal control logic is minimizing fuel consumption rate. The

performance index to evaluate the developed control logic is a conventional fuel energy equivalent of the consumed hydrogen fuel. The totally used energy is evaluated in terms of the gasoline liter equivalent per kilometer (GLEPK) with Eq. 4-16.

$$gle = \frac{LHV_{H_2} \int F_{H_2} \rho_{H_2} dt}{L} \times \frac{100}{LHV_{gas} \rho_{gas}} \tag{4-16}$$

The GLEPK is converted to miles per gallon of gasoline equivalent (MPGGE) which means the possible distance using equivalent energy of gasoline with Eq. 4-17.[128]

$$mpg = \frac{1}{\frac{gle}{100} \times \frac{0.264172}{0.539612}} \tag{4-17}$$

4.4.2. Optimal fuzzy control

Several case studies were conducted to demonstrate the developed fuzzy logic controller. The case studies are categorized into two groups as above mentioned: UDDS schedule and HWFET schedule. Furthermore, each case study is validated to three different SOH levels: 100% for high level, 87.5% for medium level and 78% for low level. Each case was evaluated by the MPGGE with SOC range shown in Table 4-6.

Fig. 4-14, 4-15 and 4-16 describe the result of the power control for FCHEV during UDDS pattern. The lithium-ion battery is on the fresh state with 100% SOH value in Fig. 4-14. The fuel cell system is operated moderately and the lithium-ion battery system is operated with rapid change to meet the peak demanded power.

The fuel cell system is operated between 7kW and 30kW of which range has high efficiency.[13] Therefore, the FCHEV is operated efficiently using suggested fuzzy logic. The MPGGE of the FCHEV is enough high at 37.56mpg as verification of system efficiency.

The lithium-ion battery system is degraded to 87.5% level with poor performance of the power and capacity in Fig. 4-15. The lithium-ion battery system could generate less power and store less charge in this state. Therefore, the battery system might generate less power than the case of 100% SOH value with rapid change of charging and discharging. The efficiency of the hybrid energy system is dropped through degradation of the battery system. The fuel cell system generates more power than previous result to cover shortages of output power from the battery. In addition, the fuel cell system is operated less moderately due to frequently charging and discharging of the battery system. The MPGGE of the FCHEV is decreased to 29.16mpg on account of inefficient hybrid energy system. Fig. 4-16 represents the worst case of the battery degradation with 78% SOH value. The battery system could generate little power and the fuel cell system generates more power. The MPGGE of the FCHEV is decreased to 23.10mpg.

Fig. 4-17, 4-18 and 4-19 describe the result of the power control for FCHEV during HWFET pattern. The lithium-ion battery is on the fresh state with 100% SOH value in Fig. 4-17. The battery system is reduced due to lack of start-up and shut-down processes. The fuel cell system is operated in highly efficient range. The MPGGE of the FCHEV is very high about 46.34mpg. The efficiency of the battery is decreased with the battery degradation in the HWFET cases. The battery is rarely operated in Fig. 4-18 and 4-19. The fuel cell system generates more power and the

efficiency is rapidly decreased. The MPGGE of the FCHEV is rapidly decreased in these situations.

4.4.3. Analysis and discussion

The rechargeable lithium-ion battery SOC is fluctuated in nominal operation range between 40% and 80% in SOH 100% condition. In addition, the SOC is operated in nominal value for degraded battery. However, the SOC operation range is moved to low and high range with exception of SOH consideration. The capacity of the battery deteriorates to low value for degraded battery. Therefore, the SOC level is more rapidly increased at the same charging current condition and decreased at the same discharging current conditions.

Furthermore, the instantaneous maximum available power of the rechargeable battery is reduced for degraded cell. The internal resistance of the battery is increased in this situation. Therefore, the battery generates more current for producing or storing same amount of power at fresh cell state. Therefore, the SOC value is fluctuated rapidly without consideration of SOH value at fuzzy control. The SOC range is increased about 49.27% at the case of 87.5% SOH value. Therefore, the SOC range is changed to 36.34% at UDDS pattern experiments. The battery system is operated over the nominal value. Moreover, the SOC range is increased about 110.73% at the case of 78% SOH value. The SOC range is changed to 51.31% at UDDS pattern experiments. Therefore, the battery is operated in dangerous range for degradation and life of the battery is rapidly shortened in this situation.[137]

Therefore, the cost of replacement is increased using fuzzy control logic without

SOH consideration. On the other hand, the rechargeable battery is operated in nominal range until EOL with suggested fuzzy control logic. The operating cost of the FCHEVs would be reduced by prolonging of battery life. Consequently, the suggested fuzzy control logic including SOH consideration is appropriate to commercialization and practical application to various types of eco-friendly vehicles.

Table 4-5. Description of two driving schedules

Driving schedule	UDDS	HWFET
Time [s]	1369	765
Distance [m]	11990	16512
Average speed [m s^{-1}]	8.75	21.55
Maximum speed [m s^{-1}]	25.35	26.78
Average acceleration [m s^{-2}]	0.50	0.19
Average deceleration [m s^{-2}]	-0.58	-0.22
Idle state time [s]	259	6

Table 4-6. MPGGE and SOC range comparison of various operating conditions.

Driving mode	SOH level [%]	MPGGE [mpg]	SOC range [%]
UDDS	100	37.56	22.35
	87.5	29.16	22.69
	78	23.10	20.33
HWFET	100	46.34	18.81
	87.5	36.75	17.20
	78	28.86	14.74

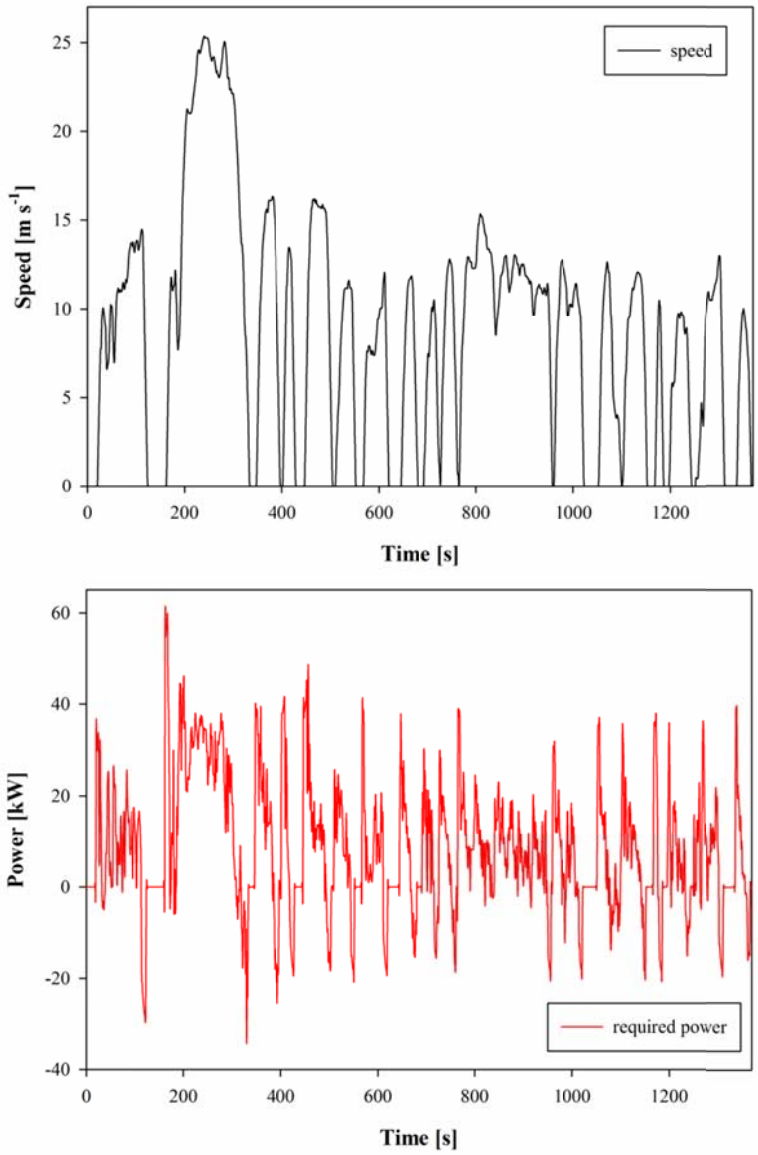

Figure 4-12. Speed and required power of the UDDS schedule.

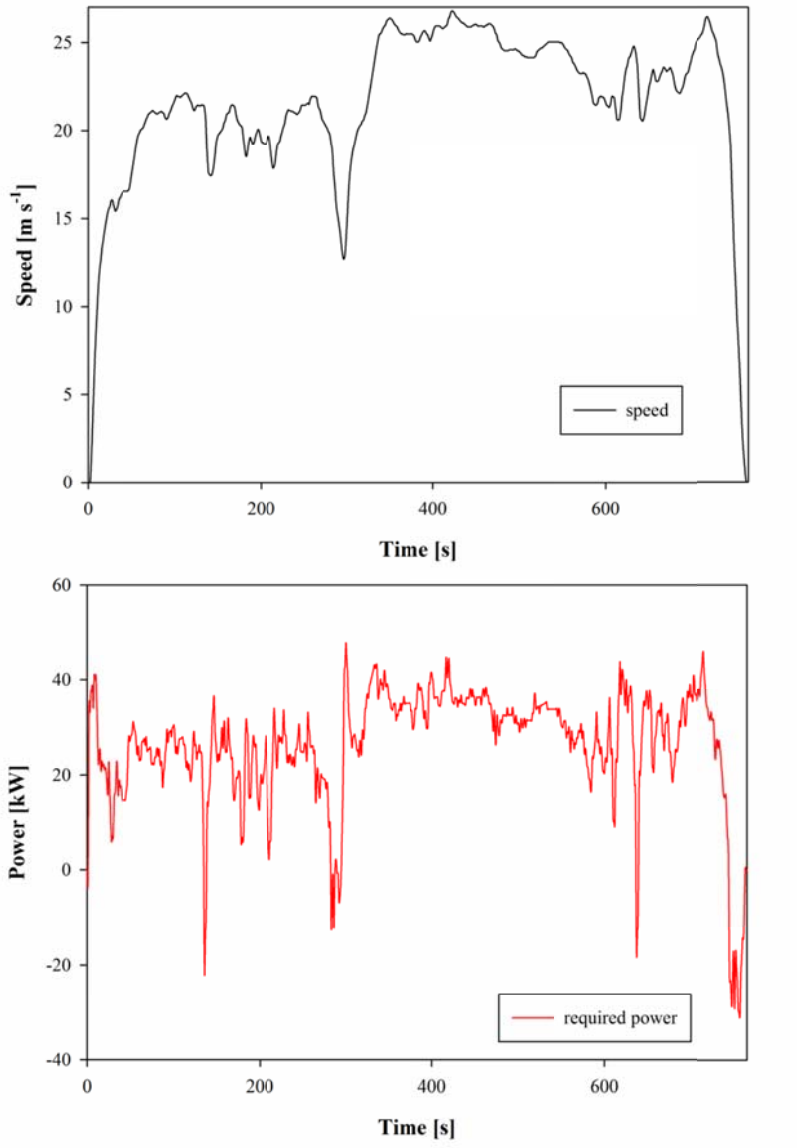

Figure 4-13. Speed and required power of the HWFET schedule.

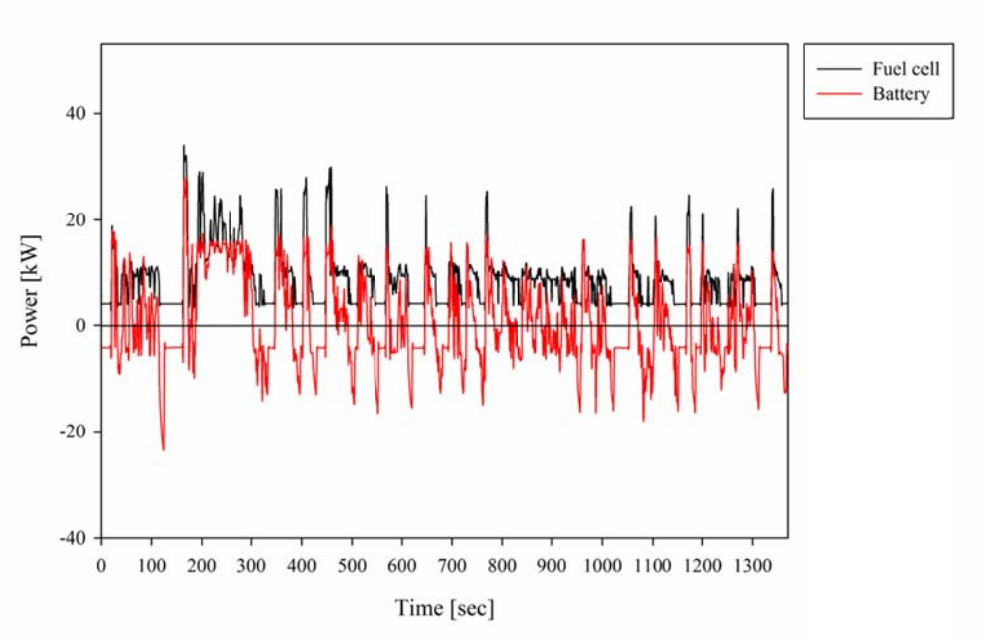

Figure 4-14. Power control for FCHEV during UDDS pattern at 100% SOH level.

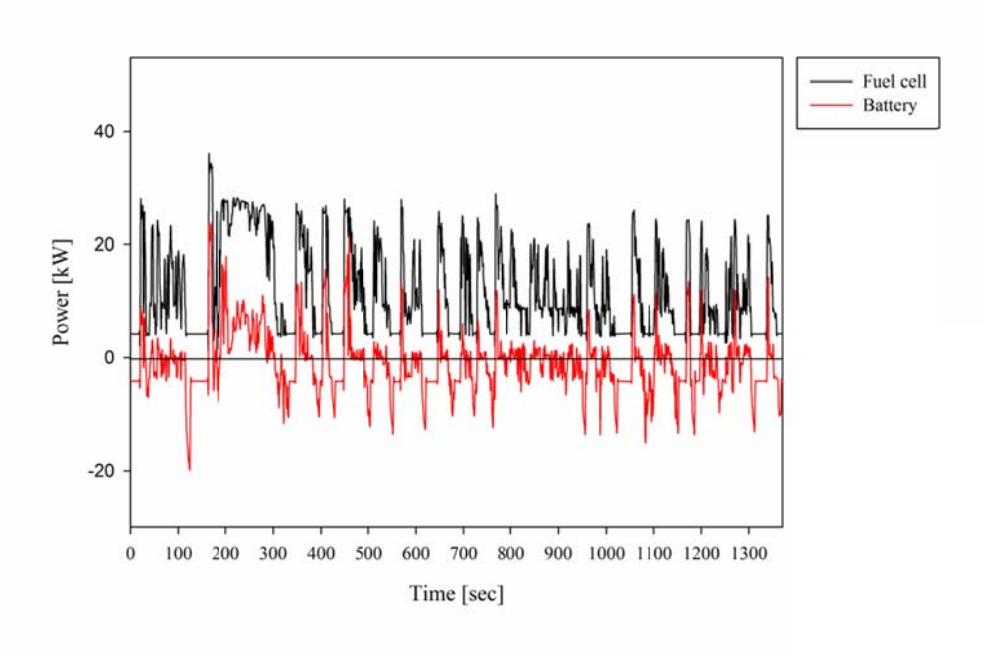

Figure 4-15. Power control for FCHEV during UDDS pattern at 87.5% SOH level.

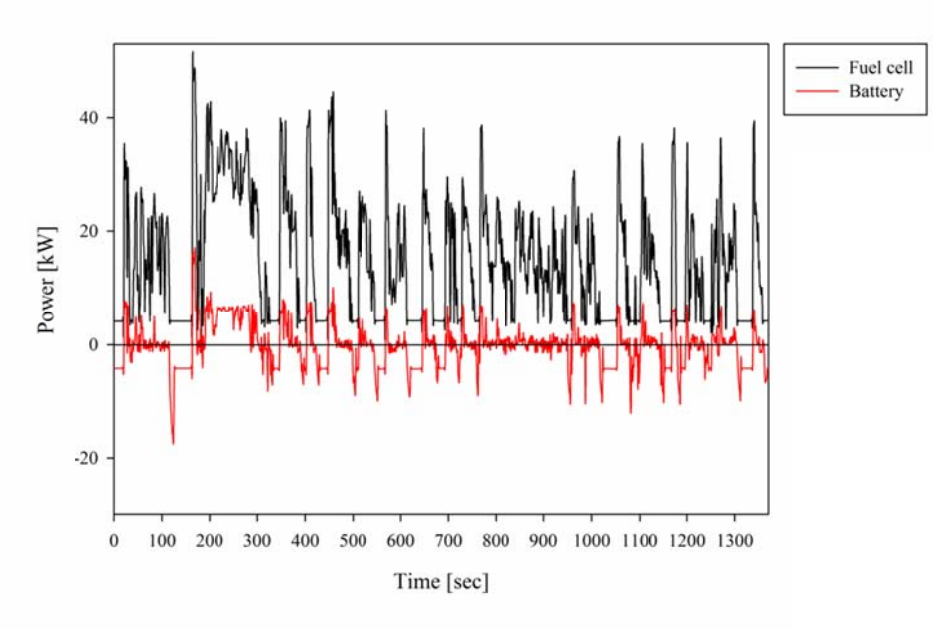

Figure 4-16. Power control for FCHEV during UDDS pattern at 78% SOH level.

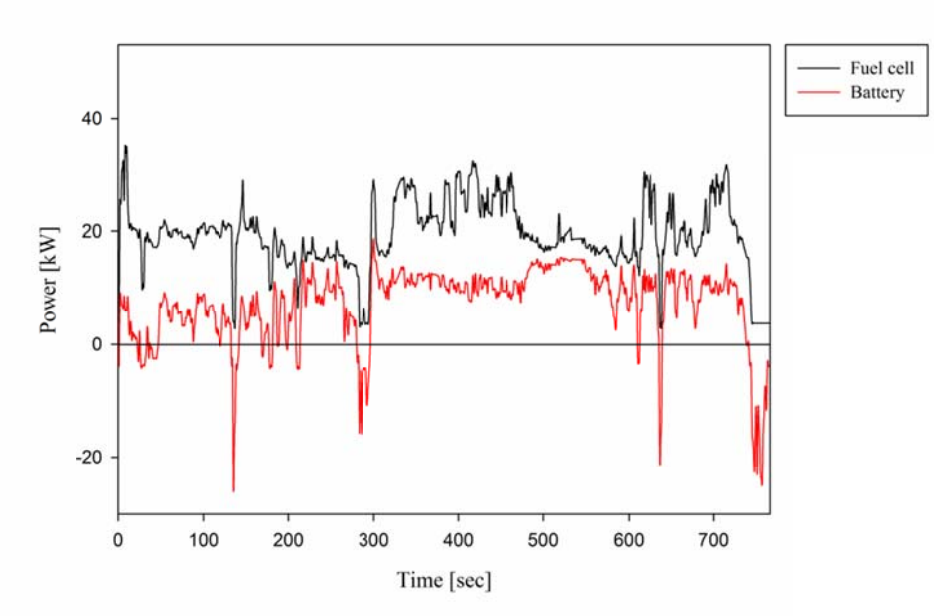

Figure 4-17. Power control for FCHEV during HWFET pattern at 100% SOH level.

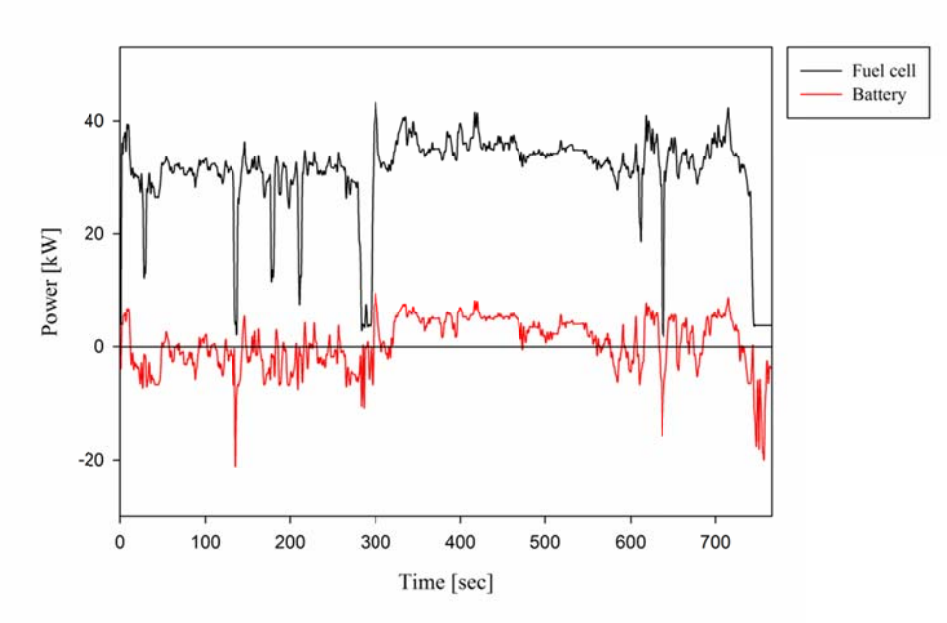

Figure 4-18. Power control for FCHEV during HWFET pattern at 87.5% SOH level.

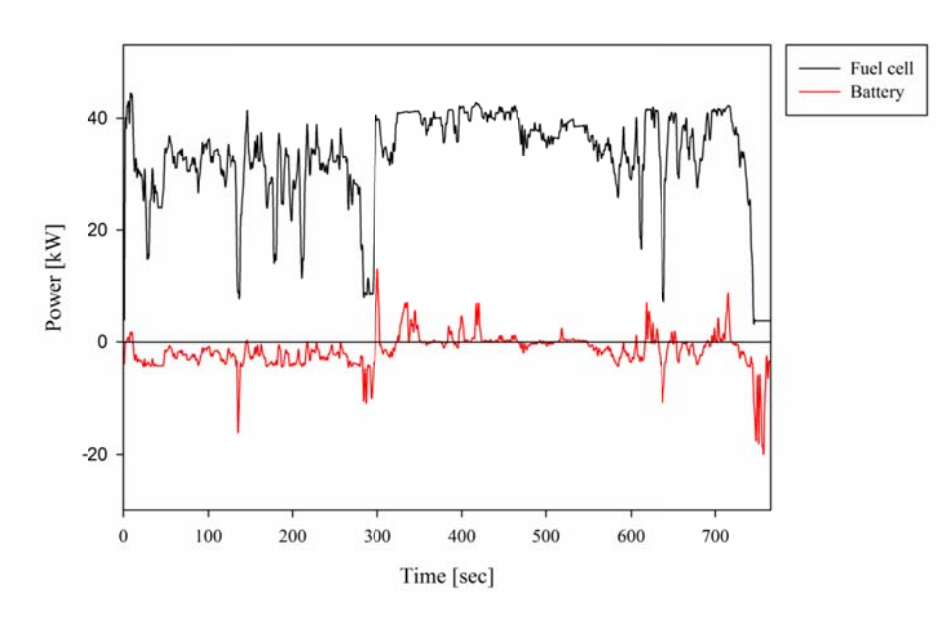

Figure 4-19. Power control for FCHEV during HWFET pattern at 78% SOH level.

4.5. Conclusions

The optimal control logic for lithium-ion battery / proton exchange membrane fuel cell hybrid energy system was developed using fuzzy logic controller. The developed lithium-ion battery system model was applied to the operation simulation. In addition, PEMFC zero dimensional process model with hydrogen recirculation and cathode humidifier was developed in this chapter. The intelligent controller was suggested by fuzzy logic control algorithm. Various input variables as SOC, SOH and demanded power of the FCHEV were used to the fuzzy logic controller to calculate the output power from the fuel cell system. The fuzzy rules were set to optimal control. The results from various operations for FCHEV applications demonstrated the performance of the developed control logic. The hybrid energy system was operated with high efficiency at 100% SOH condition. However, the efficiency was decreased with degradation of the lithium-ion battery system. The developed control logic could be applied to commercialization of hybrid energy system applications such as FCHEVs through the covering performance of various situations.

CHAPTER 5 : Concluding Remarks

5.1. Conclusions

This thesis has addressed modeling, state estimation and dynamic control of lithium-ion battery for the hybrid energy system. The developed models, methodologies and control logic were demonstrated by HEV, PHEV and FCHEV applications.

The rigorous dynamic model for lithium-ion battery was developed as equivalent circuit model. The objective of the developed model was system identification and control of lithium-ion battery system under various conditions: fluctuating currents, SOC ranges, SOH range and temperatures. The model was enhanced and refined with suggested parameter estimation technique. The error minimization technique was applied to the parameter estimation technique. The developed model was validated under various conditions for HEV applications. The average errors for ambient condition operation were under 0.2%. Furthermore, the average errors for low temperature condition operation even temperature fluctuation conditions were under 0.5%. The developed lithium-ion battery model was expected to be valuable in various applications such as BMSs in hybrid electric vehicles, plug-in hybrid electric vehicles or fuel cell hybrid electric vehicles. Furthermore, suggested battery dynamic model was applied to state estimation and control logic in this thesis.

The suggested on-line state estimation methodologies were categorized to two objects: SOC estimation and SOH estimation. The SOC estimation methodology

was a combination of the conventional current integration method and model based estimation method. Both of the SOCs were integrated in the methodology and their shortcomings were overcome with the developed battery model. The developed SOC estimation methodology was validated under various conditions for current fluctuations, temperature changes and sensor faults. As a result, the developed methodology guaranteed good accuracy and reliability against transient errors in the sensor measured data. The developed estimation methodology was expected to application in various types of lithium-ion battery system. Furthermore, suggested methodology was applied to control logic in this thesis.

The on-line SOH estimation was suggested with three types: principal algorithm, supplementary algorithm and hybridized algorithm. The principal algorithm based on the system identification method with variance inhibition based approach achieved accuracy and reliability against the inaccurate previous estimated values in estimating the capacity and power fading. The supplementary algorithm based on the simplified model had advantage of on-line computation but had a lower accuracy than that of the principal algorithm. Consequently, the hybridized algorithm was developed by combination of principal and supplementary algorithms. The results from various operation experiments for HEV and PHEV applications demonstrated the congruence of the accuracy, reliability against the inaccurate previous estimated values and computational load. The hybridized algorithm was expected to adequate methodology for accurate on-line estimation of the actual battery performance as quantitative values of capacity and power in real time. Furthermore, suggested methodologies were applied to control logic in this thesis.

Lastly, the optimal control logic for lithium-ion battery / proton exchange membrane fuel cell hybrid energy system was presented using fuzzy logic controller. The lithium-ion battery system model, PEMFC process model and FCHEV model were applied to simulate real operation of FCHEVs as the hybrid energy system. Three input variables were used to the fuzzy logic controller to calculate the output power from the fuel cell system. The results from various operations for FCHEV applications demonstrated the performance of the developed control logic. The control logic could manage the power distribution within various operation conditions. Especially, the hybrid energy system was operated with high efficiency at 100% SOH condition. However, the efficiency was decreased by the SOH value decreasing. The developed control logic could be applied to commercialization of FCHEVs through the covering performance of various situations.

5.2. Future works

Further researches for lithium-ion battery system can be considerably extended for practical application to the eco-friendly vehicles and other hybrid energy systems. The developed models and methodologies can be validated under various real world situations of field data. The parameters in the fuzzy control logic can be optimized by genetic algorithm using the field data. In addition, fault monitoring and diagnosis technique is expected to be developed for the commercialization of the eco-friendly vehicles. Also, the developed models and methodologies were conducted under equivalent cell performance. Consequently, the monitoring system of each lithium-ion battery cell in the pack is required to real world application of BMS. Lastly, the developed models and methodologies can be applied to other application of the lithium-ion battery system such as mobile phone, smart phone and portable electronics applications with a little modifications and supplementations.

Nomenclature

A	Covariance matrix for the parameter estimation
A_f	Front area of the vehicle [m^2]
a	Absolute current value [A]
a_i	Activity
a_{ii}	ith element of the diagonal of the covariance matrix
b_i	Estimated value of the parameter β_i
C_i	Electric double layer capacitor [F]
C_D	Aerodynamic drag coefficient
D	Duration of the low current [s]
eff	Efficiency
F	Faraday constant (96,485 C mol^{-1})
F_i	ith element of fuel consumption rate (L min^{-1})
f_r	Rolling resistance of the tires
g	Gravity acceleration [m s^{-2}]
gle	Gasoline liter equivalent per kilometer [L km^{-1}]
i	Current [A]
J	Jacobian matrix used for parameter estimation
k	Discrete-time increment for measured data acquisition
L	Distance [km]
LHV	Low heating value
M	Mass [kg]

m	Number of previous estimated capacity considered in moving average calculation
mpg	Miles per gallon of gasoline equivalent [mile gal^{-1}]
P_i	Power demand (kW)
p	Pressure (atm)
Q	Capacity of battery [Ah]
Q_0	Charge capacitance in equivalent circuit model [Ah]
$Q_{0,max}$	Maximum battery capacity at fresh battery state [Ah]
R	Molar gas constant (8.314 J mol^{-1} K^{-1})
R_0	Lumped series resistance [Ω]
R_i	Lumped interfacial resistances [Ω]
R_t	Lumped resistance for simplified equivalent circuit model [Ω]
s	standard deviation of the model error
T	Temperature [K]
t	Time [s]
t_a	Acceleration time [s]
$t_{(1-\alpha/2)}$	Statistic for a confidence level of (1− α) given by Student's t-distribution
V	Experimentally measured battery voltage [V]
$\hat{V}$	Model-estimated battery voltage [V]
V_0	Open circuit voltage [V]
v_f	Final speed of accelerating [m s^{-1}]
v_v	Vehicle speed [m s^{-1}]
w_m	Weighting factor for moving average calculation

w_Q	Capacity weighting factor for variance inhibiting term
w_R	Resistance weighting factor for variance inhibiting term

Greek letters

α_i	*i*th order polynomial coefficient in SOC-OCV 4th-order relationship
β_i	Unknown model parameter
γ_i	*i*th order polynomial coefficient in SOC-OCV linear relationship
δ	Mass factor
η	Electrode overpotential (V)
θ	State-of-charge (SOC) [%]
θ_c	Final estimated value of state-of-charge by SOC estimation methodology [%]
θ_i	State-of-charge estimated by current integration [%]
θ_v	State-of-charge estimated by battery model [%]
v	volumetric flow rate (L min^{-1})
ξ	Integrating factor
ρ	Density at average temperature (kg m^{-3})
Ψ	Sum square error

Subscripts

air	Air
an	Anode
cat	Cathode

fc	Fuel cell
i j	Species i, j
in	Channel inlet flow
out	Channel outlet flow
ps	Power source
rb	Rechargeable battery
veh	Vehicle

Abbreviations

BEV	Battery electric vehicle
BMS	Battery management system
EPA	Environmental Protection Agency
ECM	Equivalent circuit model
FCHEV	Fuel cell hybrid electric vehicle
GLEPK	Gasoline liter equivalent per kilometer
HEV	Hybrid electric vehicle
HWFET	Highway fuel economy driving schedule
MPGGE	Miles per gallon of gasoline equivalent
MSE	Mean squared error
OCV	Open circuit voltage
PEMFC	Proton exchange membrane fuel cell
PHEV	Plug-in hybrid electric vehicle
SOC	State-of-charge
SOH	State-of-health

SSE	Sum square error
UDDS	Urban dynamometer driving schedule

Literature cited

1. Ehsani, M.; Gao, Y.; Emadi, A., Modern electric, hybrid electric, and fuel cell vehicles: fundamentals, theory, and design. *CRC*: **2009**.

2. Jansen, A.; Kahaian, A.; Kepler, K.; Nelson, P.; Amine, K.; Dees, D.; Vissers, D.; Thackeray, M., Development of a high-power lithium-ion battery. *Journal of Power Sources*, **1999**, 81, 902-905.

3. Maggetto, G.; Van Mierlo, J. In *Electric vehicles, hybrid electric vehicles and fuel cell electric vehicles: state of the art and perspectives*, Elsevier: 2001; pp 9-26.

4. Newman, J. S.; Thomas-Alyea, K. E., Electrochemical systems. *Wiley-Interscience*: **2004**.

5. Park, H. S.; Kim, C. E.; Kim, C. H.; Moon, G. W.; Lee, J. H., A Modularized Charge Equalization Converter for a Hybrid Electric Vehicle Lithium-Ion Battery Stack. *J. Power Electronics*, **2007**, 7 (4), 343-352.

6. Eberle, U.; von Helmolt, R., Sustainable transportation based on electric vehicle concepts: a brief overview. *Energy Environ. Sci.*, **2010**, 3 (6), 689-699.

7. EIA, U., Annual Energy Outlook 2011. *Energy Information Administration*, **2010**.

8. Rosenberg, E.; Fidje, A.; Espegren, K. A.; Stiller, C.; Svensson, A. M.; Møller-Holst, S., Market penetration analysis of hydrogen vehicles in Norwegian passenger transport towards 2050. *International Journal of Hydrogen Energy*, **2010**, 35 (14), 7267-7279.

9. Offer, G.; Contestabile, M.; Howey, D.; Clague, R.; Brandon, N., Techno-economic and behavioural analysis of battery electric, hydrogen fuel cell and hybrid vehicles in a future sustainable road transport system in the UK. *Energy Policy*, **2011**.

10. Jiang, Z.; Gao, L.; Blackwelder, M. J.; Dougal, R. A., Design and experimental tests of control strategies for active hybrid fuel cell/battery power sources. *Journal of power sources*, **2004**, 130 (1-2), 163-171.

11. Ouyang, M.; Xu, L.; Li, J.; Lu, L.; Gao, D.; Xie, Q., Performance comparison of two fuel cell hybrid buses with different powertrain and energy management strategies. *Journal of Power Sources*, **2006**, 163 (1), 467-479.

12. Aguiar, P.; Brett, D.; Brandon, N., Feasibility study and techno-economic analysis of an SOFC/battery hybrid system for vehicle applications. *Journal of Power Sources*, **2007**, 171 (1), 186-197.

13. Kim, M. J.; Peng, H., Power management and design optimization of fuel cell/battery hybrid vehicles. *Journal of Power Sources*, **2007**, 165 (2), 819-832.

14. Chan, C.; Bouscayrol, A.; Chen, K., Electric, hybrid, and fuel-cell vehicles: Architectures and modeling. *Vehicular Technology, IEEE Transactions on*, **2010**, 59 (2), 589-598.

15. Miller, J. M., Propulsion systems for hybrid vehicles. *Peter Peregrinus Ltd*: **2004**; Vol. 45.

16. Simpson, A.; Laboratory, N. R. E., Cost-benefit analysis of plug-in hybrid electric vehicle technology. *National Renewable Energy Laboratory*: **2006**.

17. Elgowainy, A.; Burnham, A.; Wang, M.; Molburg, J.; Rousseau, A., Well-to-wheels energy use and greenhouse gas emissions of plug-in hybrid electric

vehicles. *SAE International Journal of Fuels and Lubricants*, **2009**, 2 (1), 627.

18. Çağatay Bayindir, K.; Gözüküçük, M. A.; Teke, A., A comprehensive overview of hybrid electric vehicle: Powertrain configurations, powertrain control techniques and electronic control units. *Energy conversion and management*, **2011**, 52 (2), 1305-1313.

19. Chan, C., The state of the art of electric and hybrid vehicles. *Proceedings of the IEEE*, **2002**, 90 (2), 247-275.

20. Chan, C., The state of the art of electric, hybrid, and fuel cell vehicles. *Proceedings of the IEEE*, **2007**, 95 (4), 704-718.

21. Paganelli, G.; Guerra, T.; Delprat, S.; Santin, J.; Delhom, M.; Combes, E., Simulation and assessment of power control strategies for a parallel hybrid car. *Proceedings of the Institution of Mechanical Engineers, Part D: Journal of Automobile Engineering*, **2000**, 214 (7), 705-717.

22. Salman, M.; Schouten, N. J.; Kheir, N. A. In *Control strategies for parallel hybrid vehicles*, IEEE: 2000; pp 524-528 vol. 521.

23. Bradley, T. H.; Frank, A. A., Design, demonstrations and sustainability impact assessments for plug-in hybrid electric vehicles. *Renewable and Sustainable Energy Reviews*, **2009**, 13 (1), 115-128.

24. Khaligh, A.; Li, Z., Battery, ultracapacitor, fuel cell, and hybrid energy storage systems for electric, hybrid electric, fuel cell, and plug-in hybrid electric vehicles: State of the art. *Vehicular Technology, IEEE Transactions on*, **2010**, 59 (6), 2806-2814.

25. Kim, M.; Sohn, Y. J.; Lee, W. Y.; Kim, C. S., Fuzzy control based engine sizing optimization for a fuel cell/battery hybrid mini-bus. *Journal of Power*

Sources, **2008**, 178 (2), 706-710.

26. Lukic, S. M.; Cao, J.; Bansal, R. C.; Rodriguez, F.; Emadi, A., Energy storage systems for automotive applications. *Industrial Electronics, IEEE Transactions on*, **2008**, 55 (6), 2258-2267.

27. Wenzl, H.; Baring-Gould, I.; Kaiser, R.; Liaw, B. Y.; Lundsager, P.; Manwell, J.; Ruddell, A.; Svoboda, V., Life prediction of batteries for selecting the technically most suitable and cost effective battery. *Journal of power sources*, **2005**, 144 (2), 373-384.

28. Kaiser, R., Optimized battery-management system to improve storage lifetime in renewable energy systems. *Journal of power sources*, **2007**, 168 (1), 58-65.

29. Peterson, S. B.; Apt, J.; Whitacre, J., Lithium-ion battery cell degradation resulting from realistic vehicle and vehicle-to-grid utilization. *Journal of power sources*, **2010**, 195 (8), 2385-2392.

30. Wood, E.; Alexander, M.; Bradley, T. H., Investigation of battery end-of-life conditions for plug-in hybrid electric vehicles. *Journal of power sources*, **2011**, 196 (11), 5147-5154.

31. Zhang, J.; Lee, J., A review on prognostics and health monitoring of Li-ion battery. *Journal of power sources*, **2011**, 196 (15), 6007-6014.

32. Schmidt, A. P.; Bitzer, M.; Imre, Á. W.; Guzzella, L., Model-based distinction and quantification of capacity loss and rate capability fade in Li-ion batteries. *Journal of power sources*, **2010**, 195 (22), 7634-7638.

33. Chiang, Y. H.; Sean, W. Y.; Ke, J. C., Online estimation of internal resistance and open-circuit voltage of lithium-ion batteries in electric vehicles.

Journal of power sources, **2011**.

34. Chau, K.; Wong, Y., Overview of power management in hybrid electric vehicles. *Energy conversion and management*, **2002**, 43 (15), 1953-1968.

35. Newnham, R.; Baldsing, W., Advanced management strategies for remote-area power-supply systems. *Journal of Power Sources*, **2004**, 133 (1), 141-146.

36. Khateeb, S. A.; Farid, M. M.; Selman, J. R.; Al-Hallaj, S., Mechanical–electrochemical modeling of Li-ion battery designed for an electric scooter. *Journal of Power Sources*, **2006**, 158 (1), 673-678.

37. Henson, W., Optimal battery/ultracapacitor storage combination. *Journal of Power Sources*, **2008**, 179 (1), 417-423.

38. Cho, S.; Jeong, H.; Han, C.; Jin, S.; Lim, J. H.; Oh, J., State-of-charge estimation for lithium-ion batteries under various operating conditions using an equivalent circuit model. *Computers & Chemical Engineering*, **2012**, 41 (0), 1-9.

39. Kornfeil, F., Some Observations on the Prediction of the State of Discharge of Batteries. *Journal of the Electrochemical Society*, **1976**, 123, 1271.

40. Rodrigues, S.; Munichandraiah, N.; Shukla, A., A review of state-of-charge indication of batteries by means of ac impedance measurements. *Journal of Power Sources*, **2000**, 87 (1), 12-20.

41. Plett, G. L., Extended Kalman filtering for battery management systems of LiPB-based HEV battery packs: Part 1. Background. *Journal of Power Sources*, **2004**, 134 (2), 252-261.

42. Gregory L, P., Extended Kalman filtering for battery management systems of LiPB-based HEV battery packs: Part 2. Modeling and identification.

Journal of power sources, **2004**, 134 (2), 262-276.

43. Gregory L, P., Extended Kalman filtering for battery management systems of LiPB-based HEV battery packs: Part 3. State and parameter estimation. *Journal of power sources*, **2004**, 134 (2), 277-292.

44. Hansen, T.; Wang, C. J., Support vector based battery state of charge estimator. *Journal of Power Sources*, **2005**, 141 (2), 351-358.

45. Plett, G. L., Sigma-point Kalman filtering for battery management systems of LiPB-based HEV battery packs: Part 1: Introduction and state estimation. *Journal of Power Sources*, **2006**, 161 (2), 1356-1368.

46. Plett, G. L., Sigma-point Kalman filtering for battery management systems of LiPB-based HEV Battery packs: Part 2: Simultaneous state and parameter estimation. *Journal of Power Sources*, **2006**, 161 (2), 1369-1384.

47. Singh, P.; Vinjamuri, R.; Wang, X.; Reisner, D., Design and implementation of a fuzzy logic-based state-of-charge meter for Li-ion batteries used in portable defibrillators. *Journal of Power Sources*, **2006**, 162 (2), 829-836.

48. Lee, S.; Kim, J.; Lee, J.; Cho, B., State-of-charge and capacity estimation of lithium-ion battery using a new open-circuit voltage versus state-of-charge. *Journal of Power Sources*, **2008**, 185 (2), 1367-1373.

49. Wang, J.; Cao, B.; Chen, Q.; Wang, F., Combined state of charge estimator for electric vehicle battery pack. *Control Engineering Practice*, **2007**, 15 (12), 1569-1576.

50. Han, J.; Kim, D.; Sunwoo, M., State-of-charge estimation of lead-acid batteries using an adaptive extended Kalman filter. *Journal of Power Sources*, **2009**, 188 (2), 606-612.

51. Kim, J.; Lee, S.; Cho, B., Discrimination of Li-ion batteries based on Hamming network using discharging–charging voltage pattern recognition for improved state-of-charge estimation. *Journal of Power Sources*, **2011**, 196 (4), 2227-2240.

52. Weigert, T.; Tian, Q.; Lian, K., State-of-charge prediction of batteries and battery–supercapacitor hybrids using artificial neural networks. *Journal of Power Sources*, **2011**, 196 (8), 4061-4066.

53. Tatur, M.; Tyrer, H.; Tomazic, D.; Thornton, M.; McDonald, J., Tier 2 Intermediate Useful Life (50,000 Miles) and 4000 Mile Supplemental Federal Test Procedure (SFTP) Exhaust Emission Results for a NOx Adsorber and Diesel Particle Filter Equipped Light-Duty Diesel Vehicle. **2005**; p Medium: X; Size: pp. 287-303.

54. Gomez, J.; Nelson, R.; Kalu, E. E.; Weatherspoon, M. H.; Zheng, J. P., Equivalent circuit model parameters of a high-power Li-ion battery: Thermal and state of charge effects. *Journal of Power Sources*, **2011**.

55. Garcia, R. E.; Chiang, Y. M.; Carter, W. C.; Limthongkul, P.; Bishop, C. M., Microstructural modeling and design of rechargeable lithium-ion batteries. *Journal of the Electrochemical Society*, **2005**, 152, A255.

56. Sikha, G.; White, R. E.; Popov, B. N., A mathematical model for a lithium-ion battery/electrochemical capacitor hybrid system. *Journal of the Electrochemical Society*, **2005**, 152, A1682.

57. Catti, M.; Montero-Campillo, M., First-principles modelling of lithium iron oxides as battery cathode materials. *Journal of Power Sources*, **2011**, 196 (8), 3955-3961.

58. Martínez-Rosas, E.; Vasquez-Medrano, R.; Flores-Tlacuahuac, A., Modeling and simulation of lithium-ion batteries. *Computers & Chemical Engineering*, **2011**.

59. Methekar, R. N.; Ramadesigan, V.; Pirkle Jr, J. C.; Subramanian, V. R., A perturbation approach for consistent initialization of index-1 explicit Differential-Algebraic Equations arising from battery model simulations. *Computers & Chemical Engineering*, **2011**.

60. Subramanian, V. R.; Boovaragavan, V.; Ramadesigan, V.; Arabandi, M., Mathematical model reformulation for lithium-ion battery simulations: Galvanostatic boundary conditions. *Journal of the Electrochemical Society*, **2009**, 156, A260.

61. Dao, T. S.; Vyasarayani, C. P.; McPhee, J., Simplification and order reduction of lithium-ion battery model based on porous-electrode theory. *Journal of Power Sources*, **2011**.

62. Jung, D. Y.; Lee, B. H.; Kim, S. W., Development of battery management system for nickel-metal hydride batteries in electric vehicle applications. *Journal of Power Sources*, **2002**, 109 (1), 1-10.

63. Junping, W.; Quanshi, C.; Binggang, C., Support vector machine based battery model for electric vehicles. *Energy conversion and management*, **2006**, 47 (7), 858-864.

64. Snihir, I.; Rey, W.; Verbitskiy, E.; Belfadhel-Ayeb, A.; Notten, P. H. L., Battery open-circuit voltage estimation by a method of statistical analysis. *Journal of Power Sources*, **2006**, 159 (2), 1484-1487.

65. Verbrugge, M. W.; Liu, P.; Soukiazian, S., Activated-carbon electric-

double-layer capacitors: electrochemical characterization and adaptive algorithm implementation. *Journal of Power Sources*, **2005**, 141 (2), 369-385.

66. Dubarry, M.; Liaw, B. Y., Development of a universal modeling tool for rechargeable lithium batteries. *Journal of Power Sources*, **2007**, 174 (2), 856-860.

67. Bergveld, H. J.; Kruijt, W. S.; Notten, P. H. L., Battery management systems: design by modelling. *Springer*: **2002**; Vol. 1.

68. Verbrugge, M. W.; Conell, R. S., Electrochemical and thermal characterization of battery modules commensurate with electric vehicle integration. *Journal of the Electrochemical Society*, **2002**, 149, A45.

69. Hildebrand, F. B., Advanced calculus for applications. *Prentice-Hall Englewood Cliffs, NJ*: **1962**; Vol. 5.

70. Verbrugge, M.; Koch, B., Generalized recursive algorithm for adaptive multiparameter regression. *Journal of the Electrochemical Society*, **2006**, 153, A187.

71. Gelb, A., Applied optimal estimation. *MIT press*: **1999**.

72. Ljung, L., System identification. *Wiley Online Library*: **1999**.

73. Santhanagopalan, S.; White, R. E., Online estimation of the state of charge of a lithium ion cell. *Journal of Power Sources*, **2006**, 161 (2), 1346-1355.

74. Sorenson, H. W., Least-squares estimation: from Gauss to Kalman. *Spectrum, IEEE*, **1970**, 7 (7), 63-68.

75. Robertson, D. G.; Lee, J. H.; Rawlings, J. B., A moving horizon-based approach for least-squares estimation. *AIChE Journal*, **1996**, 42 (8), 2209-2224.

76. Alkis, C.; Navid, M., Numerical Methods for Chemical Engineers with MATLAB Applications. *New Jersey*, **1999**.

77. Verbrugge, M.; Tate, E., Adaptive state of charge algorithm for nickel metal hydride batteries including hysteresis phenomena. *Journal of Power Sources*, **2004**, 126 (1), 236-249.

78. Jin, S.; Lim, J. H.; Oh, J.; Han, C.; Cho, S. Method for Measuring SOC of a Battery in a Battery Management System and the Apparatus Thereof. 2010/0280777, 2010.

79. Arulampalam, M. S.; Maskell, S.; Gordon, N.; Clapp, T., A tutorial on particle filters for online nonlinear/non-Gaussian Bayesian tracking. *Signal Processing, IEEE Transactions on*, **2002**, 50 (2), 174-188.

80. Cho, S.; Jeong, H.; Han, C.; Jin, S.; Lim, J. H.; Oh, J., On-line monitoring of capacity fade in lithium-ion battery. *Journal of Chemical Engineering of Japan*, **2012**, accepted paper, ASAP.

81. Huet, F., A review of impedance measurements for determination of the state-of-charge or state-of-health of secondary batteries. *Journal of power sources*, **1998**, 70 (1), 59-69.

82. Liaw, B. Y.; Jungst, R. G.; Nagasubramanian, G.; Case, H. L.; Doughty, D. H., Modeling capacity fade in lithium-ion cells. *Journal of power sources*, **2005**, 140 (1), 157-161.

83. Jin, S.; Lim, J. H.; Han, C.; Cho, S.; Jeong, H. Apparatus and Method for estimating battery life. 10-2010-0030387, 2010.

84. Jin, S.; Lim, J. H.; Han, C.; Cho, S.; Jeong, H. Apparatus and Method for reporting exchange time of battery. 10-2010-0107954, 2010.

85. Hariprakash, B.; Martha, S.; Jaikumar, A.; Shukla, A., On-line monitoring of lead–acid batteries by galvanostatic non-destructive technique. *Journal of power*

sources, **2004**, 137 (1), 128-133.

86. Bohlen, O.; Kowal, J.; Sauer, D. U., Ageing behaviour of electrochemical double layer capacitors: Part I. Experimental study and ageing model. *Journal of power sources*, **2007**, 172 (1), 468-475.

87. Bohlen, O.; Kowal, J.; Dirk Uwe, S., Ageing behaviour of electrochemical double layer capacitors: Part II. Lifetime simulation model for dynamic applications. *Journal of power sources*, **2007**, 173 (1), 626-632.

88. Pascoe, P. E.; Anbuky, A. H., A VRLA battery simulation model. *Energy Conversion and Management*, **2004**, 45 (7), 1015-1041.

89. Zhang, Q.; White, R. E., Capacity fade analysis of a lithium ion cell. *Journal of power sources*, **2008**, 179 (2), 793-798.

90. Dubarry, M.; Liaw, B. Y., Identify capacity fading mechanism in a commercial $LiFePO_4$ cell. *Journal of power sources*, **2009**, 194 (1), 541-549.

91. Anil V, V., A model for degradation of electrochemical devices based on linear non-equilibrium thermodynamics and its application to lithium ion batteries. *Journal of power sources*, **2011**, 196 (14), 5970-5984.

92. Li, Z.; Lu, L.; Ouyang, M.; Xiao, Y., Modeling the capacity degradation of LiFePO4/graphite batteries based on stress coupling analysis. *Journal of power sources*, **2011**, 196 (22), 9757-9766.

93. Ning, G.; Popov, B. N., Cycle life modeling of lithium-ion batteries. *Journal of the Electrochemical Society*, **2004**, 151, A1584.

94. Santhanagopalan, S.; Guo, Q.; Ramadass, P.; White, R. E., Review of models for predicting the cycling performance of lithium ion batteries. *Journal of power sources*, **2006**, 156 (2), 620-628.

95. Zhang, Q.; White, R. E., Calendar life study of Li-ion pouch cells: Part 2: Simulation. *Journal of power sources*, **2008**, 179 (2), 785-792.

96. Belt, J.; Utgikar, V.; Bloom, I., Calendar and PHEV cycle life aging of high-energy, lithium-ion cells containing blended spinel and layered-oxide cathodes. *Journal of power sources*, **2011**, 196 (23), 10213-10221.

97. Wang, J.; Liu, P.; Hicks-Garner, J.; Sherman, E.; Soukiazian, S.; Verbrugge, M.; Tataria, H.; Musser, J.; Finamore, P., Cycle-life model for graphite-LiFePO4 cells. *Journal of power sources*, **2011**, 196 (8), 3942-3948.

98. Delaille, A.; Perrin, M.; Huet, F.; Hernout, L., Study of the "coup de fouet" of lead-acid cells as a function of their state-of-charge and state-of-health. *Journal of power sources*, **2006**, 158 (2), 1019-1028.

99. Cao, H.; Yu, J.; Kang, L.; Yang, H.; Ai, X., Modeling and prediction for discharge lifetime of battery systems using hybrid evolutionary algorithms. *Computers & chemistry*, **2001**, 25 (3), 251-259.

100. Stamps, A. T.; Holland, C. E.; White, R. E.; Gatzke, E. P., Analysis of capacity fade in a lithium ion battery. *Journal of power sources*, **2005**, 150, 229-239.

101. Gregory L, P., Recursive approximate weighted total least squares estimation of battery cell total capacity. *Journal of power sources*, **2011**, 196 (4), 2319-2331.

102. He, W.; Williard, N.; Osterman, M.; Pecht, M., Prognostics of lithium-ion batteries based on Dempster–Shafer theory and the Bayesian Monte Carlo method. *Journal of power sources*, **2011**, 196 (23), 10314-10321.

103. Wang, S.; Verbrugge, M.; Wang, J. S.; Liu, P., Multi-parameter battery

state estimator based on the adaptive and direct solution of the governing differential equations. *Journal of power sources*, **2011**, 196 (20), 8735-8741.

104. Hu, C.; Youn, B. D.; Chung, J., A multiscale framework with extended Kalman filter for lithium-ion battery SOC and capacity estimation. *Applied Energy*, **2012**, 92 (0), 694-704.

105. Dubarry, M.; Svoboda, V.; Hwu, R.; Liaw, B. Y., A roadmap to understand battery performance in electric and hybrid vehicle operation. *Journal of power sources*, **2007**, 174 (2), 366-372.

106. Honkura, K.; Takahashi, K.; Horiba, T., Capacity-fading prediction of lithium-ion batteries based on discharge curves analysis. *Journal of power sources*, **2011**, 196 (23), 10141-10147.

107. Remmlinger, J.; Buchholz, M.; Meiler, M.; Bernreuter, P.; Dietmayer, K., State-of-health monitoring of lithium-ion batteries in electric vehicles by on-board internal resistance estimation. *Journal of power sources*, **2011**, 196 (12), 5357-5363.

108. Ljung, L., System identification: theory for the user. *Prentice Hall PTR*: **1999**.

109. Verbrugge, M. W.; Conell, R. S., Electrochemical and Thermal Characterization of Battery Modules Commensurate with Electric Vehicle Integration. *Journal of the Electrochemical Society*, **2002**, 149 (1), A45-A53.

110. Ohtsuka, T.; Fujii, H., Nonlinear receding-horizon state estimation by realtime optimization technique. *Journal of guidance, control, and dynamics*, **1996**, 19 (4).

111. Kwon, W. H.; Han, S., Receding horizon control: model predictive

control for state models. *Springer Verlag*: **2005**.

112. Bard, A. J.; Faulkner, L. R., Electrochemical methods: fundamentals and applications. *Wiley New York*: **1980**; Vol. 2.

113. Grewal, M. S.; Andrews, A. P., Kalman filtering: theory and practice using MATLAB. **2001**.

114. Franklin, G. F.; Powell, J. D.; Emami-Naeini, A., Feedback control of dynamic systems. *Addison-Wesley Reading, MA*: **1994**; Vol. 2.

115. Veziroglu, A.; Macario, R., Fuel cell vehicles: State of the art with economic and environmental concerns. *International Journal of Hydrogen Energy*, **2011**, 36 (1), 25-43.

116. Boettner, D. D.; Paganelli, G.; Guezennec, Y. G.; Rizzoni, G.; Moran, M. J., Proton exchange membrane fuel cell system model for automotive vehicle simulation and control. *Journal of energy resources technology*, **2002**, 124 (1), 20-27.

117. Bernay, C.; Marchand, M.; Cassir, M., Prospects of different fuel cell technologies for vehicle applications. *Journal of Power Sources*, **2002**, 108 (1-2), 139-152.

118. Kazim, A., Introduction of PEM fuel-cell vehicles in the transportation sector of the United Arab Emirates. *Applied energy*, **2003**, 74 (1-2), 125-133.

119. Hwang, J.; Wang, D.; Shih, N., Development of a lightweight fuel cell vehicle. *Journal of Power Sources*, **2005**, 141 (1), 108-115.

120. Offer, G.; Howey, D.; Contestabile, M.; Clague, R.; Brandon, N., Comparative analysis of battery electric, hydrogen fuel cell and hybrid vehicles in a future sustainable road transport system. *Energy Policy*, **2010**, 38 (1), 24-29.

121. Paladini, V.; Donateo, T.; de Risi, A.; Laforgia, D., Super-capacitors fuel-cell hybrid electric vehicle optimization and control strategy development. *Energy conversion and management*, **2007**, 48 (11), 3001-3008.

122. Kojima, T.; Ishizu, T.; Horiba, T.; Yoshikawa, M., Development of lithium-ion battery for fuel cell hybrid electric vehicle application. *Journal of Power Sources*, **2009**, 189 (1), 859-863.

123. Broussely, M., Battery Requirements for HEVs, PHEVs, and EVs: An Overview. *Electric and Hybrid Vehicles: Power Sources, Models, Sustainability, Infrastructure and the Market*, **2010**, 305-347.

124. Sohn, Y. J.; Kim, M.; Lee, W. Y., The computer-aided analysis for the driving stability of a plug-in fuel cell vehicle using a proton exchange membrane fuel cell. *International Journal of Hydrogen Energy*, **2011**.

125. Pérez, L. V.; Bossio, G. R.; Moitre, D.; García, G. O., Optimization of power management in an hybrid electric vehicle using dynamic programming. *Mathematics and Computers in Simulation*, **2006**, 73 (1), 244-254.

126. Schouten, N. J.; Salman, M. A.; Kheir, N. A., Energy management strategies for parallel hybrid vehicles using fuzzy logic. *Control Engineering Practice*, **2003**, 11 (2), 171-177.

127. Gao, D.; Jin, Z.; Lu, Q., Energy management strategy based on fuzzy logic for a fuel cell hybrid bus. *Journal of Power Sources*, **2008**, 185 (1), 311-317.

128. Ryu, J.; Park, Y.; Sunwoo, M., Electric powertrain modeling of a fuel cell hybrid electric vehicle and development of a power distribution algorithm based on driving mode recognition. *Journal of Power Sources*, **2010**, 195 (17), 5735-5748.

129. Hajizadeh, A.; Golkar, M. A., Intelligent power management strategy of

hybrid distributed generation system. *International Journal of Electrical Power & Energy Systems*, **2007**, 29 (10), 783-795.

130. Jeong, H.; Ha, T.; Kim, H.; Han, C., Simulation of PEM fuel cell with 2D steady-state mode. *Korean Chemical Engineering Research*, **2008**, 915-921.

131. Salmasi, F. R., Control strategies for hybrid electric vehicles: Evolution, classification, comparison, and future trends. *Vehicular Technology, IEEE Transactions on*, **2007**, 56 (5), 2393-2404.

132. Piccolo, A.; Ippolito, L.; Vaccaro, A. In *Optimisation of energy flow management in hybrid electric vehicles via genetic algorithms*, Ieee: 2001; pp 434-439 vol. 431.

133. Delprat, S.; Lauber, J.; Guerra, T. M.; Rimaux, J., Control of a parallel hybrid powertrain: optimal control. *Vehicular Technology, IEEE Transactions on*, **2004**, 53 (3), 872-881.

134. Gielniak, M. J.; Shen, Z. J. In *Power management strategy based on game theory for fuel cell hybrid electric vehicles*, IEEE: 2004; pp 4422-4426 Vol. 4426.

135. Lin, C. C.; Peng, H.; Grizzle, J. In *A stochastic control strategy for hybrid electric vehicles*, IEEE: 2004; pp 4710-4715 vol. 4715.

136. Karbowski, D.; Rousseau, A.; Pagerit, S.; Sharer, P. In *Plug-in vehicle control strategy: from global optimization to real time application*, 2006.

137. Amiri, M.; Esfahanian, M.; Hairi-Yazdi, M. R.; Esfahanian, V., Minimization of power losses in hybrid electric vehicles in view of the prolonging of battery life. *Journal of Power Sources*, **2009**, 190 (2), 372-379.

138. Vahidi, A.; Stefanopoulou, A.; Peng, H., Current management in a hybrid fuel cell power system: A model-predictive control approach. *Control Systems*

Technology, IEEE Transactions on, **2006**, 14 (6), 1047-1057.

139. Sciarretta, A.; Back, M.; Guzzella, L., Optimal control of parallel hybrid electric vehicles. *Control Systems Technology, IEEE Transactions on*, **2004**, 12 (3), 352-363.

140. Xu, L.; Li, J.; Hua, J.; Li, X.; Ouyang, M., Optimal vehicle control strategy of a fuel cell/battery hybrid city bus. *International Journal of Hydrogen Energy*, **2009**, 34 (17), 7323-7333.

141. Hajimiri, M. H.; Salmasi, F. R., A predictive and battery protective control strategy for series HEV. *Journal of Asian Electric Vehicles*, **2008**, 6 (2), 1159-1165.

142. Gao, J.; Zhu, G. M. G.; Strangas, E.; Sun, F., Equivalent fuel consumption optimal control of a series hybrid electric vehicle. *Proceedings of the Institution of Mechanical Engineers, Part D: Journal of Automobile Engineering*, **2009**, 223 (8), 1003-1018.

143. Rajagopalan, A.; Washington, G.; Rizzoni, G.; Guezennec, Y., Development of fuzzy logic and neural network control and advanced emissions modeling for parallel hybrid vehicles. *National Renewable Energy Laboratory*: **2003**.

144. Schouten, N. J.; Salman, M. A.; Kheir, N. A., Fuzzy logic control for parallel hybrid vehicles. *Control Systems Technology, IEEE Transactions on*, **2002**, 10 (3), 460-468.

145. Gomathy, C.; Shanmugavel, S. In *An efficient fuzzy based priority scheduler for mobile ad hoc networks and performance analysis for various mobility models*, IEEE: 2004; pp 1087-1092 Vol. 1082.

146. Driankov, D.; Hellendoorn, H.; Reinfrank, M., An introduction to fuzzy control. *Springer Verlag*: **1996**.

147. Li, H. X.; Zhang, X. X.; Li, S. Y., A three-dimensional fuzzy control methodology for a class of distributed parameter systems. *Fuzzy Systems, IEEE Transactions on*, **2007**, 15 (3), 470-481.

148. Seborg, D. E.; Edgar, T. F.; Mellichamp, D. A.; Doyle III, F. J., Process dynamics and control. *Wiley*: **2010**.

149. Lin, C. C.; Kim, M. J.; Peng, H.; Grizzle, J. W., System-level model and stochastic optimal control for a PEM fuel cell hybrid vehicle. *Journal of dynamic systems, measurement, and control*, **2006**, 128, 878.

150. Li, C. Y.; Liu, G. P., Optimal fuzzy power control and management of fuel cell/battery hybrid vehicles. *Journal of Power Sources*, **2009**, 192 (2), 525-533.

Abstract in Korean (요 약)

최근 휴대용 기기와 친환경 자동차의 에너지 저장 시스템이 큰 관심을 받으며, 특히 전압과 출력 면에서 높은 성능을 보이는 리튬 이온 전지가 가장 각광을 받고 있다. 이러한 리튬 이온 전지는 친환경 자동차와 같은 하이브리드 에너지 시스템의 주요 출력 공급원 또는 보조 출력 공급원으로 쓰인다. 친환경 자동차 내에 탑재되는 리튬 이온 전지의 경우 자동차에 출력을 공급하는 동시에 여분의 출력이 남는 경우 이를 저장하는 역할을 수행한다. 따라서 리튬 이온 전지의 성능이 친환경 자동차의 성능을 대표할 수 있는 중요한 요소 중 하나라고 할 수 있다. 리튬 이온 전지의 성능을 대표하여 나타낼 수 있는 것으로 가용 잔존 용량과 건전 상태를 들 수 있다. 이러한 두 종류의 상태는 센서를 통해 직접 측정이 불가능하기 때문에 이를 추정하기 위해 동적 상세 모델의 개발이 필요하다. 따라서 본 논문에서는 리튬 이온 전지에 대한 동적 상세 모델을 개발하였다. 그리고 이를 바탕으로 하여 전지의 가용 잔존 용량과 건전 상태를 추정하는 방법론을 개발하였다. 최종적으로 본 논문에서 개발한 모델 및 추정 방법론을 연료 전지 하이브리드 자동차의 최적 제어 방법론에 적용하였다.

우선, 친환경 자동차에 쓰이는 리튬 이온 전지의 가용 잔존 용량 추정 알고리즘을 제안하고자 한다. 제안된 방법론은 다양한 온도, 운전 상태 및 출력 부하에 따른 운전 조건에 부합할 수 있는 강건한 가용 잔존 용

량 추정을 기본적인 목표로 한다. 이러한 방법론은 전기화학적 모델에 기반을 둔 등가 회로 모델과 재귀 추정자를 포함하고 있다. 등가 회로 모델에 필요한 각 파라미터들은 다양한 온도 및 전류 조건에 따른 실험에 의해 추정하였다. 이러한 모델에 기반을 둔 가용 잔존 용량 추정 방법론과 전류 적산에 의한 추정 방법론의 결합을 통해 가용 잔존 용량의 추정 알고리즘을 개발하였다. 제안된 방법론은 저온 및 상온, 고온 상태에서의 다양한 운전 범위 하에서 실시된 리튬 이온 전지 팩에 대한 실험을 통해 검증하였다. 또한 각종 센서의 이상으로 인한 경우에 대해서도 검증하여 신뢰성을 입증하였다. 그 결과 제안된 방법론은 가용 잔존 용량의 추정에 적당하다는 것을 알 수 있으며 다양한 조건에 적합하고 센서 오류에 대한 문제에도 신뢰성을 가지고 있으며 계산 부하가 작기 때문에 온라인으로 적용 가능하다는 사실 또한 입증하였다.

또한 건전 상태로 대표되는 리튬 이온 전지의 실제 성능에 대한 온라인 감시를 위한 알고리즘을 개발하였다. 여러 변수 중 전지의 충전 용량이 건전 상태를 나타낼 수 있는 대표적인 변수로 선정되었다. 이러한 충전 용량의 추정을 위해 주요 알고리즘, 보조 알고리즘, 두 알고리즘을 결합한 통합 알고리즘의 세 가지 알고리즘을 개발하였다. 주요 알고리즘은 간략화한 등가 회로 모델과 소프트 센서 기술을 결합하여 개발하였다. 소프트 센서 기술은 시스템 인지 방법론과 이동 지평선 추정 방법론에 기반을 둔 방법론으로 파라미터 추정 방법에 주로 사용하였다. 그리고 주요 알고리즘의 계산 부하 문제를 해결하기 위해 보조 방법론을 개발하

였다. 그리고 이 두 알고리즘의 단점을 상쇄하고 장점을 극대화하기 위해 두 알고리즘을 결합하여 통합 알고리즘을 개발하였다. 개발된 알고리즘의 적합성을 평가하기 위해 새로운 상태의 전지와 열화된 전지에 대해 다양한 온라인 추정 시험을 거쳤다. 다양한 하이브리드 자동차 및 플러그인 하이브리드 자동차용 리튬 이온 전지에 대한 실험 결과, 개발한 알고리즘은 정확도, 신뢰성, 강건성 및 계산 부하에 대해 강점을 가지고 있어 적합하다는 결론을 내릴 수 있었다. 즉, 개발한 통합 알고리즘은 충전 용량 및 가용 출력에 대해 실시간으로 정량적인 값을 온라인 형태로 추정할 수 있어 실제 하이브리드 자동차 계열 리튬 이차 전지 시스템에 대한 응용에 적합하다는 것을 알 수 있다.

마지막으로 퍼지 제어 논리를 이용하여 고분자 전해질 연료 전지/리튬 이온 전지 하이브리드 에너지 시스템의 최적 제어 논리를 설계하였다. 이를 위해 우선적으로 앞에서 개발된 리튬 이온 전지 모델과 고분자전해질연료전지 시스템에 대해 모사를 하였다. 특히 고분자 전해질 연료 전지의 경우 수소 재활용과 공기극의 가습을 고려하여 모사하였다. 최적 제어기는 퍼지 논리 알고리즘을 활용하여 개발하였다. 이 제어기는 세 가지의 입력 변수가 있다. 그 중 첫 번째 변수인 연료 전지 하이브리드 자동차에서 요구하는 출력을 통해 연료 전지에서 생산해야 하는 출력을 계산하였다. 또한, 앞에서 개발한 방법론을 통해 추정이 가능한 가용 잔존 용량과 건전 상태 역시 제어기의 입력 값으로 사용되었다. 이렇게 개발한 퍼지 제어기를 친환경 자동차의 다양한 운전 조건 및 리튬 이온 전

지의 상태에 대해 검증하였다. 검증 결과 제안된 퍼지 논리 제어기를 통해 친환경 자동차의 운전 및 부품 교환 비용을 줄일 수 있으며 최적으로 운전을 할 수 있어 실제 이러한 시스템의 운영에 적합하다는 것을 알 수 있었다.

이러한 연구는 하이브리드 에너지 시스템을 위한 리튬 이온 전지에 대한 상태 추정 및 제어를 온라인으로 가능하게 할 수 있다. 본 논문에서 소개한 모델, 상태 추정 방법론과 제어 논리는 친환경 자동차와 같은 하이브리드 에너지 시스템에 대해 온라인으로 적용할 수 있을 것으로 보인다.

주요어: 리튬 이온 전지, 하이브리드 에너지 시스템, 등가 회로 모델, 가용 잔존 용량, 용량 저하, 퍼지 제어

학 번: 2005-21277